

ABSTRACT

Title: THE DIVALENT CATION TRANSPORTER NRAMP IN
THE PARASITE *PERKINSUS MARINUS*: GENOMIC,
MOLECULAR, STRUCTURAL, FUNCTIONAL AND
EVOLUTIONARY ASPECTS

Zhuoer Lin, Doctor of Philosophy, 2010

Dissertation directed by: Professor Gerardo R. Vasta
Department of Microbiology and Immunology
University of Maryland School of Medicine
IMET/UMB

Perkinsus marinus, the causative agent of Dermo disease in eastern oyster *Crassostrea virginica* has been a great hurdle for oyster population restoration along the atlantic and gulf coasts of USA. Iron was shown to be an essential element for *P. marinus* growth and virulence, but iron uptake pathways have not been elucidated.

The Natural Resistance-Associated Macrophage Protein (Nramp), an iron transporter initially identified in the mouse as a marker for resistance to intracellular pathogens, was also proposed as a potential virulence factor for intracellular pathogens. An Nramp homologue was identified by our laboratory in *P. marinus* (PmNramp1). In this study, two other PmNramp isotypes (PmNramp2 and PmNramp3) were identified through genome mining followed by molecular characterization. The three PmNramp isotypes are

encoded by genes of distinct organization, and are all transcribed in parasite trophozoites cultured in defined medium. Transcripts of a number of *P. marinus* genes, including PmNramp isotypes, superoxide dismutases (PmSOD), ascorbate peroxidase (PmAPX) and heat shock proteins (PmHSP70 and PmHSP90) display a trans-splicing leader (SL) highly similar to that from dinoflagellates. No changes in transcription levels of those genes were detected by real-time quantitative reverse transcription PCR (qRT-PCR), under iron/manganese overload, iron depletion, and host hemolymph exposure, suggesting a constitutive polycistronic transcription in the parasite.

Functional studies by yeast complementation assays suggested iron uptake activity by PmNramp1, but not for PmNramp2 and PmNramp3. Prediction of PmNramp1 topology by homologous modeling indicated that PmNramp1 is an integral protein with 12 transmembrane segments (TMS). The central position of the Nramp-specific triplets Asp-Pro-Gly (TMS1) and Met-Pro-His (TMS6) in a three-dimensional (3D) arrangement formed with TMS3 and TMS8 provided the mechanistic basis for iron acquisition via PmNramp1. Site-directed mutagenesis of selected residues in the TMS6 triplets in PmNramp1 resulted in loss of complementation of the mutant in yeast. A chimeric protein with PmNramp1 N- and C-termini and a PmNramp3 core structure from TMS1 to TMS12 actively complemented yeast growth, suggesting that PmNramp3 can function as an iron transporter. A phylogenetic analysis indicated that all the three PmNramp isotypes are of the archetype Nramp cluster. Protein sequence divergence among PmNramp isotypes was not related to diversification of critical functional elements, which remained constrained by purifying selection. This result was consistent with the function of both PmNramp1 and PmNramp3 as iron transporters in yeast, despite their

different evolutionary rate and substitution patterns. Subcellular localization of PmNramp isotypes in *P. marinus* trophozoites is in progress. PmNramp3 was shown to localize on cell peripheral when the parasite proliferates by binary fission. The data were consistent with the previous observation that iron is important for *P. marinus* growth.

As the first functional study of Nramp homolog in protozoan parasites, the work in this dissertation may serve as a platform for research in other protozoan Nramp and iron transporters.

THE DIVALENT CATION TRANSPORTER NRAMP IN PARASITE
PERKINSUS MARINUS: GENOMIC, MOLECULAR, STRUCTURAL, FUNCTIONAL
AND EVOLUTIONARY ASPECTS

BY

Zhuoer Lin

Dissertation submitted to the Faculty of the Graduate School of the
University of Maryland, College Park, in partial fulfillment
of the requirements for the degree of
Doctor of Philosophy
2010

Advisory Committee:

Professor Gerardo R. Vasta, Chair

Professor Mathieu F. Cellier

Professor Feng Chen

Professor Isabelle Coppens

Professor José-Antonio Fernández-Robledo

Professor Daniel C. Stein, Dean's representative for College of Life Sciences

© Copyright by

Zhuoer Lin

2010

ACKNOWLEDGEMENTS

The dissertation project was supported by the NSF grant awarded to Dr. Vasta. I would like to thank Dr. Vasta for the opportunity to work in his lab and for his support and advice during my Ph.D training process. I also would like to thank my committee member Dr. Fernández-Robledo for all the scientific discussions we had about my dissertation project. I need to thank my committee member Dr. Cellier for his great effort in my dissertation project as a collaborator. I am indebted to my committee members Dr. Coppens and Dr. Chen for their time, patience, and dedication to the completion of my research work. Furthermore, many thanks to former and present lab members in Dr. Vasta's lab for their support and expertise. Last but not least, I thank my parents and my husband for their constant support for making all of these possible.

TABLE OF CONTENTS

ACKNOWLEDGEMENTS.....	II
TABLE OF CONTENTS.....	III
LIST OF TABLES.....	IX
LIST OF FIGURES	X
LIST OF ABBREVIATIONS.....	XIII
CHAPTER 1 INTRODUCTION AND BACKGROUND INFORMATION	1
1.1 Introduction.....	1
Dermo disease and <i>P. marinus</i>	1
Importance of iron for <i>Perkinsus marinus</i> survival and virulence	1
1.2 Background.....	3
Iron is a critical trace element for both hosts and pathogens.....	3
Host iron metabolism and nutritional immunity.....	4
Iron acquisition by protozoan parasites	14
Identification of Nramp as a marker for resistance to infection	33
Nramp functions in metal homeostasis.....	34
Nramp as a potential microbial virulence factor.....	35
CHAPTER 2 MOLECULAR CHARACTERIZATION OF TWO NOVEL NATURAL RESISTANCE-ASSOCIATED MACROPHAGE PROTEIN ISOTYPES (PMNRAMP2 AND PMNRAMP3) IN <i>PERKINSUS MARINUS</i>	39

SUMMARY	39
INTRODUCTION	40
MATERIALS AND METHODS.....	41
<i>Perkinsus marinus</i> cultures.....	41
Genome mining.....	41
Nucleic acid extraction and cDNA cloning and sequencing	42
Identification of trans-splicing leader in other genes.....	43
Challenge experiment design.....	44
RNA extraction and reverse transcription.....	45
Quantitative PCR	46
RESULTS	48
Identification of two novel PmNramp isotypes	48
Gene organization of PmNramp isotypes	52
Amino acid alignment of PmNramp isotypes with human Nramp2 homolog	54
PmNramp mRNA is trans-spliced with trans-splicing leader highly identical to dinoflagellate splice leader	57
Other genes in <i>P. marinus</i> are trans-spliced	60

Trans-spliced <i>P. marinus</i> genes show no obvious transcriptional regulation	63
DISCUSSION.....	83
CHAPTER 3 PHYLOGENETIC ANALYSIS OF THE PMNRAMP ISOTYPES	
.....	88
SUMMARY	88
INTRODUCTION	89
MATERIALS AND METHODS.....	90
Phylogenetic analysis.....	90
Molecular evolutionary gene analyses.....	92
RESULTS AND DISCUSSION.....	99
Taxonomic distribution of Nramp in eukaryotes.....	99
Phylogeny of <i>Perkinsus</i> Nramp1-3 proteins.....	107
Analysis of <i>Perkinsus</i> Nramp1-3 gene evolution	110
Detailing evolutionary patterns of <i>Perkinsus</i> Nramp1-3 genes domains....	111
CHAPTER 4 FUNCTIONAL CHARACTERIZATION OF THE PMNRAMP ISOTYPES.....	
.....	114
SUMMARY	114
INTRODUCTION	114
MATERIALS AND METHODS.....	115

Yeast strains and plasmid.....	115
Culture and transformation of yeast cells	116
Transformation and expression of PmNramp isotypes in transformed yeast	116
Construction of chimeric PmNramp2 and PmNramp3	117
IFAs to detect PmNramp protein expression in <i>fet3fet4</i>	121
Yeast complementation assay of transformed <i>fet3fet4</i>	122
Complementation assay of yeast <i>smf1smf2</i>	122
RESULTS	123
Expression of PmNramp isotypes in <i>fet3fet4</i>	123
PmNramp1 complements the growth of <i>fet3fet4</i>	126
<i>Fet3fet4</i> complementation assay of chimeric PmNramp2 and PmNramp3	129
Yeast complementation assay in <i>smf1smf2</i>	132
DISCUSSION.....	135
CHAPTER 5 STRUCTURAL AND MECHANISTIC STUDIES OF THE PMNRAMP ISOTYPES.....	137
SUMMARY	137
INTRODUCTION	137

MATERIALS AND METHODS.....	140
Structural analysis of PmNramp1 by homology modeling.....	140
Site-directed mutagenesis	140
RESULTS	141
Functional features predicted from protein sequence structural modeling analysis.....	141
Site-directed mutagenesis of PmNramp1 predicted functional residues	148
DISCUSSION.....	153
CHAPTER 6 SUBCELLULAR LOCALIZATION OF THE PMNRAMP	
ISOTYPES.....	158
SUMMARY	158
INTRODUCTION	158
MATERIALS AND METHODS.....	163
Generation of PmNramp antibodies.....	163
Western blot analysis of PmNramp isotypes	166
IFAs in <i>P. marinus</i> cells.....	166
RESULTS	167
Western blot on parasite lysates using purified PmNramp IgG.....	167

Localization of PmNramp3 in log-phase <i>P. marinus</i> trophozoites.....	171
DISCUSSION.....	175
CHAPTER 7 SUMMARY AND FUTURE DIRECTIONS.....	179
Functional studies of PmNramp isotypes	179
Domain swapping as a novel approach for functional studies of protozoan Nramp in heterologous systems	181
<i>P. marinus</i> and oyster hemocyte interaction: the “tug-of-war” for iron.....	181
Other potential iron uptake pathways in <i>P. marinus</i>	182
<i>P. marinus</i> genomic organization and post-transcription regulations	182
BIBLIOGRAPHY.....	185

LIST OF TABLES

TABLE 1. COMMON PROTOZOAN PARASITES AND THEIR PARASITIC NICHES IN HOST	17
TABLE 2. THE COMPOSITION OF <i>PERKINSUS MARINUS</i> CULTURE MEDIUM.....	42
TABLE 3. PRIMERS USED FOR AMPLIFYING <i>PERKINSUS</i> NRAMP GENES	42
TABLE 4. PRIMERS USED IN TESTING OF TRANS-SPLICING LEADER IN OTHER GENES	44
TABLE 5 PRIMERS USED IN QUANTITATIVE PCR	47
TABLE 6 IDENTITY AND SIMILARITY OF PMNRAMP ISOTYPES	54
TABLE 7. TAXONOMIC DISTRIBUTION OF KNOWN EUKARYOTIC NRAMP HOMOLOGS.....	104
TABLE 8. PRIMERS USED IN N- AND C-TERMINUS SWAPPING AND YEAST COMPLEMENTATION.....	117
TABLE 9. SITE DIRECTED MUTAGENESIS OF PMNRAMP1	141

LIST OF FIGURES

FIG. 1. MAMMALIAN IRON METABOLISM IS REGULATED BY INNATE IMMUNITY.....	12
FIG. 2. SUMMARY OF IRON UPTAKE PATHWAYS IDENTIFIED IN EXTRACELLULAR PROTOZOAN PARASITES.....	26
FIG. 3. SUMMARY OF IRON UPTAKE PATHWAYS IDENTIFIED IN <i>LEISHMANIA</i> AMASTIGOTES.....	32
FIG. 4. RT-PCR ANALYSIS OF PMNRAMP ISOTYPES IN <i>P. MARINUS</i> TROPHOZOITES.....	51
FIG. 5. GENE ORGANIZATION OF <i>PMNRAMP</i> HOMOLOGS.....	53
FIG. 6. MULTIPLE ALIGNMENT OF DEDUCED AMINO ACID SEQUENCES OF PMNRAMP1, PMNRAMP2 AND PMNRAMP3 WITH HUMAN NRAMP2 (HSNRAMP2).....	56
FIG. 7. THE CONSERVED SL SEQUENCE FROM <i>P. MARINUS</i> NRAMP MRNAS.....	59
FIG. 8. THE CONSERVED SL SEQUENCE FROM OTHER GENES IN <i>P. MARINUS</i>	62
FIG. 9. EXPRESSION OF PMNRAMP1 UPON DIFFERENT TREATMENTS.....	66
FIG. 10. EXPRESSION OF PMNRAMP2 UPON DIFFERENT TREATMENTS.....	68
FIG. 11. EXPRESSION OF PMNRAMP3 UPON DIFFERENT TREATMENTS.....	70
FIG. 12. EXPRESSION OF PMSOD1 UPON DIFFERENT TREATMENTS... ..	72
FIG. 13. EXPRESSION OF PMSOD2 UPON DIFFERENT TREATMENTS... ..	74

FIG. 14. EXPRESSION OF PMAPX1 UPON DIFFERENT TREATMENTS. . .	76
FIG. 15. EXPRESSION OF PMAPX2 UPON DIFFERENT TREATMENTS. . .	78
FIG. 16. EXPRESSION OF PM18S UPON DIFFERENT TREATMENTS.	80
FIG. 17. EXPRESSION OF PMHSP70 AND PMHSP90 TRANSCRIPT UPON TEMPERATURE CHANGES.....	82
FIG. 18. AMINO ACID ALIGNMENT OF THE THREE PMNRAMP ISOTYPES	95
FIG. 19. CODON-BY-CODON CDNA ALIGNMENT OF PMNRAMP ISOTYPES	98
FIG. 20. SIMPLIFIED PHYLOGENY OF PMNRAMP1-3	102
FIG. 21. PHYLOGENETIC ANALYSES OF SEQUENCES DERIVED FROM TAXONOMICALLY DIVERSE UNICELLULAR EUKARYOTES DEMONSTRATE PREVALENCE OF PROTOTYPE NRAMP (PN).	106
FIG. 22. DETAILED PHYLOGENY OF <i>P. MARINUS</i> NRAMP HOMOLOGS (PMNRAMP1-3) DEMONSTRATES THEY BELONG TO THE NRAMP ARCHETYPE II GROUP.....	109
FIG. 23. N- AND C-TERMINI SWAPPING OF PMNRAMP1 TO PMNRAMP2 AND PMNRAMP3	120
FIG. 24. TRANSFORMATION AND EXPRESSION OF PMNRAMP ISOTYPES IN <i>FET3FET4</i>	125
FIG. 25. YEAST COMPLEMENTATION ASSAY OF PMNRAMP ISOTYPES IN <i>FET3FET4</i>	128
FIG. 26. COMPLEMENTATION OF IRON DEFICIENCY PHENOTYPE OF YEAST <i>FET3FET4</i> MUTANT BY CHIMERIC PMNRAMP3.	131

FIG. 27. COMPLEMENTATION ASSAY OF YEAST STRAIN <i>SMF1SMF2</i> IN SOLID MEDIUM.	134
FIG. 28. DISPLAY OF PREDICTED STRUCTURE BY ALIGNMENT OF PMNRAMP ISOTYPES WITH HUMAN NRAMP2.	145
FIG. 29. HYPOTHETIC MODEL FOR TRANSMEMBRANE SYMPORT OF DIVALENT METALS AND PROTONS VIA PMNRAMP1.	147
FIG. 30. COMPLEMENTATION ASSAYS OF YEAST <i>FET3FET4</i> MUTANT AFTER MUTATIONS OF KEY RESIDUES IN PMNRAMP1.....	152
FIG. 31. A DIAGRAMMATIC DRAWING OF CELL CYCLE OF CULTURED <i>P. MARINUS</i>	162
FIG. 32. RABBIT ANTISERUM WAS RAISED AGAINST PEPTIDES PREDICTED TO BE THE LOOPS BETWEEN TMS7 AND TMS8.	165
FIG. 33. WESTERN BLOT ANALYSIS OF PMNRAMP ISOTYPES USING PURIFIED IGG	170
FIG. 34. LOCALIZATION OF PMNRAMP3 IN LOG-PHASE <i>P. MARINUS</i> BY FLUORESCENCE MICROSCOPY.....	173

LIST OF ABBREVIATIONS

3D	three-dimensional
ACO	aconitase
ApcT	amino acid-polyamine-organocation transporter
APX	ascorbate peroxidase
BetP	betaine transporter
BLAST	basic local alignment search tool
bp	base-pair
CNS	central nerve system
Dcytb	duodenal cytochrome-b
DFO	deferoxamine
CHO	Chinese hamster ovary
DME	Dulbecco modified Eagle's
DMT1	divalent metal transporter 1
ER	endoplasmic reticulum
ESTs	expressed sequence tags
FBS	fetal bovine serum
FLVCR	feline leukemia virus, type C, receptor
FPN1	ferroportin-1
GDF15	growth differentiation factor 15
HAM12	Ham's F12
HCP1	heme carrier protein-1
HIFs	hypoxia-inducible factors
HJV	hemojuvelin
HO	heme oxygenase

Hp	hephaestin
HSP	heat shock protein
IRE/IRP	iron responsive element/iron responsive protein
IRP1	iron responsive protein-1
IRT	iron regulated transporter
LD	lethal dose
LeuT	leucine transporter
Lf	lactoferrin
LIP	labile iron pool
LIT	<i>Leishmania</i> iron transporter
LPS	lipopolysaccharide
Mhp 1	sodium-benzylhydantoin transport protein
MntH	manganese transport, H ⁺ -dependent
Nramp	natural resistance-associated macrophage protein
PCR	polymerase chain reaction
PGC	polycistronic gene cluster
PV	parasitophorous vacuole
QPCR	quantitative PCR
RACE	rapid amplification of cDNA ends
RBCs	red blood cells
RMSD	root mean square deviation
RNAi	RNA interference
RNS	reactive nitrogen species
ROS	reactive oxygen species
SGLT1	sodium-coupled glucose transporter

SL	splicing leader
Slc	solute carrier
SOD	superoxide dismutase
STEAP3	six-transmembrane epithelial antigen of the prostate-3
Tf	transferrin
TMS	transmembrane segment
UTR	untranslated region
VSG	variant surface glycoprotein
ZIP	Zrt, Irt-like protein

CHAPTER 1 INTRODUCTION AND BACKGROUND INFORMATION

1.1 Introduction

Dermo disease and *P. marinus*

Perkinsus species, are parasites of oysters, abalones, clams, and scallops, and have caused substantial damage to these fisheries worldwide [1, 2]. *P. marinus* is a facultative intracellular parasite that causes “Dermo” disease in the eastern oyster *C. virginica* [3]. Over the last 10-15 years, the range of *P. marinus* infection has extended along the Atlantic coast from New Jersey to Maine [4-6] with catastrophic consequences for local fisheries and the health of coastal waters [7]. The life cycle of *P. marinus* includes a free-living stage (zoospore) and a non-motile vegetative stage (trophozoite). Upon entering the host, most commonly by ingestion during filter-feeding, trophozoites are phagocytosed by oyster hemocytes where they are able to survive and proliferate inside a phagosome-like structure. Although the infection mechanism has not been fully elucidated, a galectin of unique structure plays a significant role in parasite entry into the host hemocytes [8]. Migration of infected hemocytes throughout the host tissues leads to systemic infection and eventually death [3, 9]. In the environment, transmission of *P. marinus* between oysters likely occurs when released trophozoites from infected oysters are filtered by adjacent individuals [7].

Importance of iron for *Perkinsus marinus* survival and virulence

Iron is a critical factor for *Perkinsus* growth and infection. In the eastern oyster *C. virginica*, the infection intensity of the protozoan parasite *P. marinus* increases with

environmental iron concentrations in a dose-dependent manner [10]. By adding deferoxamine (DFO) into the culture medium, the parasite growth was significantly inhibited; however, supplementing with the appropriate iron equivalents to saturate the DFO can rescue the parasite's growth [11]. One potential explanation for the importance of iron for *P. marinus* infection is that iron is the cofactor for the enzymes in the antioxidant pathways in the parasite. The hypothesis was proposed that *P. marinus* can overcome oyster oxidative burst by degradation of host-originated reactive oxygen species (ROS) [12, 13]. The identification of the key elements PmSOD1, PmSOD2, PmAPX and PmAPX2 in *P. marinus* antioxidant pathway [14-16] provided a molecular evidence for the ROS detoxification activity in the parasite. The fact that both the two SOD isotypes in *P. marinus* are iron-dependent indicates a potential connection between iron acquisition and *P. marinus* anti-oxidant pathway function. Despite our long acknowledgement of the importance of iron for *P. marinus*, no iron uptake pathways were identified. The research work in the dissertation is essentially the first exploration of iron acquisition pathways in this parasite. The outline for the following part of the dissertation is as below

- Background
 - Iron-uptake in host and protozoan parasites
 - role of Nramp in the tug-off war for iron
- Chapter 2: molecular identification of two other *P. marinus* Nramp isotypes (PmNramp2 & PmNramp3) after the characterization of PmNramp1

- Chapter 3: functional analysis of PmNramp isotypes in the aspects of transported substrates and 3D structure
- Chapter 4: subcellular localization of PmNramp isotypes in *P. marinus*
- Chapter 5: phylogeny analysis of PmNramp isotypes
- Chapter 6: summaries and future directions

1.2 Background

Iron is a critical trace element for both hosts and pathogens

Iron is an essential trace element for almost all organisms. Function as enzyme cofactor makes iron indispensable in a variety of biological activities, including oxygen transport in red-blood animals [17], DNA synthesis [18], electron transport [19] and others. The delicate balance orchestrated by iron uptake, transport, storage and release is pivotal since this metal can be a double-edged sword due to its redox-activity [20]. Therefore, every single taxon has evolved a rigorously controlled iron homeostasis system that fits its ecological niche. At the host-pathogen interface, the control of the balance becomes more intricate when two highly-evolved iron-acquisition systems compete directly with each other. During co-evolution of hosts and pathogens, pathogens have evolved efficient iron scavenging machineries to divert iron from host molecules, while the hosts have developed coordinated responses to infection, embargoing access to endogenous iron reserves. This strategy constitutes the basis of the concept of “nutritional immunity” [21, 22].

The iron-metabolism systems of host cells have been summarized in recent reviews [20, 23-25]. Based on functions, the elements involved in host iron homeostasis fall into at least eight categories: redox active (*e.g.*, Dcytb), sensing (*e.g.*, transferrin receptor 2), delivery (*e.g.*, transferrin), import (*e.g.* divalent metal transporter 1, transferrin receptor 1), recovery (*e.g.* haptoglobin), storage (*e.g.* ferritin), export (*e.g.* ferroportin), metabolic regulation (*e.g.*, intracellular, iron responsive protein 1 and endocrine, hepcidin). Some of these functions have been adapted to host defense against microbial pathogens. During infections, a large amount of lactoferrin is released for tight binding of ferric iron even in acid conditions. Siderocalin, also called lipocalin2, is able to interfere the pathogenic siderophores function via direct binding. The host resistance marker to intracellular pathogens, Nramp1 is recruited to the phagosomal membrane to withdraw iron away from pathogens [20, 23].

Host iron metabolism and nutritional immunity

Mammalian hosts use iron as the oxygen carrying element. Approximately 70% of the body iron exists in hemoglobin in red blood cells (RBCs) and erythroid precursors. As the biggest iron sink in the body, the iron supply for hemoglobin production in erythroid precursors is mostly through the iron delivery molecule Tf (transferrin) that undergoes the endocytosis pathway. Two of the other highly-expressed molecules, six-transmembrane epithelial antigen of the prostate-3 (STEAP3) [26, 27] and DMT1 (divalent metal transporter) [28] are the ferrireductase and the ferrous iron transporter in the endosomes (Fig. 1). Iron delivery to other tissues may involve different molecules, such as H- and L-ferritin which allow iron entry into cells via distinct endocytic receptors

TIM-2 [29] and Scara5 [30], respectively. Also DMT1 and Zip14 facilitate non-Tf bound iron uptake [31].

There are two potential ways for the endosomal iron to reach mitochondria, the factory for heme and iron-sulfur cluster synthesis. One way of endosomal iron supply to mitochondria comes from low molecular weight complexes in the cytosolic labile iron pool (LIP); beside, protein-to-protein or compartment-to-compartment iron delivery to mitochondria was also proposed based on the study in *hbd* mutant mice [32-35]. It is believed that mitochondria have redundant iron transporters and one of the identified carriers is mitoferrin [36, 37]. Cytotoxic over-accumulation of free iron or heme is avoided in the erythroid precursors by the expression of two isoforms of ferroportin (+/- IRE, [38]) and the heme exporter Feline leukemia virus, type C, receptor (FLVCR) [39, 40], respectively.

Mammalian erythroid precursors eventually develop into mature RBCs that have no nucleus and little repair capacity [41]. After 100 to 120 days spent in the blood circulation, RBCs become senescent. In the absence of infection, macrophages recycle iron from senescent RBCs, through erythrophagocytosis, and more generally from effete cells (e.g., PMNs, polymorphonuclear neutrophils). Senescent cells are engulfed and broken down within macrophages and iron is liberated from heme molecules by heme oxygenases (HO1 and HO2). Besides active phagocytosis of senescent cells, macrophages are also able to scavenge Tf-bound and Lf (lactoferrin)-bound [42] iron as well as hemoglobin-haptoglobin complexes. During hemolysis, haptoglobin binds to hemoglobin to prevent oxidative activities [43, 44]. The membrane receptor CD163 can interact with the hemoglobin-haptoglobin complex and internalize both molecules

through endocytosis. If severe hemolysis happens and haptoglobin is exhausted, CD163 can scavenge hemoglobin directly through the same pathway [45]. Unless under pathological conditions, macrophages normally accumulate little iron, and when plasma level is high, the excess is primarily stored in the ferritin of hepatocytes.

Macrophages expressing the exporter ferroportin-1 (FPN1) release iron into the circulation, acting as the recycling factory for ~90% of body iron. This activity corresponds to M2 macrophages in terms of activation states [46, 47]. M2 macrophages, by definition, stimulated with the Th2 cytokines interleukin 4 (IL4) and/or IL13, are functionally distinct from M1 macrophages, stimulated with the Th1 cytokine interferon gamma, IFN γ and/or bacterial lipo-polysaccharide (LPS) [48]. M2 macrophages are heterogeneous and include immunologically quiescent cells (M0). In steady state conditions, these phagocytes contribute to maintain self-tolerance and efficient iron recycling through anti-inflammatory circuits that are enforced by lipid ligands of the nuclear receptors families PPAR and LXR [49-51] as well as binding of external phosphatidyl-l-serine to stereospecific receptors [52, 53]. M2 macrophages are also crucial for tissue repair and the resolution phase of inflammatory responses [54].

However, sensing infection through activation of pattern recognition receptors [*e.g.*, Toll-like receptors (TLRs), NOD-like receptors (NLRs), RIG-I-like receptors (RLRs) etc.] activates macrophage microbicidal functions (M1), which are amplified by inflammation and the acute phase response. Notably, M1 macrophages sequester iron by secreting hepcidin, reducing FPN1 expression and increasing the synthesis of H-ferritin [46, 47] (Fig. 1). Both M1 macrophages and hepatocytes secrete H-ferritin; the presence of this acute phase protein has profound immunological consequences because its

receptor TIM-2 acts as a negative regulator of Th2 cytokines [29]. Consistent with macrophage polarization towards iron recycling vs. iron sequestration, all known iron metabolism-related molecules expressed in macrophages are tightly regulated during immune responses [25]. These apparently opposite roles of macrophages in iron metabolism make them key players in host-pathogen interactions.

As most of the iron required for erythropoiesis comes from macrophage erythrophagocytosis, the remaining portion that is necessary to compensate body losses is obtained from diet. Dietary free iron is acquired through the apical membrane of epithelial cells from the small intestine (enterocytes). The duodenal cytochrome-b (Dcytb) [55, 56] and possibly other reductases convert ferric iron into ferrous iron ready to be transported into the cell by DMT1, also described as Nramp2 [28, 57]. Enterocytes are also able to absorb iron from heme molecules using the heme carrier protein-1 (HCP1) through the endocytic pathway. When diet is replete with iron, uptake through DMT1 dominates because HCP1 remains located inside endosomal vesicles, but heme uptake provides an alternative pathway in conditions where iron is scarce [58]. After transit through enterocytes, iron is relocated to the basal membrane and exported through FPN1 [59, 60]. Subsequently iron is oxidized by hephaestin (Hp), and released into the circulation system in the form of transferrin-bound iron (diferric transferrin, Fig. 1).

RBCs, macrophages, enterocytes and hepatocytes play different roles in iron homeostasis but cellular activities are generally subjected to both endogenous regulators and a systemic, integrated control. Eukaryotic cells rapidly and coordinately regulate iron and energy metabolisms by sensing the intracellular free iron status as well as the presence of ROS, reactive nitrogen species (RNS) and/or hypoxia through the use of

labile 4Fe-4S cluster-protein complexes, such as the cytoplasmic aconitase/iron response protein 1 (IRP1) or Fe- and 2-oxoglutarate-dependent dioxygenases [that target hypoxia-inducible factors (HIFs), and IRP2 for degradation). Reduction in available iron stimulates IRP activities which modulate the stability mRNA encoding iron trafficking and storage factors that functions to replenish cellular stores. Hypoxia (mimicking iron deficiency) triggers HIFs activities which reduce the expression of hepcidin in hepatocytes [61] and upregulate iron uptake in enterocytes [62].

Hepatocytes scavenge circulating iron from Tf, heme and ferritin. Most of iron homeostasis proteins, for instance, Tf, haptoglobin and hepcidin are synthesized by hepatocytes [20]. Identification of hepcidin as the key molecule for systemic regulation of iron metabolism was instrumental in understanding the complexity of iron homeostasis [63, 64]. Circulating hepcidin binds specifically to FPN1 on the membrane of cells (e.g. macrophages, enterocytes and hepatocytes) and triggers intracellular degradation of FPN1 that prevents iron exit from cells [65-67]. Hepcidin binding to FPN1 also transduces regulatory signals in macrophages that suppress pro-inflammatory secretions [68]. Liver hepcidin secretion is finely tuned by various sensors of body iron, which include TfR2 and Human hemochromatosis protein (HFE), neogenin, hemojuvelin (HJV) and Bone Morphogenetic Proteins (BMPs) or the growth differentiation factor 15 (GDF15). TfR2, a low affinity receptor, senses Tf saturation (apo/diferric Tf) and depends on the MHC Class I-like molecule HFE to activate hepatocytes' secretion of hepcidin [69]. The bone morphogenic protein BMP6 also contributes to sense systemic iron levels; its binding to hepatocyte BMP receptors is regulated by neogenin and HJV and can lead to mothers against decapentaplegic homolog (SMAD)-dependent activation

of hepcidin antimicrobial peptide (HAMP) gene [70]. In contrast, hepcidin expression is down-regulated by elevated serum levels of GDF15, a member of the transforming growth factor beta (TGF- β) superfamily secreted by erythroid precursors from thalassemia patients [71].

Hepcidin secretion is also regulated in coordination with host immune response to infection. This is not surprising given that this amphipatic peptide is a member of the defensin family of antimicrobial peptides [72]. Host response to infection stimulates the release of hepcidin together with inflammatory cytokines both from hepatocytes and M1 macrophages [46, 47], forming a complex iron immunity network (Fig. 1). Hepcidin secreted by M1 macrophages works in an autocrine fashion to down-regulate FPN1 and ensure iron retention in macrophages [73, 74]; hepcidin localized inside mycobacteria-containing phagosomes showed anti-microbial activity [75]. Circulating IL-6 further stimulates hepcidin expression and release by hepatocytes [76]. In addition to blocking cellular iron efflux, hepcidin also impairs the expression of DMT1 and Dcytb in enterocytes and limits dietary iron uptake [77, 78]. Pro-inflammatory cytokines such as IL-1, TNF- α and IL-6 also upregulate ferritin expression and down-regulate TfR expression in the reticuloendothelial system. IFN- γ and TNF- α also increase NRAMP1 and DMT1 expression [79, 80] and contribute to iron sequestration in M1 macrophages. Increased iron retention in cells causes hypoferremia and eventually sabotages erythropoiesis by handicap of hemoglobin synthesis, a phenomenon alternatively termed anemia of chronic disease or anemia of inflammation [81].

In contrast, anti-inflammatory cytokines, such as IL-4, IL-10 and IL-13 induce the expression of CD163 by M2 macrophages for uptake of hemoglobin/haptoglobin

complex [82] as well as necessary molecular functions to maintain iron flux and homeostasis (e.g., Tf, TfR1, HFE, STEAP3, DMT1, FPN1, IRPs, [46, 47]). Thus, hepatocytes and macrophages are key cells for maintenance of iron homeostasis which perform distinct functions depending on the physiological context, indicating either steady state conditions or immune response to infection and/or inflammation.

Fig. 1

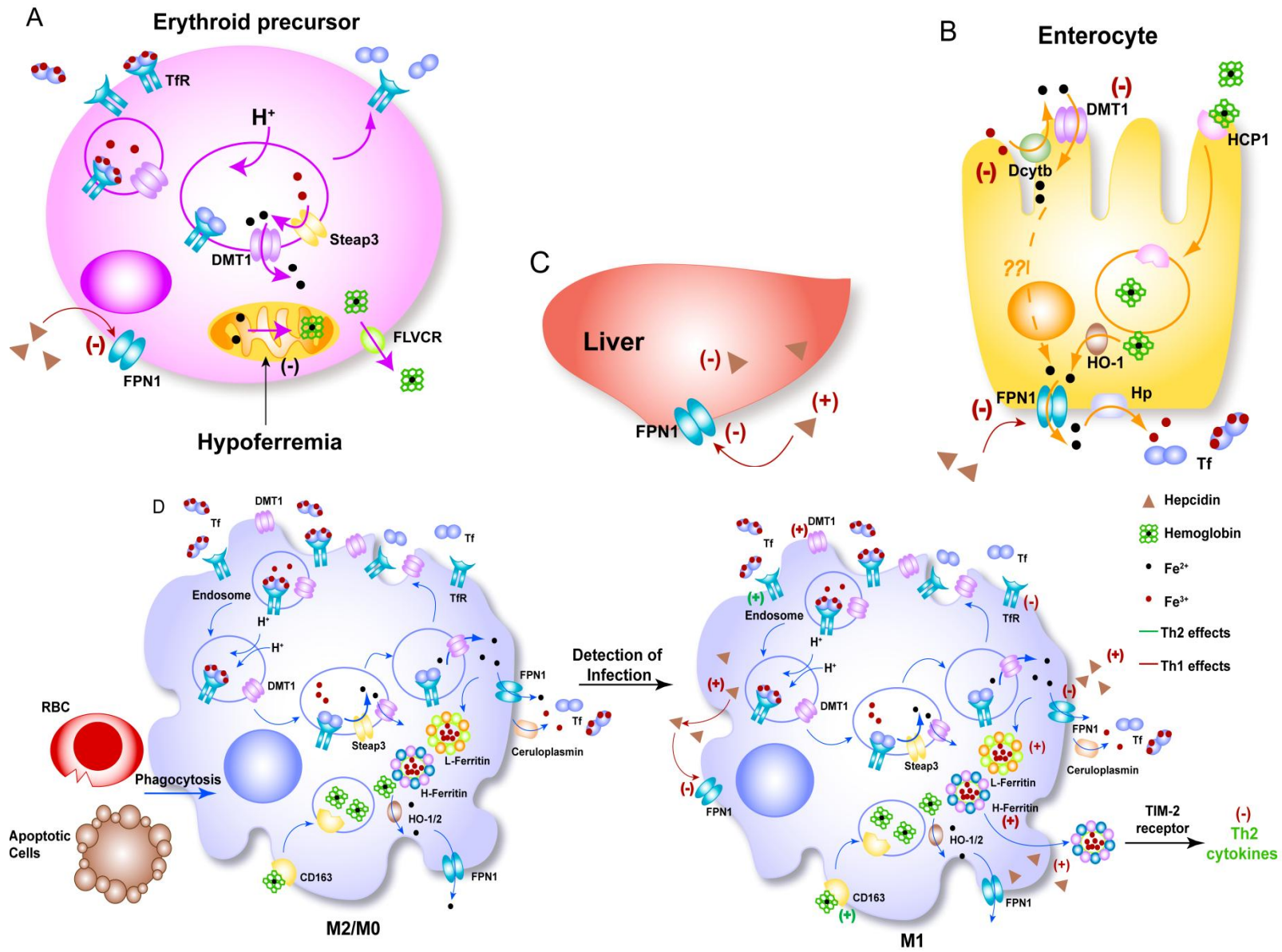


Fig. 1. Mammalian iron metabolism is regulated by innate immunity.

A. Iron homeostasis in erythroid precursors. Bone marrow precursors that generate RBC acquire iron mostly via the Tf-TfR pathway. The highly-expressed Steap3 reduces ferric iron to ferrous iron. DMT1 transports divalent iron out of the endosomes for downstream usage, mostly heme synthesis in mitochondrion. As a protection against heme overload, surface FLVCR can transport excess heme out of erythroid precursors.

B. Iron homeostasis in Enterocytes. Enterocytes mediate dietary iron uptake to upload Tf in the circulation. Ferric iron in the proximal intestinal lumen is first reduced to ferrous iron by the iron reductase Dcytb, and is then transported into enterocytes by DMT1. Heme uptake by surface receptor HCP1 is a backup system for iron acquirement under conditions of iron depletion.

C. Liver constitutes the headquarters for iron metabolism regulation. Most molecules involved in iron metabolism are synthesized in hepatocytes which can acquire iron through multiple pathways. In addition, hepatocytes release hepcidin, the peptide hormone that regulates iron metabolism systemically.

D. Macrophages serve as an iron recycling factory in resting conditions. Senescent RBCs and apoptotic cells are engulfed and degraded by macrophages which become polarized towards M2 phenotype for efficient iron recycling. Iron is released after the heme molecules are oxidized by HO and NRAMP1 may promote iron recycling from the phagosome. Besides, M2 macrophages can also scavenge hemoglobin directly by the surface receptor CD163, and acquire other iron-containing molecules, including Tf, Lf (refer to the text for details). M2 macrophages release iron through the exporter FPN1.

Upon detection of pathogen-associated molecular patterns, macrophages up-regulate M1 functions and secrete hepcidin locally. Hepcidin, together with the inflammatory cytokines released during the immune response form a complex iron immunity network that coordinates host defenses against pathogens. The effects of stimuli that polarize macrophages towards a type 1 (e.g., PAMPs/LPS, IFN γ , TNF α , IL1 and IL6) or type 2 (e.g., IL10 and IL4/13 cytokines) phenotypes are indicated in red and green colors respectively. Their impact on the functions of hepatocytes, enterocytes and erythroblasts. “+” or “-” represents up- or down-regulation respectively. Pro-inflammatory cytokines block body iron cycling by increasing intracellular retention, which reduces Tf saturation in the circulation; they also stimulate microbicidal functions of M1 macrophages. In case the immune response is inefficient, it will lead to tissue damage, hypoferremia and eventually anemia of chronic disease. In contrast, anti-inflammatory cytokines can reverse this trend by promoting iron circulation and tissue repair, and restoring iron and immune homeostasis (refer to text for details).

Iron acquisition by protozoan parasites

As antagonists of host iron homeostasis, pathogens have developed an array of mechanisms to acquire iron and interfere with host regulation of iron metabolism, including carrier, uptake and storage functions. Iron acquisition in pathogens has long been recognized as an expression of virulence [83-85] and iron starvation constitutes a possible avenue for pathogen elimination [86, 87]. Our knowledge about bacterial [84, 88] and fungal [85, 89, 90] iron uptake pathways is better established than that of protozoan parasites. However, utilization of drugs targeting pathogen iron trafficking pathways as a treatment for parasite infection preceded that for bacteria [87]. Artemisinin extracted from plant *Artemisia annua* has been used as anti-malaria drugs in China since 17th century. The working mechanism of artemisinin has not been fully elucidated, but it is known to have multiple targets in the parasite *Plasmodium falciparum* [91]. It is generally accepted that iron, heme and ROS are important in the antimalarial activity of Artemisinin, possibly interrupting ferriheme storage, the final step in the unique *P. falciparum* iron trafficking pathway [87] by inducing rapid and dramatic iron-catalyzed ROS accumulation in plasmodia mitochondria [92]. Iron chelators, such as DFO, salicylaldehyde isonicotinoyl hydrazone (SIH) and deferiprone that actively kills malaria parasites in vitro were selected for further evaluation as a regimen or potential chemotherapeutic adjuvant treatment in human [93, 94].

As previously mentioned, host iron metabolism is closely regulated by cytokines to ensure that iron is sequestered away from pathogens detected by the host. Most, if not all, pathogens interfere with host innate immune system by modulating cytokine production, and potentially creating a micro-environment conducive for iron uptake.

Indeed, protozoan parasites are able to disturb host innate immune responses notably by “confusing” macrophages. A comparative study of macrophage response to the kinetoplastid parasites *Leishmania* spp. and *Trypanosoma cruzi* by Zhang and colleagues [95] indicated that *L. mexicana* infected macrophages show no significant transcriptional response. IL-12 is a key cytokine for the generation of protective immunity to *L. major* infection. It has been reported that IL-12 secreted by M1 macrophages (and/or mature dendritic cells) can activate NK cells and CD8⁺ T cells to drive the development of a Th1 type immune response, including the production of IFN- α [96, 97]. However, *L. major* promastigotes are able to inhibit the macrophage release of IFN- α/β [98]. It seems that the major strategy used by *Leishmania* spp. is impeding the host Th1 immune response, while *T. cruzi* actually induces a delayed activation of IFN response [95, 99] that can be related to the parasite’s unique ability to escape from the parasitophorous vacuole (PV) to the cytosol. Moreover, the transcriptional profile of macrophages infected by *T. cruzi* is closer to the response of macrophages stimulated by cytokine IL-4, IL-10 and IL-17 than M1 macrophages [95]. Different from these two kinetoplastid parasites, *Toxoplasma gondii* is a strong inducer of cell-mediated immunity, and a large amount of proinflammatory cytokine is produced during in vivo infection. However, intracellular infection by *T. gondii* actively down-modulates host proinflammatory signaling pathways potentially by histone modification of inflammatory cytokine genes [100].

It is probable that by interfering with host innate immunity, parasites are able to deregulate iron metabolism and ensure access to iron for their survival. It seems that protozoan parasites are able to obtain different forms of iron depending on their living environment. Protozoan parasites can usually be classified as extracellular or intracellular

pathogens, while some have complicated life cycles involving extracellular and intracellular stages. A summary of common protozoan parasites, their particular parasitic niches, and the iron-containing molecules in those niches is illustrated in table 1. For some parasites listed, however, there is no information available on iron acquisition pathways, and comparing information about the parasites living in a similar niche may reveal some clues to the elucidations for iron uptake.

Table 1. Common protozoan parasites and their parasitic niches in host

Infected organ/ host cell types	Iron containing molecules ^a	Protozoan parasite
Gut/NA	Transferrin, lactoferrin	<i>Giardia, Entamoeba, Isospora, Balantidium</i>
GU tract ^b /NA	Transferrin, lactoferrin	<i>Trichomonas, Trtrichomonas</i>
Bloodstream/ NA	Transferrin, hemoglobin, lactoferrin	<i>Plasmodium, Trypanosoma, Leishmania</i> promastigotes
Liver/ NA	Transferrin, lactoferrin, hemoglobin, ferritin	<i>Entamoeba</i>
CNS ^c / NA	Neuroglobin	<i>Naegleria</i>
Spleen, liver/ Macrophage	Transferrin, ferritin, hemoglobin	<i>Leishmania</i> amastigotes, <i>Toxoplasma gondii</i>
Muscle/ Muscle cells	Myoglobin	<i>Trypanosoma cruzi, T. gondii</i>
CNS/ Astrocyte	Neuroglobin	<i>Trypanosoma, T. gondii</i>

^a All the potential iron-containing molecules in the particular organs are listed. Only some of them were identified to be the iron source for protozoan parasites

^b Genitourinary tract

^c Central nerve system

1. Iron acquisition by extracellular protozoan parasites

One advantage for mammalian bloodstream parasites is that they reside in the largest iron reservoir. Around 70% of the total iron in the host exists in the form of hemoglobin [101]. In addition, 90% of iron recycling from RBCs depends on the endosomal transferrin cycle (Tf-TfR1-Steap3-Dmt1). As a tradeoff for easy access to iron though, bloodstream parasites are under the direct challenge of humoral immunity. *T. brucei*, the parasite causing African trypanosomiasis, stays and multiplies in mammalian bloodstream throughout the whole infection cycle, obtaining iron from host Tf and using surface antigenic variation as primary mechanism of immune evasion. In chronic trypanosomiasis, the parasite can also invade CNS. In contrast, *Plasmodium* sporozoites get into host bloodstream when infected insect vectors, *Anopheles* spp. are taking a blood meal. After their invasion into hepatocytes, *Plasmodium* sporozoites develop into merozoites that are released again into the circulation to invade RBCs. *T. cruzi* and *Leishmania* spp. have also complicated life cycles with intracellular and extracellular stages. They are both injected by insect vectors into host subcutaneous tissues and reach the host cells within which they multiply (muscle cells for *T. cruzi* and macrophages for *Leishmania*). *Entamoeba histolytica* is a strictly extracellular parasitic protozoan that infects humans and other primates. The non-infectious cysts enter the host via contaminated food and water, and undergo maturation and a unique excystation process, in which one single cyst is converted into eight trophozoites that migrate to the large intestine and invade the intestinal mucosa. As the infection develops, the parasites gain access to liver, lung and brain via the blood circulation [24].

Leishmania promastigotes

As early as 1994, Wilson and colleagues demonstrated the acquisition of iron from host transferrin and lactoferrin by *Leishmania* promastigotes, and at the same time, they ruled out the possibility of other iron uptake pathways, such as siderophore-mediated iron chelation and cleavage of host iron-binding proteins [102]. In addition, it was shown that transferrin uptake is delayed relatively to the lactoferrin uptake. The potential explanation given by the authors was that the transferrin acquisition mechanism had to be up-regulated. This study also presented several possible mechanisms for transferrin and lactoferrin uptake. A membrane receptor for transferrin and/or lactoferrin may be involved in the uptake and the inhibition of uptake of lactoferrin or transferrin by each other, suggesting a common receptor or a convergent pathway for uptake, which would be difficult to reconcile with the lag in transferrin uptake. A second line of thought is that a reductase is involved in iron acquisition, a strategy that has been demonstrated in *Cryptococcus neoformans* [103], *Saccharomyces cerevisiae* [104], and *Histoplasma capsulatum* [105]. Those potential uptake pathways were tested in a subsequent paper by the same group. It was found that host lactoferrin and transferrin bind non-specifically to a 70kDa parasite protein (Fig. 2). On the other hand, iron uptake using transferrin and lactoferrin was inhibited by competing ferric reductase activity and enhanced in the presence of a reducing agent like DTT. Therefore, these authors proposed a model for promastigote uptake of iron, in which the reduction of extracellular iron is followed by the transport of ferrous iron through transporter(s). The transporter involved in this process was identified recently by Huynh and colleagues [106] in *Leishmania amazonensis* and *L. major*. This *Leishmania* iron transporter (LIT1) is a membrane protein extensively similar to the ferrous iron transporter from *Arabidopsis thaliana* IRT

(iron regulated transporter), a member of the ZIP (Zrt-, Irt-like proteins) family. In *L. amazonensis*, a GFP-tagged LIT construct is expressed at the plasma membrane and in a perinuclear compartment, likely a megasome.

In contrast to lactoferrin and transferrin uptake, hemoglobin endocytosis by *L. donovani* promastigotes is mediated through a specific protein located in the flagellar pocket [107]. Hemoglobin uptake as an avenue for heme acquisition is secondly relevant since *Leishmania* lacks a complete heme biosynthesis pathway. Electron and immunofluorescence microscopy showed that uptake begins with the binding of hemoglobin in the flagellar pocket, and is followed by internalization in early-endosome-like compartments, and eventual dispersion through the whole parasite cell [108] (Fig. 2).

Trypanosoma brucei

For *T. brucei*, the major source of iron is host transferrin [109]. First, transferrin binds to the flagellar pocket via a hetero-dimeric glycosylphosphatidylinositol-anchored receptor encoded by the genes *ESAG-6* and *ESAG-7* which are expressed in mammalian hosts [109]. Both *ESAG-6* and *ESAG-7* are localized upstream of and are co-transcribed with the gene coding for the parasite variant surface glycoprotein (VSG) in poly-cistronic transcription units [109]. There are several distinct expression sites containing different copies of these genes that encode TbTfR subunits with quite distinct affinities for Tf.

Two hypotheses have been proposed for the advantages of expressing transferrin receptors with different affinities. First, due to its complex life cycle, *T. brucei* may need a repertoire of high affinity transferrin receptors directed toward proteins from different hosts. At any particular time point, the *T. brucei* population in a host expresses transferrin receptors encoded by different expression sites, with one of these being active in the

majority of the population. Despite that the host immune system may kill a large portion of the parasite population; this is also the tactic for the parasites to “fool” the immune system for the selection of the next population to expand. The other theory is that the diversified TfR can ensure the efficient iron uptake during chronic infection when the host immune system generates anti-TbTfR antibodies. It is still under debate what benefit exactly the parasite gains from the multiple and various TfR genes [109-111]. After binding, Tf is internalized through clathrin-coated vesicles to the endocytic pathway for degradation in the parasitic lysosomes [24] (Fig. 2). One cysteine protease is essential for the digestion of Tf [112].

Entamoeba histolytica

Iron availability is critical for anti-oxidative activity in *E. histolytica* since the parasite has iron-type SOD [113], further, iron is an important factor in adherence and cytotoxicity of *E. histolytica* to CHO cell monolayers [114]. The effect of Lf on the amoeba depends on the host iron physiological and dietary conditions. Holo-lactoferrin can specifically bind to two membrane proteins, internalized by caveolin-like protein to endosomal/lysosomal pathway. It is noteworthy that apo-lactoferrin can be used synergistically with human milk IgA and lysozyme as an anti-amoeba drug. It was shown that apo-lactoferrin binds to amoebic phospholipids and cholesterol, which are released before lysis. The same microbicidal effect of apo-lactoferrin was demonstrated in *Giardia lamblia* infection [24].

E. histolytica is an aggressive iron scavenger capable of acquiring iron from almost all host iron-containing molecules. The parasite can spread to multiple organs through the systemic circulation and produce enzymes to rupture host cells. It has been

revealed by electron microscopy that *E. histolytica* trophozoites can ingest both dead and live RBCs [115]. Surface proteins, such as haemolysins and phospholipases [116] can bind and lyse the membrane of RBCs so that released hemoglobin is internalized for degradation. It seems that extracellular parasites, such as *Leishmania* promastigotes and *E. histolytica* have developed a repertoire of surface proteins to bind to host iron-containing molecules. At least two surface proteins from *E. histolytica* can bind to Tf, and one of them might be homologous to human TfR1 since it can be recognized by anti-human TfR1 monoclonal antibody. After binding, Tf is internalized through clathrin-coated vesicles [117], similar to *T. brucei* Tf scavenger pathway. The more astonishing in *E. histolytica* iron mining strategy is that this parasite can lyse enzymatically the hepatocyte membrane and absorb iron directly from host ferritin, which contains 1000-fold more iron than Hb. Ferritin molecules are first bound to the surface protein, followed by cleavage into fragments, and internalization via clathrin-coated vesicles to the lysosomes [24] (Fig. 2).

Tritrichomonas and Trichomonas

Like *E. histolytica*, *Tritrichomonas* spp. can produce adhesive molecules to increase adherence to vaginal epithelial cells [118, 119]. Iron uptake pathways of *Tritrichomonas* spp. show versatile iron utilization by mucosal parasites. In *Tritrichomonas*, the majority of iron is associated with ferridoxin [120] that plays a critical role in glycolysis. The lack of mitochondria makes glycolysis the only energy generating avenue for the parasite. In its unique organelle, the hydrogenosome, carbohydrate metabolism activity is closely correlated with iron availability [121]. Therefore, it is not surprising that *Tritrichomonas* can acquire iron from wide-range

molecules via multiple pathways. Iron from different kinds of siderophores [122] can be used by *T. foetus* through pinocytosis, and siderophore-associated iron is probably released in acidic vesicles in the parasites. Since *T. foetus* can parasitize both the bovine vagina and uterus, it has access to both Lf and Tf [123]. Lf is taken through the endocytosis [124] pathway via a specific-receptor [125], while, Tf is processed by non-specific pathways similar to those discussed in *Leishmania* promastigotes. An acidic environment is built around the parasites to release iron from Tf, followed by reduction of ferric iron and transport of ferrous iron [85, 123]. The *in vitro* uptake of low-molecular weight iron complex occurs in the same manner as Tf acquisition *in vivo* [125] (Fig. 2).

The causative agent of human trichomoniasis, *Trichomonas vaginalis* uses adhesins, such as AP51 and AP65, for double functions as both adhesive molecules and binding proteins to heme and hemoglobin [126]. There are interesting reports about IRE/IRP-like systems in *T. vaginalis* to regulate expression of virulence factors such as adhesion and cysteine proteinase that induce apoptosis of host cells [127, 128], consistent with the ancient origin of the IRE/IRP system in evolution. Further, a lactoferrin-specific binding protein has been reported [129]. Like *E. histolytica*, *T. vaginalis* can also specifically bind to RBC and alternatively use hemoglobin as the iron source [130].

Other extracellular protozoan parasites

The iron uptake pathways identified in extracellular protozoan parasites discussed above are illustrated in Fig. 2. However, our knowledge about iron acquisition pathways used by extracellular parasitic protozoans is still lacking for most species. Although it has been demonstrated that *Giardia* infection results in decreased iron level in patient serum [18], which is probably an outcome from hypoferrremia due to the host

immune response to withhold iron, nothing is known about *Giardia* iron uptake. We don't know how *Naegleria fowleri* acquire iron from the host, while inhibition of the parasite by iron chelators was reported [131]. Iron-type mitochondrial SOD was identified in *Cryptosporidium parvum* [132] and based on a recent report, an ATP half-transporter CpABC4 in the parasite was characterized as iron-sulfur cluster transporter [133]. There is not yet any report on the iron uptake in parasites *Isospora* or *Balantidium*.

Fig. 2

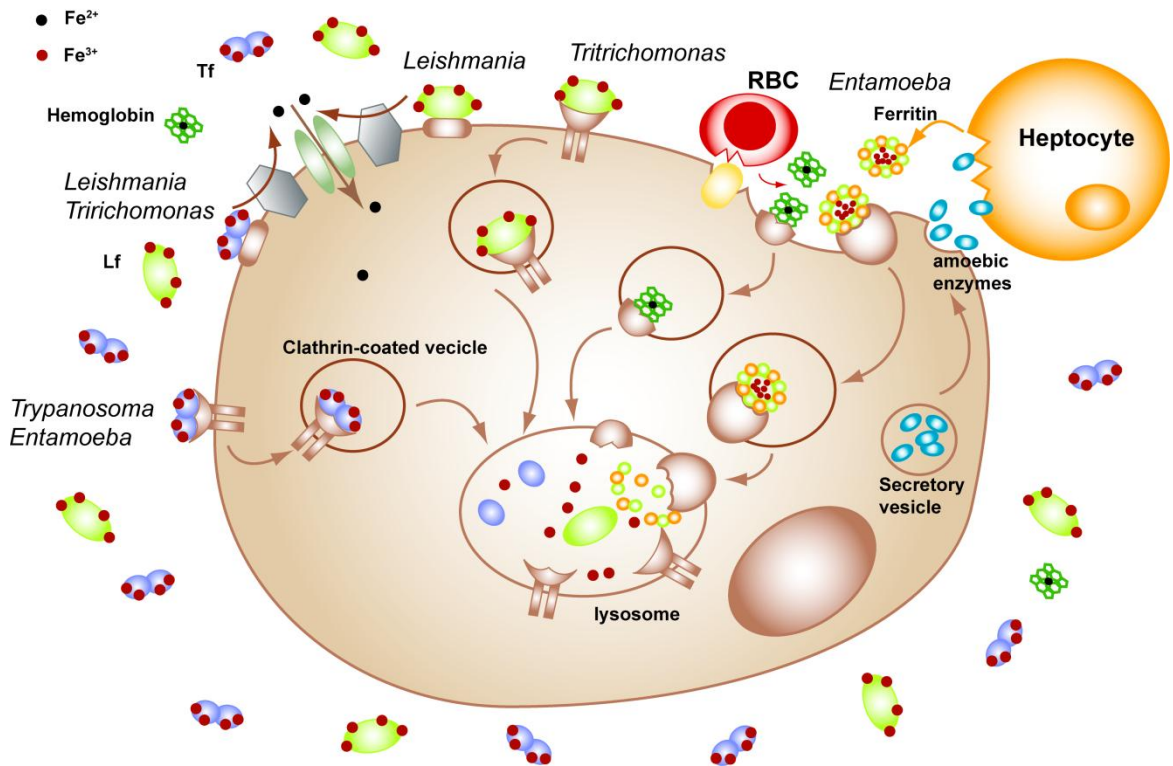


Fig. 2. Summary of iron uptake pathways identified in extracellular protozoan parasites.

Extracellular parasites are surrounded by high concentrations of host iron-associated molecules. Host Tf can be obtained by extracellular parasites following specific- and non-specific binding. Examples of specific-binding of Tf by parasite surface receptors are provided by *Trypanosoma* and *Entamoeba*. The system for non-specific binding and uptake of Tf is generally coupled with a ferric reductase and a ferrous iron transporter. This strategy is shared by *Leishmania* and *Trichomonas*. Host Lf can also be acquired via specific- and non-specific pathways. *Leishmania* expresses non-specific surface protein to capture Lf while *Tritrichomonas* owns Lf-specific receptors. In addition to Tf uptake pathways, *Entamoeba* can also acquire iron from hemoglobin and ferritin. *Entamoeba* has the ability to bind and rupture RBC, or even engulf the whole RBC. *Entamoeba* is also an example of iron acquisition from hepatocyte ferritin by secreting perforing enzymes that destroy the hepatocyte membrane and digesting the liberated ferritin. All receptor-specific binding of host molecules are followed by internalization inside vesicles and degradation in lysosomes. Details can be found in text.

Iron acquisition by intracellular protozoan parasites

As compared to extracellular pathogen varieties, our knowledge about iron acquisition mechanisms in intracellular parasites, with the exception of *Leishmania* amastigotes, is even more limited.

Leishmania amastigotes

The intracellular parasite lifestyle of *Leishmania* amastigotes comprises the same set of iron acquisition pathways as promastigotes [134] that is supplemented to facilitate iron delivery of through the physical and immune barriers inside host cells. Tf has been suggested to be the source of iron for *L. amazonensis* and *L. pifanoi*, because gold-labeled Tf was detected in the parasitophorous vacuole (PV) seven day post-infection [135]. This was unexpected since Tf is delivered through the early endosomal pathway while the PV is formed after late endosomal pathway. To explain the unusual appearance of Tf in the PV, evidence was presented in pulse-chase experiments that the macrophage endosomal pathway is subverted by *Leishmania* infection. Recently, it has been found that in addition to developing ways to acquire host iron from different sources, *Leishmania* parasites deplete the labile iron pool of *Nramp1*^{-/-} macrophages [136]. As mentioned above, upon infection macrophages normally reduce their capacity for iron uptake and increase the expression of the iron storage protein ferritin. But within 12 h after *L. donovani* infection, mouse TfR1 (mTfR1) was up-regulated; similar up-regulation was detected in macrophage treated with DFO. Increased mTfR1 expression was the result of enhanced mRNA stability via the augmented IRE/IRP interaction [136]. Notably, though all the experiments by Das *et al.* (2009) were performed within 24 h after infection, and detection of Tf in PV was carried on day 7 after infection [135], re-routing of transferrin

was observed both at 60 min and 18h post-infection [136]. Combining those results, it may be inferred that depletion of the host cell labile iron pool can benefit the parasite during early stages of infection. Meanwhile, alteration of host endosomal trafficking pathway actually starts as early as the first hour of infection, which sets the stage for gaining iron later in the process as host cells are stimulated to replenish their iron pool.

It remains unclear how the parasite actually depletes the host labile iron pool. Das and colleagues pointed out the possible role of *Leishmania* intracellular iron scavenging pathways and suggested that they may provide new drug targets. But macrophages used in these studies lacked a functional Nramp1, which artificially limited host cell capacity to counter-act *Leishmania* activity and expel iron from PV. Nevertheless, another interesting finding [137] is that a protein from *L. tarentolae* extracts can interact with mammalian IRE. An alternative possibility might thus be that *Leishmania* secrete a protein to perturb directly the host cell IRP/IRE regulatory network, “simulating” iron starvation to upregulate TfR1 and reduce ferritin expression. In any case LIT is another important player for iron acquisition by amastigotes. LIT expression is accelerated under iron depletion conditions, such as expression of host Nramp1, suggesting competition for iron between LIT and host Nramp. LIT knockout has no significant effect on differentiation of promastigotes into amastigotes, but it abolishes amastigote division and the parasite virulence, indicating that LIT has a critical role at the intracellular stage.

Other intracellular protozoan parasites

The exact iron acquisition pathway in malaria parasite *Plasmodium* spp. is still unknown though it is clear that malarial pathogenesis results in delocalization of systemic iron (Nweneka CV et al., 2009). In 1988, it was pointed out that if host Tf is one of the iron

sources for the parasites, it is not delivered via host TfR1 [138]. Detection of ferric transferrin reductase on the plasma membrane of infected RBCs and the expression of parasite-derived TfR in RBC membrane indicated a possible transferrin-dependent iron uptake [139]. Radioactive-labeled transferrin failed to enter the parasites; however, radioactive-labeled low molecular-weight iron-complex can reach both uninfected, infected RBC and the parasites, suggesting a transferrin-independent iron uptake pathway [140]. It would be very surprising that *Plasmodium* embedded in a huge hemoglobin pool cannot exploit this easy iron source. It is known that inhibition of heme synthesis can impair hepatic development of *P. yoelii* [141]. The HOs that catalyze iron release from heme molecules were thought to be absent in the parasites until recently, when such activity was detected for a HO-like protein located in apicoplast [142]. Also, it seems worth noting that plasmodia genomes encode a predicted Nramp homolog,

It is not clear either how *T. gondii* parasites gain access to host iron, although two *Toxoplasma* proteins from endocytic rhoptries were demonstrated to bind human lactoferrin [143]. Further information may be obtained from *T. gondii* intracellular parasitism of placental trophoblasts. The concomitant presence of pregnancy and intracellular infections for which host protection depends on Th1 response is well documented. Immunocompetent individuals resolve *T. gondii* infection by relying on secretions of IFN γ , IL1 β and TNF α , but during pregnancy, anti-inflammatory cytokines such as IL-4, IL-10 and TGF- β dominate to maintain immunological tolerance, together with innate antimicrobials such as defensins [144]. Fetal growth depends on transfer from maternal blood of various nutrients and molecules, including diferric Tf, which proceeds across polarized epithelial cells by receptor-mediated transcytosis [145]. Trophoblasts are

frequently parasitized by *T. gondii*, and in vitro this infection can be controlled by neutralizing endogenous IL-10 and TGF- β and providing IFN- γ [146]. This suggests that this parasite hijacks a vulnerable iron pool within trophoblasts. Besides, *T. gondii* [147] and *Trypanosoma cruzi* [148, 149] can invade muscle cells and CNS, and it was hypothesized that host myoglobin and neuroglobin could protect the parasites from nitrosative stress. The above reports imply that the parasites have access to the particular iron-containing molecules, but whether they use those molecules as iron source needs further investigation.

Fig. 3

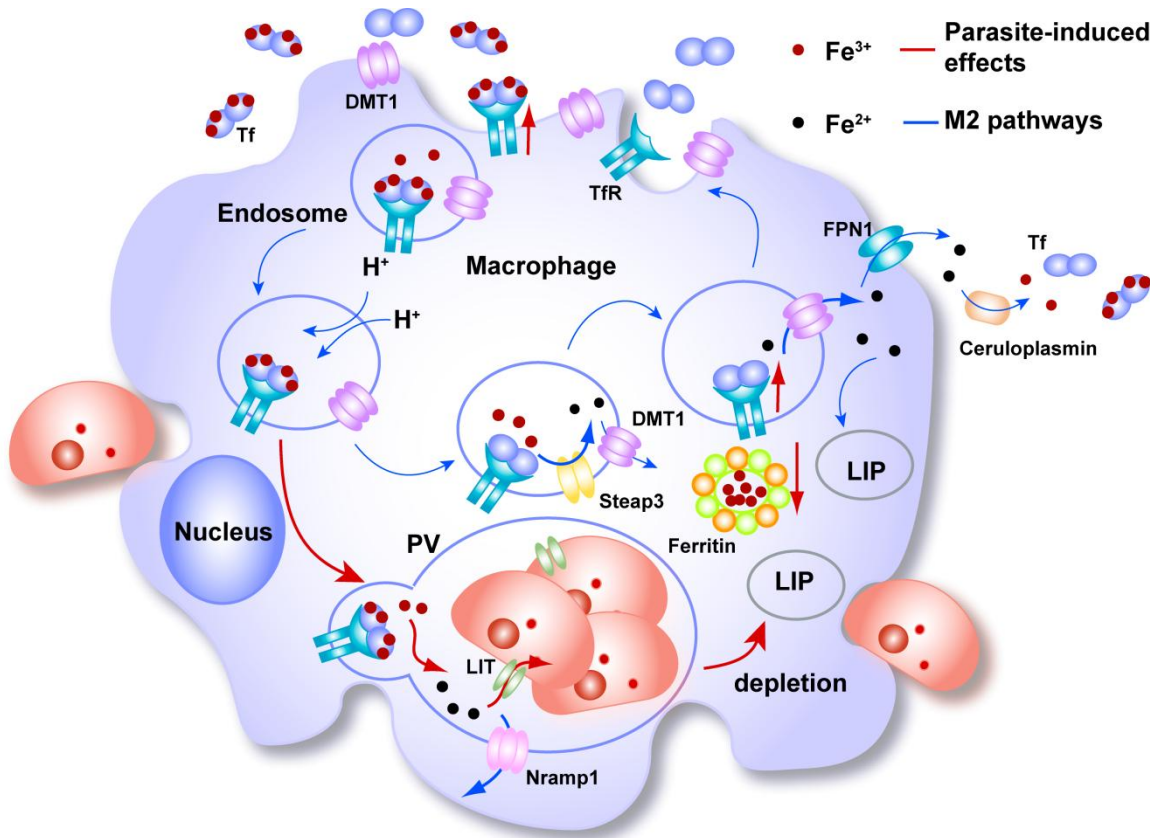


Fig. 3. Summary of iron uptake pathways identified in *Leishmania* amastigotes.

For intracellular parasites (*e.g.* the *Leishmania* spp. amastigote stage), new challenges arise from the host's physical and immune barriers that defend iron store against potential pathogens. The blue arrows indicate the pathways in uninfected or M2 host macrophages, and the red arrows represent steps following the parasite entry. In uninfected host cells, transferrin receptors bind circulating transferrins and are endocytosed. In addition, M2 macrophages phagocytose effete cells and recycle their internal iron. Following acidification of endosomes/phagosomes, ferric iron is released and converted to ferrous iron by Steap3, before being translocated by Nramp2/Dmt1 into the host cytoplasmic LIP, together with iron extracted from heme. Because M2 macrophages express FPN1, the majority of cytoplasmic ferrous iron is exported, oxidized by ceruleoplasmin and then loaded onto Tf while the excess is stored in ferritin in the ferric form. *Leishmania* amastigotes may be able to deplete host cell LIP by mimicking iron starvation that would ultimately down-regulate host ferritin while up-regulating transferrin receptor expression (indicated by red arrows). Increased trafficking of diferric transferrin into the endocytic pathway would facilitate parasite-driven delivery of host iron to PV. As part of host iron recycling machinery and macrophage defense system, Nramp1 is recruited to the membrane of late endosomes/lysosomes and PV to withdraw iron from these compartments. However, parasitic LIT may compete with Nramp1 to secure iron import from the PV lumen into the amastigote parasites.

Identification of Nramp as a marker for resistance to infection

Nramp1 (natural resistance-associated macrophage protein 1) was identified from a survey of inbred mouse strains in a model of *Salmonella typhimurium* infection. Results showed that resistant ($LD_{100} > 10^4 - 10^5$ bacteria) or susceptible ($LD_{100} < 100$ bacteria) phenotypes to *Salmonella* infection were controlled by a single locus (*Ity*) [150]. Similarly, another group showed independently that the replication of *Leishmania donovani* in mouse tissues was either allelic or tightly linked to *Lsh* [151]. More recently, a third locus (*Bcg*) was mapped to the same region of mouse chromosome 1 (*Bcg/Lsh/Ity* locus) [152] in *in vivo* studies of mycobacteria replication [151-154]. In each case the resistant allele that permitted restriction of intracellular replication of the infectious agents was shown to be dominant. By positional cloning the chromosomal region covering the *Bcg/Lsh/Ity* locus was found to encode six candidate genes, and was expressed exclusively in macrophages extracted from spleen and liver [152]. The highly hydrophobic integral trans-membrane protein encoded by this mRNA was reminiscent of a transporter or an ion channel. Later studies rigorously demonstrated that *Nramp1* (*Bcg/Lsh/Ity* gene or Slc11, Solute carrier 11) was involved in host resistance to intracellular infections. Interestingly, it was a single Gly169Asp substitution in predicted TMS4 of the protein that was responsible for the susceptibility trait. These findings spiked the search for Nramp in humans where it was also shown to be associated with resistance to infection with a variety of intracellular pathogens. This studies revealed that Nramp as a promising marker for resistance to intracellular pathogens. Prompted by this possibility, strong interest was generated in searching for this marker in agriculturally

important animal species such as of chickens and cattle, to increase the overall level of genetic resistance by using selective breeding programs [155-157]. Pursuing the same objectives, the *Nramp* gene has also been described in numerous wild and farmed fishes [158-163].

Nramp functions in metal homeostasis

Functional studies revealed that Nramp homologs are proton-dependent divalent metal transporter with a high affinity for Mn^{2+} and Fe^{2+} . Heterologous expression studies of Nramp family members from various organisms have identified several metal substrates, including Cd^{2+} , Cu^{2+} , Co^{2+} [164-166], and even Ca^{2+} [167]. Besides the mammalian Nramp1, the Nramp isotype, Nramp2, or DMT1 was identified and characterized [168]. A mutation (G185R) at the Nramp2 locus causes microcytic anemia and iron deficiency in the *mk* mouse and the Belgrade rat [169, 170], a pathology associated with decreased iron uptake in the duodenum, and impaired iron metabolism in peripheral tissues. Nramp2 is believed to function as the major transferrin-independent iron uptake system at the intestinal brush border, and in the transport of transferrin iron across the membrane of acidified endosomes as part of transferrin cycle [171].

Nramp homologs are ubiquitously present in virtually all taxa. In yeast, the Nramp homologs SMF1 and SMF2 transport Mn^{2+} , but also Cd^{2+} , Cu^{2+} and Co^{2+} at lower rate, while SMF3 is presumed to mostly transport Fe^{2+} [166]. The fruit fly *Nramp* homologue, *malvolio*, is expressed primarily in the brain, and mutations at this locus cause a sensory-neuron defect in taste discrimination. The mutant phenotype can be corrected by dietary Fe^{2+} or Mn^{2+} , and by expression of mammalian *Nramp1* in *malvolio* transgenic flies [172]. The plant Nramp family has been well documented in both

genomic and EST databases, demonstrating that genes from this family are present in virtually all plants studied at the molecular level. Functionally, plant Nramp genes complement yeast mutants deficient in the uptake of several metals, including Fe^{2+} , Mn^{2+} , and Zn^{2+} , suggesting that their function as metal transporters is conserved across various taxa. *Schistosoma mansoni*, an intravascular human parasite with a high nutritional and metabolic demand for iron, has two Nramp homologues (SmDMT1A and SmDMT1B) with different expression patterns and subcellular compartmentalization. SmDMT1 localizes primarily to the tegument, suggesting that the parasite uses this transporter for iron acquisition [173].

Nramp as a potential microbial virulence factor

As mentioned above, iron, and possibly other divalent cations are necessary for the growth of microbial pathogens and parasites; therefore, their metal transporters have been investigated as candidate virulence factors. Manganese was recognized as necessary for virulence in certain bacteria, and one of the reasons is that some bacteria use manganese as their SOD cofactor [174]. The bacterial Nramp homologs MntH (H⁺-dependent Mn transporter) are widespread. Disruption of *MntH* in *Escherichia coli* and *S. typhimurium* does not affect bacterial growth under aerobic conditions in minimal or rich medium, implying that MntH is not essential for growth under normal laboratory conditions [175, 176], and at least one potentially redundant manganese acquisition system (*e.g.* ATP-binding cassette transporter) is present in pathogenic enterobacterial microorganisms [177]. The lack of a strong growth phenotype suggests either that Mn^{2+} is not critical for growth or that other enterobacterial transporters can compensate for the loss of MntH-mediated uptake. However, elimination of the Gram positive *Bacillus*

subtilis mntH gene prevented bacterial growth in Mn-limited medium, implying that bacterial physiology influences *mntH* phenotype [177]. It was demonstrated in *E. coli* that overexpression of *mntH* from a plasmid could restore growth of the temperature sensitive *hflB1* mutant, which requires high intracellular metal concentrations to grow at non-permissive temperatures [177]. In addition, when MntH was overexpressed, *E. coli* cells become more sensitive to Mn^{2+} , Cd^{2+} , Co^{2+} , Fe^{2+} , Ni^{2+} , and Cu^{2+} and direct measurements of radio-label uptake showed that *E. coli* MntH has higher affinity for Mn^{2+} [176]. Likewise, it was confirmed that overexpression of *mntH* renders both *E. coli* and *S. typhimurium* more sensitive to growth inhibition by Mn^{2+} and Cd^{2+} , and that the loss of *mntH* rendered them more sensitive to hydrogen peroxide but not to superoxide. Although bacterial pathogens acquire host iron and other divalent metals via multiple routes, Nramp homologs (MntH) identified in *M. tuberculosis* [178], *M. leprae* [179], and *Salmonella* spp. [175] represent potential virulence factors.

A “tug-of-war” for iron through host and pathogen Nramp homologs

The concept of "nutritional immunity" defines the dynamic interaction between pathogens and hosts, including the competition for essential nutrients such as small organic molecules, amino acid, fatty acids, nucleotides and other co-factors [22]. Hence, the innate resistance to infection by intracellular pathogens is, at least in part, derived from basal metabolic functions, and influenced by genetic factors [21]. An instructive example for nutritive host–pathogen competition is represented by the mutual requirement for iron, manganese, and potentially other divalent cations. One illustrative example is the divalent cation transporter Nramp, which plays roles in both trace metal acquisition and natural defense against intracellular pathogens.

Two different theories have been proposed about how the host Nramp1 functions in defense against intracellular pathogens. One theory implies that Nramp1 might increase intraphagosomal Fe^{2+} , and through the Haber-Weiss/Fenton reaction facilitates the generation of microbicidal reactive oxygen species [180, 181]. The second suggests that Nramp1 deprives the intraphagosomal pathogen of Fe^{2+} and other divalent cations critical for growth and for the pathogen's effective antioxidant defense [182-184].

Accumulating evidence further supports the prime role of Nramp as a first line defense that limits essential metal availability to intracellular pathogens, not only in animal hosts but also in amoeba and plants [185]. In *M. tuberculosis*, it has been suggested that the prokaryotic Nramp homolog (MntH) might be in direct competition with the host Nramp for iron and other divalent cations [178]. A proposed “tug-of-war” for iron between oyster and *P. marinus* Nramp is illustrated in Fig. 4, in which the host Nramp1 mediates efflux of divalent cations (including Fe^{2+} and Mn^{2+}) from inside the phagosome and into the cytoplasm. Acidification of the phagosomal space by vacuolar H^+ /ATPase would provide the proton gradient as the driving force for metal efflux. Deprivation of Mn^{2+} and Fe^{2+} could deplete the parasite of nutritional metals, prevent success of individual survival strategies (virulence factors), and/or disable the pathogen-encoded detoxifying enzymes (SOD, APX, among others). The microbial archetype Nramp homologs likely function by a similar mechanism, both for the acquisition of metals from the environment, and in the competition for the same substrate(s) with their host counterpart(s). This question was raised whether there is a “tug-of-war” for iron between oyster hemocytes and intracellular *P. marinus*. As mentioned before, iron is critical for *P. marinus* growth and prevalence of infection, but no iron uptake pathway has been identified. Exploring

Nramp homologs in *P. marinus* and the functional characterization of the homolog(s) may not only provide a novel avenue for disease intervention, but also shed some light on the Nramp-involved iron metabolism in other intracellular protozoan parasites.

CHAPTER 2 MOLECULAR CHARACTERIZATION OF TWO NOVEL NATURAL RESISTANCE-ASSOCIATED MACROPHAGE PROTEIN ISOTYPES (PMNRAMP2 AND PMNRAMP3) IN *PERKINSUS MARINUS*

SUMMARY

Perkinsus marinus, a pathogenic intracellular protozoan parasite of the eastern oyster, *Crassostrea virginica*, requires iron for proliferation and virulence. In a previous study, a divalent metal transporter (PmNramp1) was described as a potential iron transporter in the parasite. In this chapter, two extra *P. marinus* Nramp homologs designated PmNramp2 and PmNramp3 are described. Among the three PmNramp isotypes, PmNramp2 was similar to PmNramp1 in the aspects of amino acid sequence and exon-intron boundaries. Nucleotide and amino acid sequences analyses indicate that PmNramp2 and PmNramp3 encode predicted membrane proteins of 649 and 559 amino acids respectively. Topology prediction software programs suggest 10 to 12 TMS in both PmNramp2 and PmNramp3. Regular RT-PCR was performed to detect the transcript of the three PmNramp isotypes, and indeed, the three Nramp isotypes are transcribed in cultured *P. marinus* trophozoites. All the PmNramp isotypes have a SL at the 5' ends. The sequence of the SL is highly similar to dinoflagellate SL. Further examination proved the presence of the SL in other genes of the parasite. *P. marinus* heat shock proteins (PmHSP70 and PmHSP90) and antioxidant genes, including superoxide dismutases (PmSOD1 and PmSOD2) and ascorbate peroxidases (PmAPX1 and PmAPX2) are trans-spliced. Iron overload, iron depletion and host serum challenge did not change the transcript level of PmNramp isotypes and tested antioxidant genes as accessed by

quantitative PCR (Q-PCR). Temperature change did not have a significant impact in PmHSP transcription. The identification of SL and the lack of change in transcription suggest a constitutive polycistronic transcription in *P. marinus*.

INTRODUCTION

Once inside the oyster hemocyte, *P. marinus* must acquire from the host trace elements, such as iron, which are essential for pathogen survival. A putative divalent cation membrane transporter that may be responsible for iron uptake is previously identified in *P. marinus* (hereafter designated as PmNramp1) [186], which is the first report about Nramp homologs in alveolates. The cDNA sequence of PmNramp1 was obtained and sequenced. PmNramp1 cDNA turns out to be 2,082 base-pair (bp) long with a CDS for 518 amino acids. Topology prediction implies that PmNramp1 is an integral membrane protein with 12 TMS. Southern blot analysis indicates PmNramp1 exists as a single copy gene in *P. marinus* strain TXsc (ATCC number 50849) [186].

In mammals, two different Nramp isotypes are characterized [162, 168, 169, 187]. While baker yeasts, *Saccharomyces cerevisiae*, has three Nramp homologs [188, 189]. *P. marinus* genome database provides a powerful tool for searching genes of interest. As a continuous study of the identification of PmNramp1, the possibility of other Nramp isotypes in *P. marinus* was explored since Nramp can exist as several different forms in an organism. In this chapter, two new PmNramp isotypes were described in the aspects of gene organization and transcription regulation.

MATERIALS AND METHODS

***Perkinsus marinus* cultures**

The *Perkinsus marinus* strain CB5D4 (ATCC# PRA-240) [190] was propagated in *Perkinsus* standard culture medium [Dulbecco modified Eagle's (DME): Ham's F12 (1:2) with 5% fetal bovine serum (FBS)] at 28 °C [191]. The details about the culture medium composition are listed in table 2.

Genome mining

cDNA and amino acid sequences of *P. marinus* Nramp (PmNramp1) [186] were used as query in the search of potential homologs in the *P. marinus* genomic database (<http://blast.jcvi.org/er-blast/index.cgi?project=pmg>). Two contigs were identified in the TIGR database using BLASTn, or tBLASTn programs in the BLOSUM62 matrix, respectively. The consensus sequences of the contigs were then used in NCBI BLASTx program (www.ncbi.nlm.nih.gov) to confirm their identity as Nramp homologs.

Table 2. The composition of *Perkinsus marinus* culture medium

Chemical name	Final concentration
Dulbecco' modified Eagle's medium (DMEM) (Sigma Aldrich, St. Louis, MO)	5 mg/ml
Ham's F12 nutrients mixture (HAM's F12) (Sigma Aldrich, St. Louis, MO)	10 mg/ml
artificial seawater (Instant Ocean, Mentor, OH)	15 mg/ml
4-(2-hydroxyethyl)-1-piperazineethanesulfonic acid (HEPES)	50 mM
sodium bicarbonate	3.6 mM
penicillin G	100 U/ml
streptomycin sulfate	100 U/ml
fetal bovine serum (FBS)	5%

* Adjust pH to 6.6

Nucleic acid extraction and cDNA cloning and sequencing

Parasite cultures in log phase were harvested by centrifugation for 10 min at 500 g and the pellets were used for either total RNA extraction with the RNeasy Mini Kit (Qiagen, Valencia, CA) or DNA extraction with the QIAamp tissue kit (Qiagen) following the manufacturer's instructions.

Table 3. Primers used for amplifying *Perkinsus* Nramp genes

Primer	Primer sequence	PCR reaction
PmNR1f	5'-TCT TCG CTG TTG GCA TAT TG-3'	RT-PCR of PmNramp1
PmNR1r	5'-TCT ATG GAA GCA GCA CAT CG-3'	
PmNR2f	5'-CGC TAG GCT CGG TTT TGT AA-3'	RT-PCR of PmNramp2
PmNR2r	5'-ATG CAT TGA TGC CGT TCA TA-3'	
PmNR3f	5'-CGC TAG GCT CGG TTT TGT AA-3'	RT-PCR of PmNramp3
PmNR3r	5'-CAC TGC GGA ACC CAA TAC TT-3'	
PmNR2fullcDNAf	5'-ATT ATT ATG TCT ATT GTC GC-3'	Amplification of PmNramp2 full cDNA
PmNR3fullcDNAf	5'-ATG GGG TCG TCC GAA CCA TA-3'	Amplification of PmNramp3 full cDNA

One microgram of *P. marinus* RNA was transcribed into cDNA using GeneRacer Core Kit (Invitrogen, San Diego, CA) according to the manufacturer's protocol; another microgram of total RNA was used to generate first-strand cDNA as reported elsewhere [192]. Based on the partial sequences of the PmNramp homologues obtained from genome mining, gene specific primers (PmNR2f, PmNR2r, PmNR3f, and PmNR3r, Table 2) were designed using the web-based software Primer3 (<http://frodo.wi.mit.edu/>) for RT-PCR. The 5' and 3' ends were subsequently obtained by rapid amplification of cDNA ends (RACE) with the GeneRacer kit (Invitrogen). For 3' RACE, the method described by Borson was also used [192]. The 5' and 3' RACE products were cloned into the pGEM-T vector (Promega, Madison, Wisconsin), and sequenced (3120X/Genetic Analyzer, Applied Biosystems, Carlsbad, California). Finally, to confirm the full-length PmNramp2 and PmNramp3 cDNA sequences, primers were designed to target the predicted 5' UTR (Table 2) to amplify the full cDNA by 3' RACE. Products were cloned and sequenced as above. All PCR reactions were performed using High Fidelity *Taq* DNA polymerase (Takara, Otsu, Shiga, Japan), with the following settings: 94°C /5min, 35 cycles of 94°C/1 min per kbp, 50-60°C/30sec, and 72°C/2-4min.

Identification of trans-splicing leader in other genes

In order to test if other genes in *P. marinus* are trans-spliced, a forward primer was designed based on the 22 nucleotide sequence (SL forward, Table 4) and reverse primers were designed based on the cDNA sequenced of *P. marinus* SOD1, SOD2, APX1, APX2 cDNA sequences [14, 15]. Reverse primers were also designed based on partial cDNA sequences of two potential heat shock proteins, HSP70 (Accession # XM_002774278) and HSP90 (Accession # AY391259) identified in *P. marinus* genome

database (Table 4). RT-PCR using *P. marinus* cDNA as template was performed. PCR product was purified and sequenced to verify that the targeted anti-oxidant genes are actually amplified.

Table 4. Primers used in testing of trans-splicing leader in other genes

Primer	Primer sequence
SL forward	5'-TCC GTA GCC ATC TTG GCT CAA G-3'
SOD1 reverse	5'-CAG CAG CGA TGC TAT TCA AA-3'
SOD2 reverse	5'-GCC TTT CGC ATG AAG TTC TC-3'
APX1 reverse	5'-CGA TAC CCT CCT TTC CAT CA-3'
APX2 reverse	5'-CCT CGC TAC CGT TGG TGT AT-3'
HSP70 reverse	5'- GTTGCTCTTGCCAGTGGACTTA-3'
HSP90 reverse	5'- CAACACGGACCTTGTCAGCA-3'

Challenge experiment design

Perkinsus marinus cells were grown as described above to log phase (optical density at 600 nm = 1.2). Cells were pelleted by centrifugation at 1000 g for 5 min, washed with culture medium (DME-HAM based) to remove FBS and inoculated into culture mediums including fetuin (1.7 mg/ml) as iron supplement to a final cell number around 8×10^6 cell/ml (optical density at 600 nm = 0.64).

Cation overload and depletion conditions were set up in DME-HAM base medium with fetuin as follows: (1) iron overload: FeCl₂ (Sigma) stock solution (25 µg/ml) was added to the medium to reach the final concentration of 100 and 400 µM. (2) manganese overload: MnCl₂ (Sigma) stock solution (1M) was added to the medium to reach the final concentration of 0.3 and 0.8 µM. (3) iron depletion: DFO (Sigma) stock solution (20 mg/ml in *P. marinus* culture medium) was added to the culture medium to the final concentration of 0.01 and 0.08 mg/ml. To study the effect of host factor on the

expression of PmNramp isotypes, over one hundred oysters were ordered from Mook Sea Farm, Inc. (Walpole, ME). All the oysters were notched and hemolymph was withdrawn from the adductor muscle with a 22 G needle and 3 ml syringe and collected in 1.5 ml eppendorf tubes on ice. A piece of oyster tissue was dissected from every oyster for DNA extraction using DNeasy Blood&Tissue Kit (Qiagen) followed by infection check via PCR-based assay [193]. Due to a high infection rate, a limited amount of uninfected oyster sera was available and the final concentration of oyster serum in the culture medium was 5%. All the culture medium was filter sterilized with 0.2 μ m VacuCap 90 (Gelman Sciences, Port Washington, NY) after preparation. To test the transcription regulation of PmHSP70 and PmHSP90, *P. marinus* culture was grown to log-phase (OD=0.6) and split to three groups: one stayed in optimal 28°C, one was put in 4°C and the other one in 37°C for 2 hs.

All the challenge experiments were carried out in duplicates. During the time of experiment, parasite cells were incubated in 75 ml cell culture flask (Corning, Corning, NY) under 28°C. 0.5 ml culture was withdrawn for OD measurement using UV-1601 UV-visible spectrophotometer (Shimadzu, Columbia, MD) at different time points (at $t=0$, 18 hours, 2 days, 4 days, 7 days and 9 days). Meanwhile, 7.5 ml culture was taken from each flask for RNA extraction and eventually Q-PCR.

RNA extraction and reverse transcription

P. marinus cells were pelleted by centrifugation at 1000 g for 5 min. QIAshredder (QIAGEN) was used to homogenize the cells. RNeasy Mini Kit (QIAGEN) was used for RNA extraction from all the samples. Elimination of DNA contamination was achieved by using the RNase-Free DNase Set (QIAGEN). The final concentration of RNA from

each sample was measured by NanoDrop ND-1000 spectrophotometer (NanoDrop Products, Wilmington, DE). One microgram of RNA was used for the synthesis of the first-strand cDNA using RevertAid™ First Strand cDNA Synthesis Kit (Fermentas, Ontario, Canada).

Quantitative PCR

The primers used in QPCR were designed using the free primer design tool OligoPerfect™ Designer from Invitrogen (<http://tools.invitrogen.com/content.cfm?pageid=9716>). All the primers sets (Table 5) used in QPCR were confirmed to have application efficiency from 90% to 110%. All the genes that are known to be trans-spliced, including the three PmNramp isotypes, PmSOD isotypes and PmAPX isotypes were tested for transcriptional change. Partial cDNA sequences of *P. marinus* 18S gene (Accession number ti:1520534126), heat shock protein were obtained from *P. marinus* genome database (http://blast.ncbi.nlm.nih.gov/Blast.cgi?PROGRAM=blastn&BLAST_SPEC=TraceArchive&BLAST_PROGRAMS=megaBlast&PAGE_TYPE=BlastSearch) was also included in the QPCR. All QPCR reactions were performed using Sybr Green PCR master mix (Applied Biosystems) in 7500 Fast Real-Time PCR system (Applied Biosystems), with the following settings: 50 °C /2 min, 95°C /10 min, 40 cycles of 95°C /15 sec, 60 °C/ 1 min.

Table 5 Primers used in quantitative PCR

Target gene	Forward primer	Reverse primer
Pm18S	5'-GCATTTGCCAAGGATGTTTT-3'	5'-AAATTAACGACCCCCAATCC-3'
PmNramp1	5'-TTTGCTGCACGGTATCAGAG-3'	5'-GGCATAATAACTGCGCCAAT-3'
PmNramp2	5'-GGCATTACAGGTTCCAGT-3'	5'-CCTCTACGGCAATTCTCTGC-3'
PmNramp3	5'-CAGCCGCTGATACTTTCACA-3'	5'-GAAGCAAGCGCACATTATCA-3'
PmSOD1	5'-CTGGCAAGCCTTTTAACCAG-3'	5'-CGCTGAACTCCTCCTTGAAC-3'
PmSOD2	5'-GGGGAGAATGTGTTCAATGC-3'	5'-GCCTTTCGCATGAAGTTCTC-3'
PmAPX1	5'-GCCTTCAAAGATCGTTCTGG-3'	5'-CGATACCCTCCTTCCATCA-3'
PmAPX2	5'-GGGCTTCAATGATCAGGAGA-3'	5'-CCTCGTACCGTTGGTGTAT-3'
PmHSP70	5'-GATAACCAGCCTGGTGTGTTGA-3'	5'-GTTGCTCTTGCCAGTGGACTTA-3'
PmHSP90	5'-AGGCCAATGGCACCCCTTACT-3'	5'-CAACACGGACCTTGTCAGCA-3'

RESULTS

Identification of two novel *PmNramp* isoforms

Genome mining of *PmNramp* homologs was performed with bi-direction BLAST. Both *PmNramp1* cDNA and amino acid sequences were used as queries in BLASTn and tBLASTn programs respectively in the *P. marinus* genomic databases (<http://blast.jcvi.org/er-blast/index.cgi?project=pmg>, previous TIGR *Perkinsus marinus* Sequence Database). Two contigs were returned as hits. One contig (No. 21203) came out as hit when *PmNramp1* cDNA sequence was used as query; another different contig (No. 22669) was shown as hit when *PmNramp1* amino acid sequence was used as query. The consensus sequences from the two contigs were then used as queries in NCBI BLASTx program (<http://blast.ncbi.nlm.nih.gov/Blast.cgi>) and both of them turned out to be *Nramp* homologs. Gene specific primers were designed based on the consensus sequences and used in regular RT-PCR. As shown in Fig.4, all the three *PmNramp* isoforms cDNA was amplified by those primers, indicating that all the three *PmNramp* are transcribed in the parasite trophozoites cultured in standard medium.

The full cDNA sequences of the two new *Nramp* genes, hereafter designated *PmNramp2* (GenBank accession No. EU589239) and *PmNramp3* (GenBank accession No. EU836690) were obtained. The first in-frame initiator methionine codon of CDS is located at position 37 of the *PmNramp2* cDNA sequence. *PmNramp2* CDS was 1,947-bp long, encoding a putative protein of 649 amino acid residues with a predicted molecular mass of 70.5 kDa. The *PmNramp3* cDNA was 1,726-bp long with a 1,677 bp CDS. The

putative PmNramp3 protein has 559 amino acids and is predicted to be 60.0 kDa. No canonical polyadenylation signals were identified in *PmNramp2* or *PmNramp3*.

Fig. 4

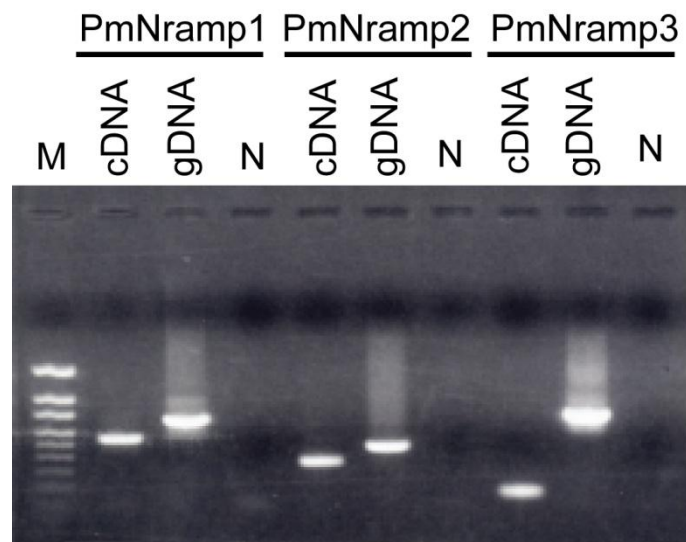


Fig. 4. RT-PCR analysis of PmNramp isotypes in *P. marinus* trophozoites.

cDNA of *P. marinus* trophozoites was used as template in regular RT-PCR. Gene-specific primers used in the RT-PCR are listed in Table 3. cDNA: *P. marinus* cDNA; gDNA: *P. marinus* genomic DNA; N: water as negative control; M: 100-1.5kb DNA marker. 1.2% agarose gel, ethidium bromide, 1X tris-acetate-EDTA.

Gene organization of PmNramp isotypes

Gene structures were compared between the three PmNramp isotypes. Exon-intron boundaries were obtained by alignment of sequences of genomic DNA and cDNA from the three PmNramp isotypes using the commercially-available software Sequencher 4.2.2 (Gene Codes Corporation, Ann Arbor, MI). A side-by-side comparison of gene organization of the three PmNramp isotypes was shown in Fig. 2. PmNramp2 has 7 exons interrupted by 6 introns. Most of the exon/intron boundaries were characterized by the canonical splicing signal (GT/AG) with the exception of GT/GC non-canonical splicing signal in *PmNramp2* intron 3. The translational start codon was within the exon 1 and the termination codon (TGA) was located in exon 7, which has a 3' UTR more than 1 kb-long. PmNramp3 has 14 exons interrupted by 13 introns and the start and stop codons were located in the first and the last exons, respectively. The exon/intron organization of PmNramp2 is similar to PmNramp1, which contained 8 exons, instead of the 7 exons reported in a previous study [186].

Fig. 5

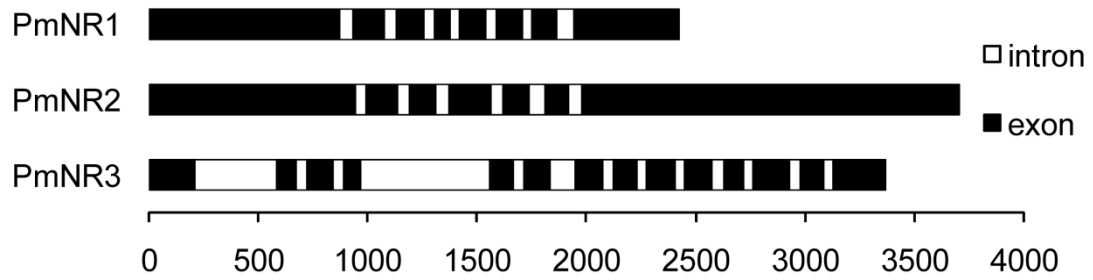


Fig. 5. Gene organization of *PmNramp* homologs.

Comparison of cDNA and gDNA sequences revealed exon-intron structures of the three *PmNramp* isotypes. Exons and introns are indicated by filled or open boxes, respectively. The x-axis indicates size in bp.

Amino acid alignment of PmNramp isotypes with human Nramp2 homolog

A pairwise amino acid sequence alignment (Fig. 6) of PmNramp2 and PmNramp3 with human Nramp2 (GenBank accession No. BAA24933) and PmNramp1 (GenBank accession No. AAQ94879) is shown in fig. 6 and the identity and similarity of the compared Nramp homologs are summarized in table 6. It seems that PmNramp1 and PmNramp2 display the highest identity in protein sequences (51%). Despite the low identity and similarity, conserved domains can be seen from the alignment (Fig. 6). In addition, PmNramp1 and PmNramp2 share most of the same exon boundaries in the amino acid sequence as indicated by numbered arrows (Fig. 6).

Table 6 Identity and similarity of PmNramp isotypes

Identify (Similarity)	PmNramp2	PmNramp3	HsNramp2
PmNramp1	51% (67%)	47% (63%)	35% (51%)
PmNramp2		40% (56%)	30% (47%)
PmNramp3			33% (50%)

Fig. 6

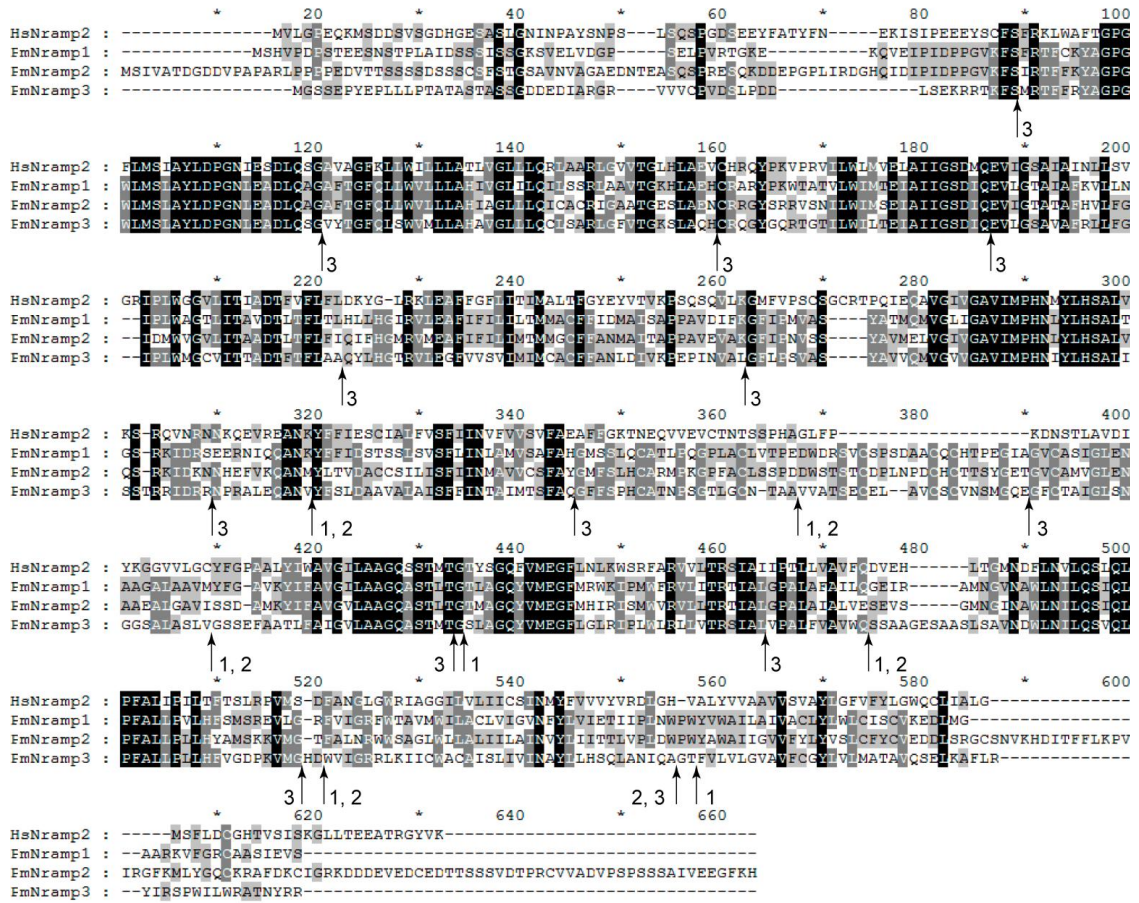


Fig. 6. Multiple alignment of deduced amino acid sequences of PmNramp1, PmNramp2 and PmNramp3 with human Nramp2 (HsNramp2).

Amino acid sequences of PmNramp isotypes were aligned using Mega 4.0 [194, 195] and displayed with GeneDoc [196]. Identical residues were highlighted at three cutoffs (50, 75 and 100 %). Arrows represent the exon boundaries in the protein sequence with the number indicating corresponding PmNramp isotype number.

PmNramp mRNA is trans-spliced with trans-splicing leader highly identical to dinoflagellate splice leader

Analysis of the 5' cDNA sequences of *PmNramp2* and *PmNramp3* revealed a 20 nt stretch that was absent in *PmNramp2* and *PmNramp3* genomic vicinities (Fig. 7A). Reexamination of the 5' sequence of *PmNramp1* [186] revealed the same feature (Fig. 7A). This stretch of nucleic acid sequence has a good but not perfect match is displayed with the SL sequence from dinoflagellates (Fig. 7B). All mRNA of the three *P. marinus* Nramp genes are trans-spliced with a conserved SL.

Comparison of genomic DNA and cDNA of *PmNramp* isotypes revealed that at the junction between SL sequence and the 5' UTR of *PmNramp*, the genomic DNA sequence bears a dinucleotide AG (Fig. 7B) consistent with the common canonical cis- and trans-splicing acceptor boundary, apparently serving as the acceptor site of SL [197]. In dinoflagellate, a conserved "CGTGTGC" sequence was identified immediately upstream of the 3' acceptor splice site AG of analyzed genes [198]. However, no such conserved sequence was found in any of the three *PmNramp* isotypes. Interestingly, some SL sequences from both *PmNramp2* and *PmNramp3* isotypes carry a thymidine deletion at the same position (Fig. 7A).

Fig. 7

A.

```

                *      20      *      40
PmNR1cDNA : ACCGTAGCCATCTTGGCTCAAGATTGTTAGTCCTAGTAGAATG : 43
PmNR1gDNA : ttcatgctttcataaactttagattgtagtcctagtagaatg : 43

                *      20      *
PmNR2cDNA : TCCGTAGCCATCTTGGCTCAAGGAAGTATTATTATTATG : 39
PmNR2gDNA : gcttagttacgtttgcttttaggaagtattattattatg : 39

                *      20      *      40
PmNR3cDNA : ACCGTAGCCATCTTGGCTCAAGGGTTTTTAATATTTGTCACCATCGATG : 49
PmNR3gDNA : cccccgacttgagatgtggcagggtttttaaatattttgacccatcgatg : 49

```

B.

```

                *      20      *      40      *      60      *
dino       : DCCGTAGCCATCTTGGCTCAAG----- : 22
PmNR1-SL   : ACCGTAGCCATCTTGGCTCAAGATTGTTAGTCCTAGTAGAATGTCACACGTCCCGATCCGTCTACGGAGG : 71
PmNR2-SL1  : TCCGTAGCCATCTTGGCTCAAGGAAGTATTATTATTATGTCTATGTCCGGACCGATGGTGTATGATGTCCC : 70
PmNR2-SL2  : TCCGTAGCCATCTTGGCTCAAGGAAGTATTATTATTATGTCTATGTCCGGACCGATGGTGTATGATGTCCC : 71
PmNR3-SL1  : TCCGTAGCCATCTTGGCTCAAGGGTTTTTAATATTTGTCACCATCGATGGGGTGTCCGAACCATACGAGC : 71
PmNR3-SL2  : ACCGTAGCCATCTTGGCTCAAGGGTTTTTAATATTTGTCACCATCGATGGGGTGTCCGAACCATACGAGC : 71
PmNR3-SL3  : TCCGTAGCCATCTTGGCTCAAGGGTTTTTAATATTTGTCACCATCGATGGGGTGTCCGAACCATACGAGC : 70

```

Fig. 7. The conserved SL sequence from *P. marinus* Nramp mRNAs.

A. alignment of the 5'UTRs of *P. marinus* Nramp cDNAs and corresponding gDNA sequence revealed the 22-nt SL marked by box. The canonical splicing acceptor sites AG and the translation starting sites ATG were also highlighted. B. Alignment of the 5' end of *PmNramp* isotype cDNA. The consensus SL sequence from dinoflagellates is compared with that from *P. marinus*. dino: dinoflagellate consensus SL (D = T, A or G); The 22-nt SL sequence is highlighted by a square box. PmNR1-SL: all the SL sequences from three independent clones of *PmNramp1* show the same sequence; PmNR2-SL1 and PmNR2-SL2: two different SL sequences with a deletion in one of them were obtained from three independent clones; PmNR3-SL1, PmNR3-SL2 and PmNR2-SL3: three SL sequences with either deletion or nucleotide substitution were identified in 5' ends of *PmNramp3* mRNA.

Other genes in *P. marinus* are trans-spliced

RT-PCR using forward primer designed based on SL sequence and reverse primer based on cDNA sequences of *P. marinus* SOD1, SOD2, APX1, APX2, HSP70 and HSP90 generated amplification product that was subsequently sequenced. Sequencing result indicates that all the four genes in *P. marinus* antioxidant pathway, and two of the heat shock proteins, HSP70 and HSP90, are trans-spliced with the same SL as in PmNramp genes. Alignment of 5' end sequences is shown in Fig. 8.

Fig. 8

```

                *           20           *           40           *           60
DINO           : DCCGTAGCCATTTGGCTCAAG----- : 22
FmSOD1_SL     : TCCGTAGCCATCTTGGCTCAAGTAGTTTATTGTTCAATAAGTTGATATGTTATCCGTCTG : 60
FmSOD2_SL     : TCCGTAGCCATCTTGGCTCAAGTTGGGTTGCTATGCGGGCTCTCTGGCTCTGATGGAAGGC : 60
FmAPX1_SL     : TCCGTAGCCATCTTGGCTCAAGTTTGTTCGCGCCTCAATATGGTACAGAGTGATCCCAAG : 60
FmAPX2_SL     : TCCGTAGCCATCTTGGCTCAAGTTGTATTTCGAGTCGTCTTCAYCCATGGGAAACATCT : 60
FmHSP70_SL    : TCCGTAGCCATCTTGGCTCAAGTACTTCCAGTCCCTAGTATTGCCCTAACCCGGCAGCC : 60
FmHSP90_SL    : TCCGTAGCCATCTTGGCTCAAGTCAAACACAATCTATCAAATACACTATGTCTTCTCT : 60
```

Fig. 8. The conserved SL sequence from other genes in *P. marinus*

5' end of *P. marinus* SOD1, SOD2, APX1, APX2, HSP70 and HSP90 cDNA are aligned with dinoflagellate SL sequence. The black box indicates the SL identified in mRNA of those genes.

Trans-spliced *P. marinus* genes show no obvious transcriptional regulation

Transcriptional regulation of PmNramp isotypes and *P. marinus* anti-oxidant genes were investigated under several conditions, including iron overload, manganese overload, iron depletion, and oyster serum challenge. Transcription regulation of PmHSP70 and PmHSP90 were tested under drastic temperature change. There was no obvious change in the transcript level for all the tested genes despite the affected *P. marinus* growth under the treatments (Fig. 9 to 17).

P. marinus growth shows no significant difference when the iron concentration is as high as 60 times (400 μM Fe) of the standard medium (Fig.9), implying the parasite's capability to adapt to a high-iron environment. A 15-time manganese overload (0.3 μM Mn) shows no significant impact on *P. marinus* growth while a 500-time overload (10 μM Mn) shows approximately 15% inhibition in cell multiplication. Iron depletion caused by 0.01 and 0.08 mg/ml DFO result in a 5% and 12% decrease in growth respectively. A 10% reduction in cell growth was induced by 5% oyster serum in the medium. For all the tested conditions, the change in Ct value under the challenging conditions did not significantly exceed the change in the control group (standard medium with no supplements) during the time window of the study. In addition, all the PmNramp isotypes and PmSODs transcript gave a highly similar Ct value; while the two PmAPX isotypes shared a similar transcriptional level as indicated by the similar Ct value. The first-strand cDNA with 10-time dilution was used to test the expression of 18S rRNA gene, and it shows the slightest change among all the test genes during the study. In order to confirm that the lack of change in transcription indicated by QPCR is not an artifact, *P. marinus* heat shock protein HSP70 and HSP90 transcript were tested when the

temperature was changed to 4°C and 37°C for 2 h. There is not significant change in Ct values (Fig. 17) despite the possible of HSP protein expression regulation [199]. The examination of 5' cDNA sequences of HSP70 and HSP90 revealed the presence of trans-splicing leader shown in Fig. 9. The lack of transcription regulation by QPCR reflects the probability of constitutive polycistronic transcription suggested by the trans-splicing of those genes. Since there was no significant change in Ct values, all the Ct values presented from Fig. 9 to Fig. 17 are raw data without normalization.

Fig. 9

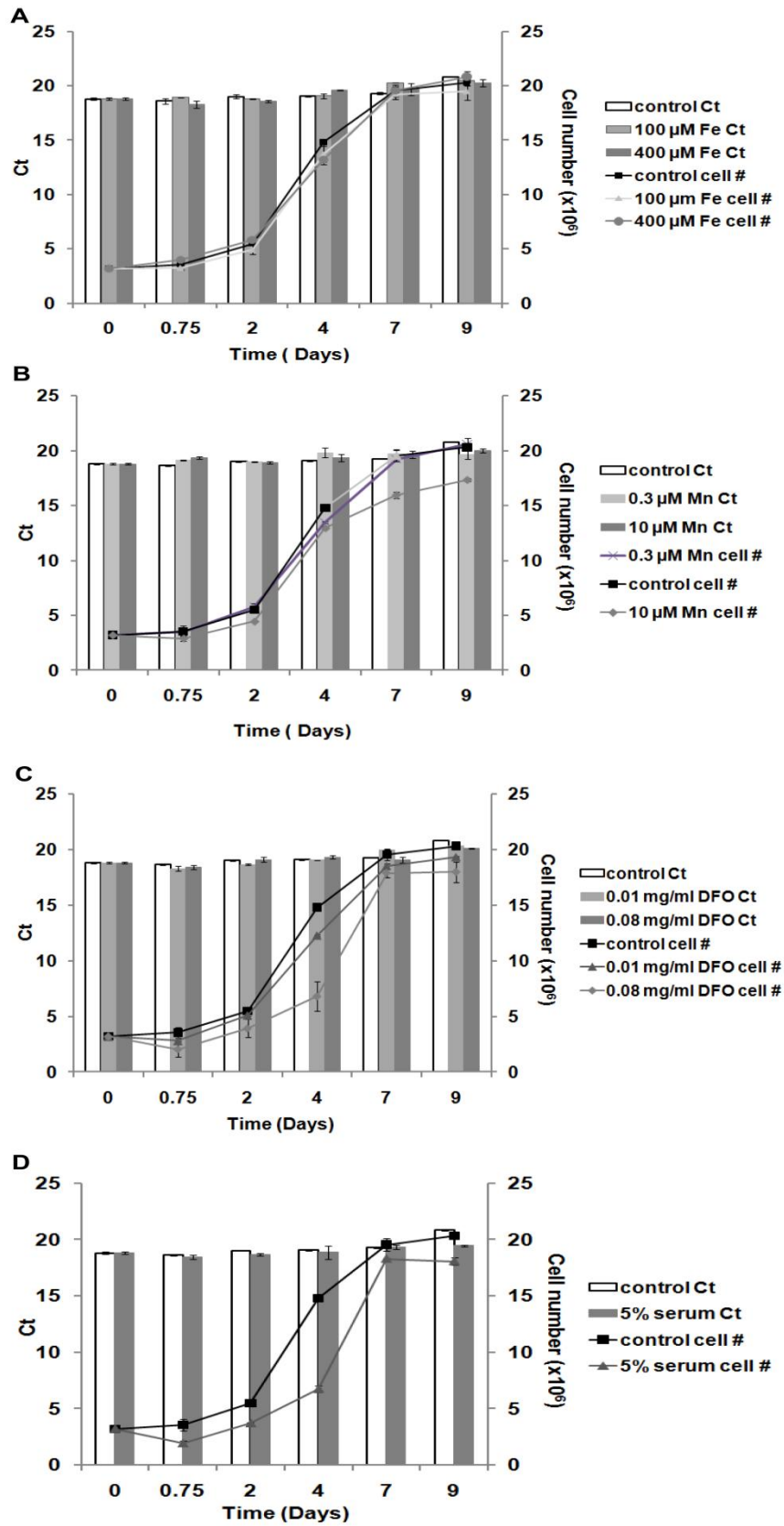


Fig. 9. Expression of PmNramp1 upon different treatments.

Ct values obtained by QPCR are indicated in colons and the growth of *P. marinus* (cell number) is indicated by lines. A. iron overload (100 and 400 μ M). B. manganese overload (0.3 and 10 μ M). C. iron depletion by DFO (0.01 and 0.08 mg/ml). D. oyster serum challenge (5%).

Fig. 10

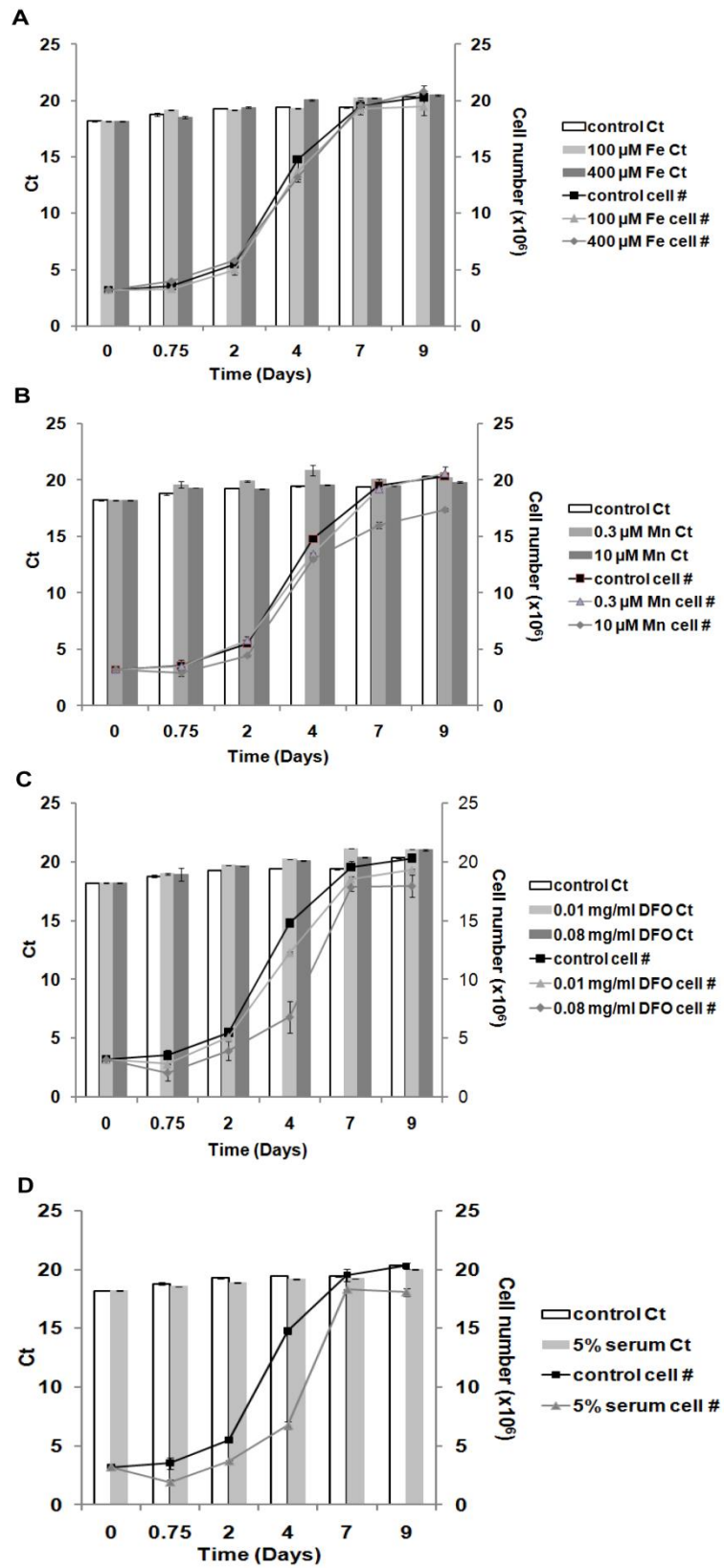


Fig. 10. Expression of PmNramp2 upon different treatments.

Ct values obtained by QPCR are indicated in colons and the growth of *P. marinus* (cell number) is indicated by lines. A. iron overload (100 and 400 μ M). B. manganese overload (0.3 and 10 μ M). C. iron depletion by DFO (0.01 and 0.08 mg/ml). D. oyster serum challenge (5%).

Fig. 11

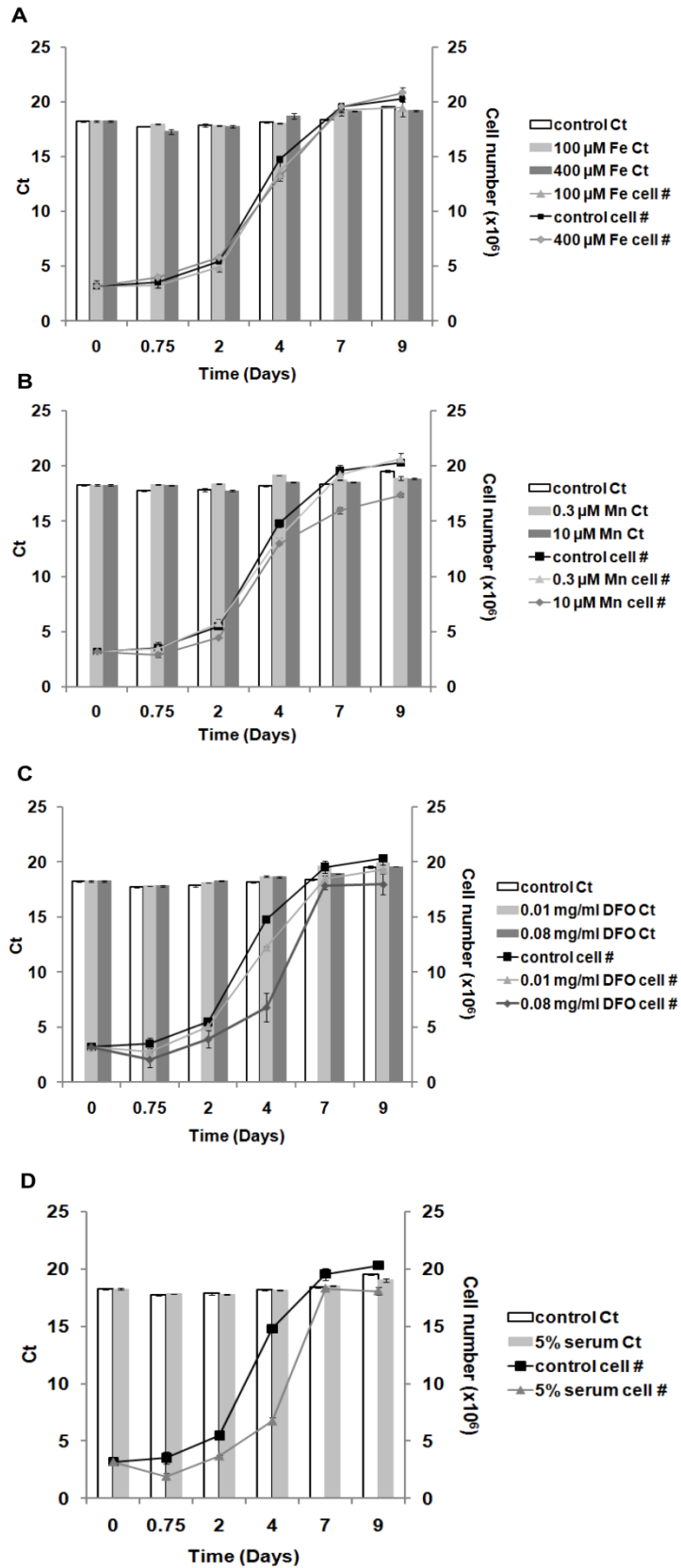


Fig. 11. Expression of PmNramp3 upon different treatments.

Ct values obtained by QPCR are indicated in colons and the growth of *P. marinus* (cell number) is indicated by lines. A. iron overload (100 and 400 μ M). B. manganese overload (0.3 and 10 μ M). C. iron depletion by DFO (0.01 and 0.08 mg/ml). D. oyster serum challenge (5%).

Fig. 12

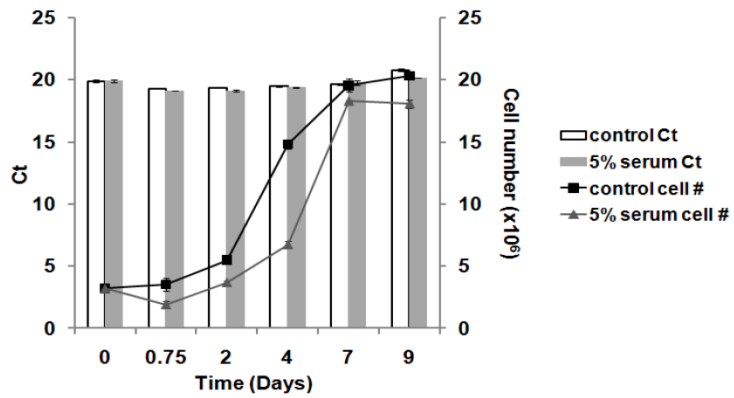
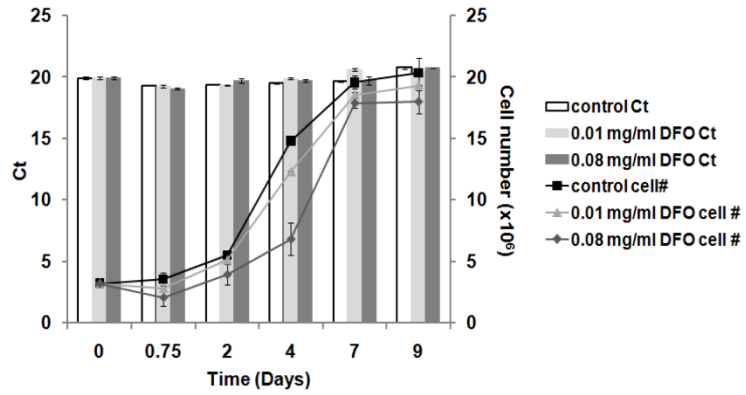
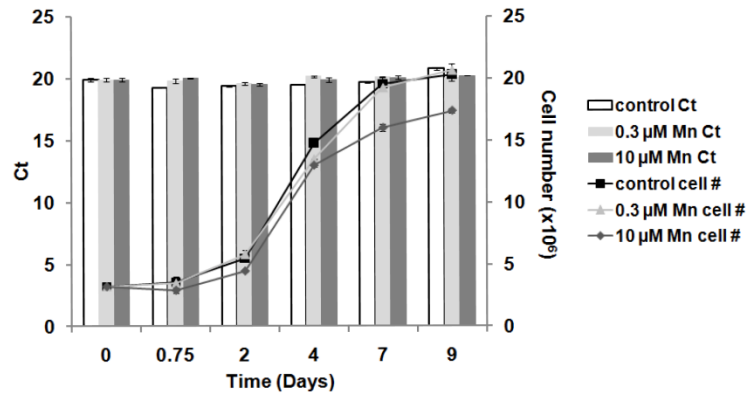
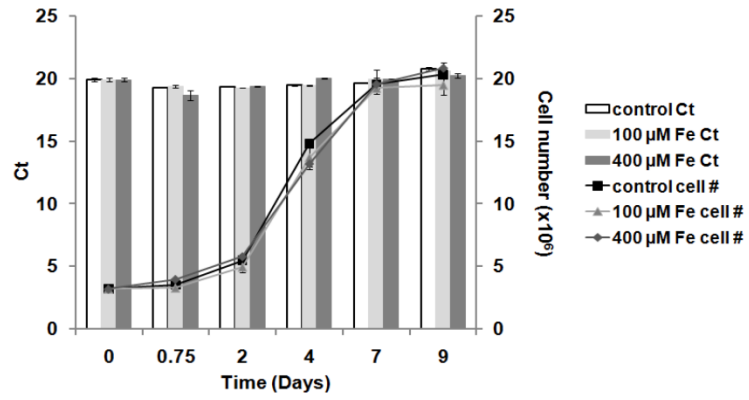


Fig. 12. Expression of PmSOD1 upon different treatments.

Ct values obtained by QPCR are indicated in colons and the growth of *P. marinus* (cell number) is indicated by lines. A. iron overload (100 and 400 μM). B. manganese overload (0.3 and 10 μM). C. iron depletion by DFO (0.01 and 0.08 mg/ml). D. oyster serum challenge (5%).

Fig. 13

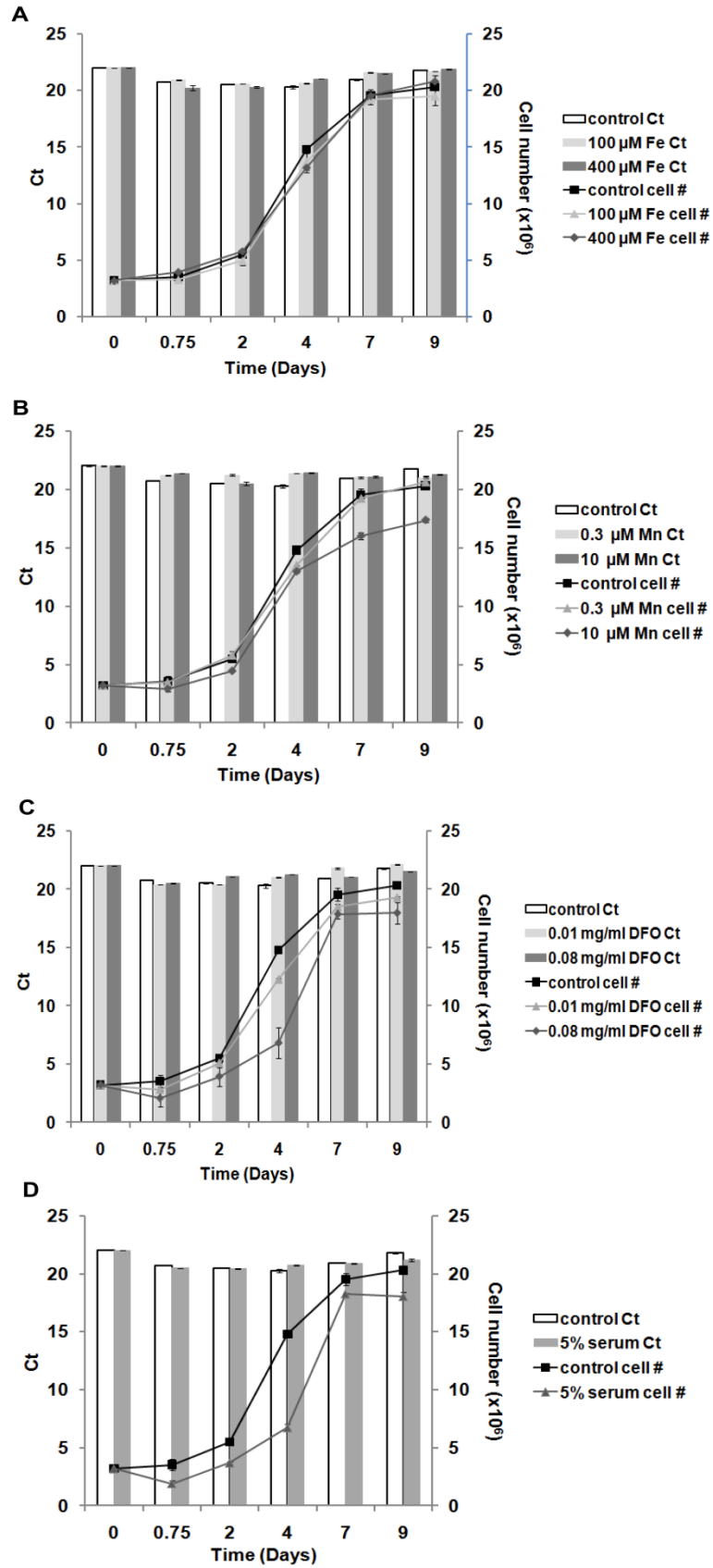


Fig. 13. Expression of PmSOD2 upon different treatments.

Ct values obtained by QPCR are indicated in colons and the growth of *P. marinus* (cell number) is indicated by lines. A. iron overload (100 and 400 μ M). B. manganese overload (0.3 and 10 μ M). C. iron depletion by DFO (0.01 and 0.08 mg/ml). D. oyster serum challenge (5%).

Fig. 14

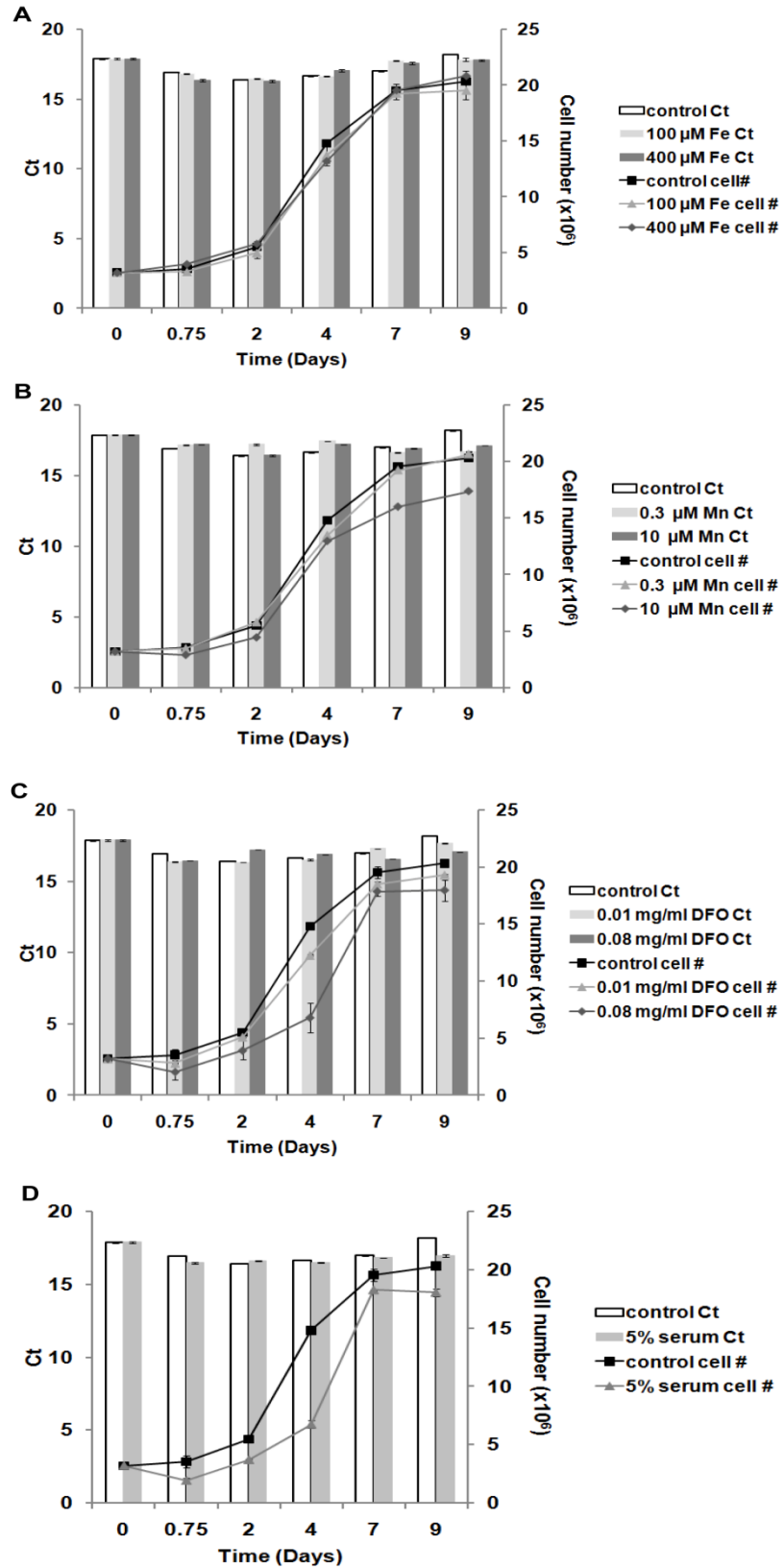


Fig. 14. Expression of PmAPX1 upon different treatments.

Ct values obtained by QPCR are indicated in colons and the growth of *P. marinus* (cell number) is indicated by lines. A. iron overload (100 and 400 μ M). B. manganese overload (0.3 and 10 μ M). C. iron depletion by DFO (0.01 and 0.08 mg/ml). D. oyster serum challenge (5%).

Fig. 15

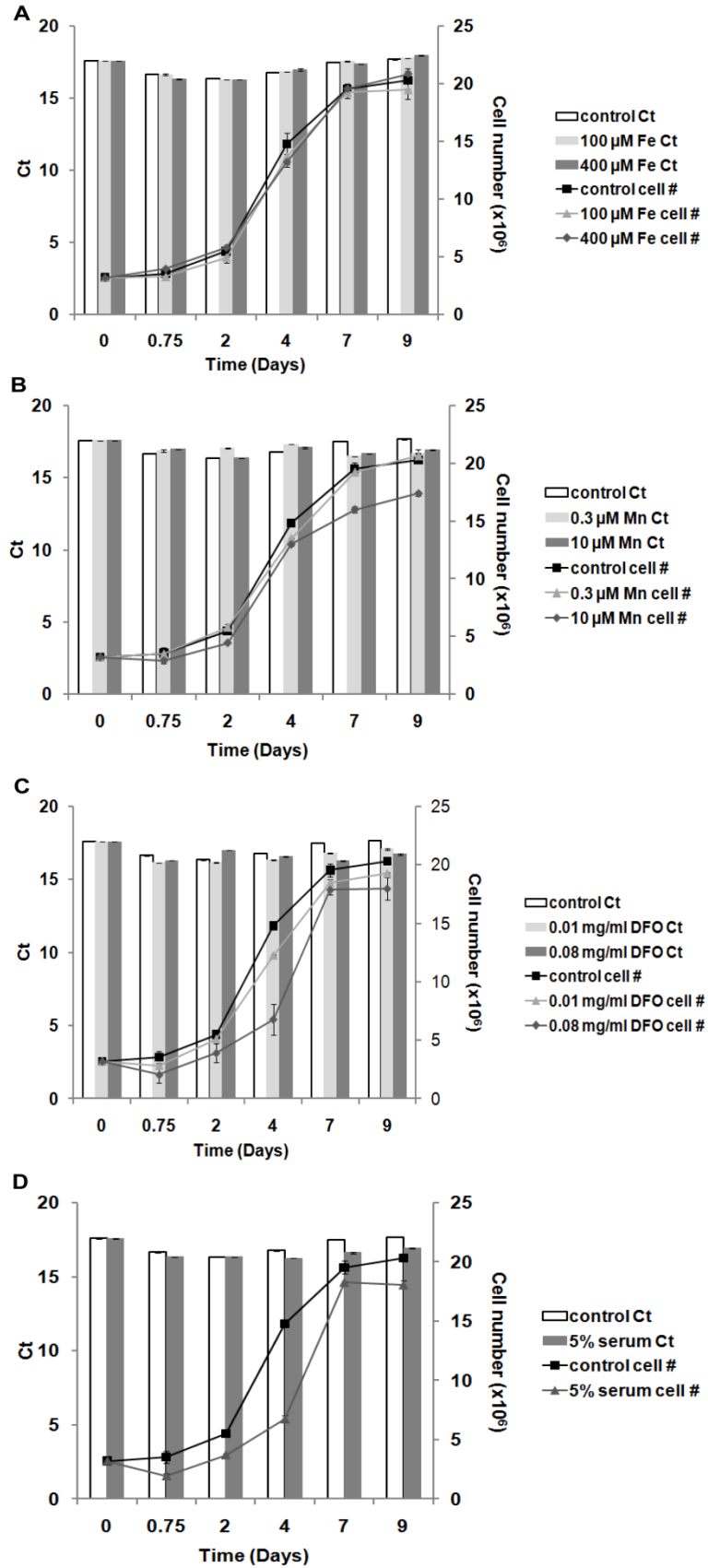


Fig. 15. Expression of PmAPX2 upon different treatments.

Ct values obtained by QPCR are indicated in colons and the growth of *P. marinus* (cell number) is indicated by lines. A. iron overload (100 and 400 μ M). B. manganese overload (0.3 and 10 μ M). C. iron depletion by DFO (0.01 and 0.08 mg/ml). D. oyster serum challenge (5%).

Fig. 16

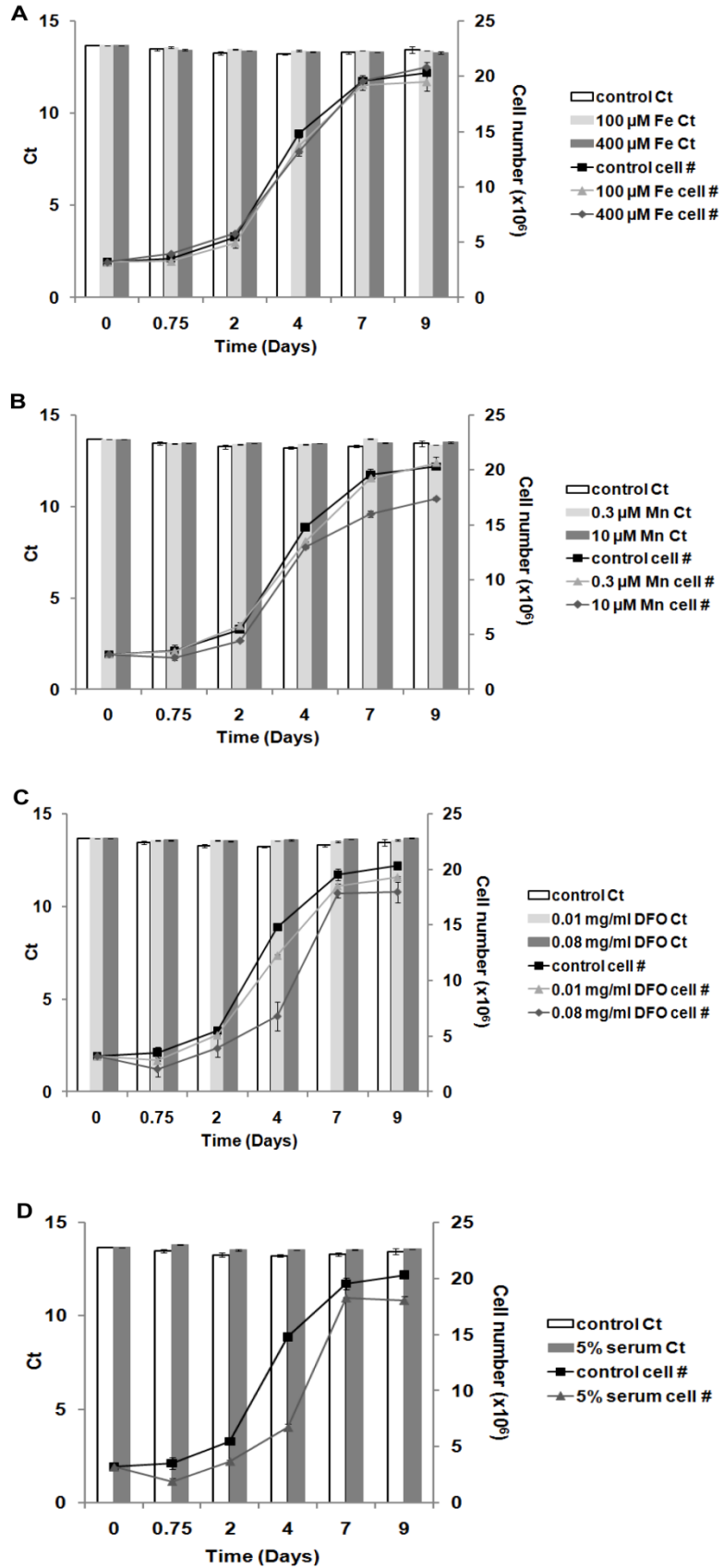
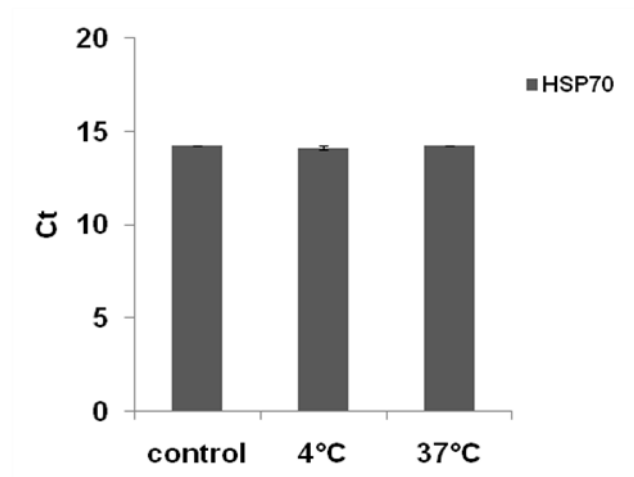


Fig. 16. Expression of Pm18S upon different treatments.

Ct values obtained by QPCR are indicated in colons and the growth of *P. marinus* (cell number) is indicated by lines. A. iron overload (100 and 400 μM). B. manganese overload (0.3 and 10 μM). C. iron depletion by DFO (0.01 and 0.08 mg/ml). D. oyster serum challenge (5%).

Fig. 17

A



B

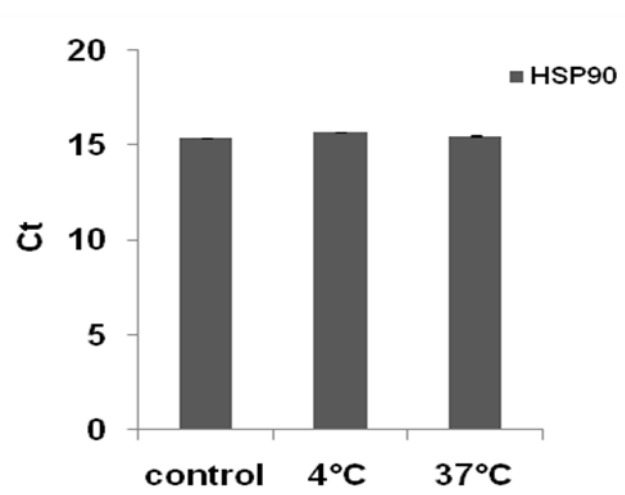


Fig. 17. Expression of PmHSP70 and PmHSP90 transcript upon temperature changes.

Lon-phase *P. marinus* trophozoites were incubated in three different temperatures. After two-hour incubation, cells were harvested for QPCR analysis. Ct values are presented in colons.

DISCUSSION

Research work on Nramp was incipiently focused on host homologs mostly because Nramp was first identified in mammals as resistance marker [152-154]. After that, Nramp homologs were characterized in other animals, plants [156, 159], protozoans [186], and bacteria [176, 200], almost all the taxonomic groups. Therefore, Nramp has been considered as a molecule that involves in host-pathogen interaction. The number of Nramp isotypes varies substantially from organism to organism as mentioned in introduction. With regards to protozoan parasites, a single putative Nramp archetype was annotated in the genome databases of *Plasmodium* spp. (<http://plasmodb.org/plasmo/>), *T. gondii* (<http://toxodb.org/toxo/>), and *Neospora caninum* (<http://toxodb.org/toxo/>, Gene ID NCLIV_038890), respectively. PmNramp1 was the first characterized Nramp homolog in protozoan parasites. It was considered as a single copy gene in the oyster parasite *P. marinus* based on the Southern blot analysis [186]. In order to answer the question whether there are more Nramp isotypes in the parasite, genome mining was performed in the *P. marinus* genome database (<http://www.tigr.org/tdb/e2k1/pmg/>). Two contigs containing partial Nramp homolog were fished out by BLAST using cDNA and amino acid sequences respectively. RT-PCR result shows the expression of the three PmNramp isotypes, indicating potentially critical functions of these genes in parasite metal metabolism during this particular life stage.

Analysis of the full cDNA sequences reveals the presence of the predicted SL in all *PmNramp* cDNAs. The same SL was found in the 5' end of cDNA of *P. marinus* antioxidant pathway, such as SOD1, SOD2 [14, 15], APX1, and APX2 (unpublished data). Trans-splicing has been detected in nematodes, platyhelminths, cnidarians, rotifers,

ascidians, appendicularians, and dinoflagellates [197, 198, 201, 202]. This process makes it possible to translate polycistronically transcribed nuclear genes. A recent thorough investigation of transcript and genomic arrangement of the SL RNA in phylogenetically and ecologically diverse dinoflagellates from four different orders reveals that the majority of dinoflagellate SL RNA transcripts are 56-59 nt although the size of SL RNA can range from 42 to 92 nt. The SL RNA genes are organized in both single gene tandem repeats and in mixed SL RNA-5S rRNA arrangements. The highly complex and diversified genomic arrangements of SL RNA gene in dinoflagellates is the result of genomic duplication and recombination in each dinoflagellate lineage, while the length and the secondary structure of the SL RNA is conserved during evolution [203]. However, the bigger picture about dinoflagellate spliced leader RNA gene arrangement in genomic level is still unavailable. Since *P. marinus* genome annotation is still underway, it is not known if *P. marinus* has various SL RNA genes with different sequence length and genomic arrangement as dinoflagellates. Constitutive polycistronic transcription and trans-splicing also occur in flagellated trypanosomatid parasites, including *Leishmania*, *Trypanosoma brucei*, and *T. cruzi* [204]. Analysis of the complete genome of *L. major* [205], *T. brucei* [206], and *T. cruzi* [207] reveals that majority of genes are organized in the form of PGCs (polycistronic gene clusters) in all the chromosomes. A striking synteny is observed in the genome of trypanosomatids for protein-coding genes [208]. All the genes that reside on the same PGC are transcribed at the same level as the consequence of polycistronic transcription [204]. This is a reminisce of the interesting result in QPCR that all the PmNramp isotypes and PmSOD isotypes transcript give a highly similar Ct value presenting a similar transcriptional level. The questions raised

here are first, whether *P. marinus* genes are organized into PGCs and if so, whether they are located in the same PGC. Furthermore, unique machinery for transcription and processing of mRNA has been uncovered behind this unique genomic organization in trypanosomatid parasites. In *L. major*, the transcription of the whole chromosome 1 starts bidirectionally towards the telomere in the TSS (transcription start sites) between the two divergent PGSs [209]. Long G- or C-tracts instead of canonical promoter elements, such as TATA box were found in TSSs. The polyadenylation of a gene is dictated by the trans-splicing of the upstream adjacent genes since the selection of splice site determines that selection of the polyadenylation site [210], which can also explain the absence of polyadenylation signal in PmNramp genes. The completion of genome annotation of *P. marinus* can answer some fundamental questions about gene expression and regulation of the parasite.

The lack of transcription regulation of PmNramp isotypes implies a significant role of post-transcription regulation. In *Trypanosoma* spp., all the genes are trans-spliced [211, 212] and the SL is a conserved 35-nt stretch. The constitutive transcription of all the genes makes RNA interference (RNAi) an important avenue for expression regulation for the parasite and a widely-used knockdown technique in *Trypanosoma* research [213-216]. In the *P. marinus* genome database, some components of the RNAi machinery have been identified by BLAST, indicating a possible regulation of expression through RNAi [217]. Acquisition of iron and other divalent cation is vital for *P. marinus*; therefore, the presence of PmNramp mRNA ready for protein synthesis would secure an immediate response to metal requirements. *P. marinus* may have one or two ferritins, based on querying the genome with *Chlamydomonas reinhardtii* ferritin sequences (GenBank

accession No. AF503338 and EU223296) [218], suggesting the potential iron storage ability and consistent with high-iron tolerance in *P. marinus*.

Bioinformatic searches for regulatory RNA elements [219] in either 5' or 3' UTR of the *PmNramp* mRNA sequences failed to identify any sequence motifs, such as IRE. In vertebrates, the biosynthetic rates for ferritin and the TfR1 are regulated by iron. A highly conserved IRE in the 5' UTR of the *ferritin* mRNA and the 3' UTR of mammalian *TfR1* mRNA mediates iron-dependent post-transcriptional control of their expression [213, 214]. A similar element has been reported in the 3'-UTR of vertebrate *Nramp2* sequences [215, 216]. The IRE functions by forming a specific stem-loop structure that interacts with IRP in an iron-dependent fashion. Though both animal cytosolic aconitase (ACO) and bacterial ACO are able to switch to IRP function, playing a key role in the regulation of iron homeostasis, plant ACO, however, is not converted into an IRP. Thus, the absence of IRE in *P. marinus* may not be surprising since IRP/IRE signaling may have been preserved only in metazoans [220]. Nevertheless, it can still be too early to exclude IRE/IRP systems as mean of regulation for *PmNramp* expression. IRE/IRP like systems has been reported in some protozoan parasites. In *Trichomonas vaginalis* [127] and *Plasmodium falciparum* [221], atypical IREs have been identified despite the structure deviation compared to the consensus mammalian IRE. Binding activity of the IRP-like protein to mammalian IRE was demonstrated in *P. falciparum* [222, 223] and *Leishmania tarentolae* [137]. The definite function of the IRE/IRP like system in protozoan parasites still awaits further investigation

The regulation of *Nramp* expression can be realized through different ways for different isotypes in a single organism. In yeast, the three *Nramp* prototypes are regulated

differently: the vacuolar iron transporter Smf3 is controlled at the transcriptional level [188], while the manganese transporter Smf1 and Smf2 proteins are constitutively expressed and trafficked to either degradation or secretory pathways depending on manganese availability [224]. Since manganese is so critical for yeast metabolic activity, quick response to manganese limitation or toxicity is important. In addition, Nramp transporters display broad selectivity for divalent metals, including some that are highly toxic. Hence, rapid trafficking of transporters may allow dynamic control of metal-ion fluxes, and be beneficial for unicellular organisms. Because all three *PmNramp* isotype transcript lacks known nucleotide sequence motifs and are detected in trophozoites cultured in standard conditions, it is possible that the proteins are subject to translational and post-translational regulation mechanisms. In addition, the localization of the transporters can be changed by protein trafficking so as to regulate the protein function in the parasite.

CHAPTER 3 PHYLOGENETIC ANALYSIS OF THE PMNRAMP ISOTYPES*

SUMMARY

Phylogeny analysis indicates that the three PmNramp isotypes form a moderately tight set of archetype Nramp subgroup II. They are fairly close relatives of animal and higher plant Nramp, and to a less extent to homologues from apicomplexans and ciliates. No evidence of positive selection was found among the three isotypes. PmNramp3 stands out from the three isotypes when they are subjected to molecular evolutionary analysis. By Tajima's test of relative evolutionary rate, a similar evolutionary rate is shown in PmNramp1 and PmNramp2, while PmNramp3 shows a distinct rate; PmNramp1 and PmNramp2 display a homogenous substitution pattern, however, PmNramp2 and PmNramp3 demonstrate heterogeneous pattern. It seems that PmNramp genes evolved by successive duplications of PmNramp2, first yielding PmNramp3 and more recently PmNramp1. Protein sequence divergence among PmNramp isotypes was not related to diversification of critical functional elements, which remained constrained by purifying selection. This result is in consistence with the function of both PmNramp1 and PmNramp3 as iron transporter in yeast despite their different evolutionary rate and substitution patterns.

* The results in this chapter is obtained through the collaboration with Dr. Mathieu F. Cellier

INTRODUCTION

Five Nramp phylogroups were identified to provide a plausible pathway describing the evolution of the Nramp family, from sodium- or proton-motive substrate symport in bacteria, to metal nutrition, eukaryotic host cell defense and brain function [225]. Among the five subgroups of Nramp, the most ancient homologs are prokaryotic MntH B that can date back to the apparition of anoxygenic photosynthetic organism. With the increase of the oxygen concentration in the atmosphere, MntH A homologs merge during the aerobic organism evolution. The origin of eukaryotic prototype Nramp is likely to be MntH A, which is transfer to Eukaryotes due to an endosymbiotic event. Early gene duplication of prototype Nramp gives rise to archetype Nramp. Close relationships between MntH C group and some prototype Nramp, and within MntH C group irrespective of bacterial phylogeny, indicate eukaryotic gene transfer toward bacteria [226]. However, no direct eukaryotic source of *mntH C* genes has been identified to date, and this complication warrants careful phylogenetic studies of Nramp homologs in unicellular eukaryotes. Therefore, a hypothetic evolutionary pathway of Nramp is presented as Outgroup > MntH B > MntH A > eukaryotic duplication/divergence of proto- and archetype Nramp > MntH C ($C\alpha$, $C\beta$, $C\gamma$) [227].

The current taxonomic distribution of Nramp phylogenetic subgroups is the outcome of the Nramp evolution combined with the selective loss of certain subgroup in certain organisms. MntH A homologs are broadly shared, while *mntH B* genes are prevalent among anaerobic genera. The distribution of MntH C ranges from wide (MntH $C\alpha$) to limited to gut-associated bacteria (MntH $C\beta$) or Gram negative soil bacteria (MntH $C\gamma$). In eukaryotes, the taxonomic distribution of both archetype and prototype

Nramp is diverse, including Bikonts (Plantae, Chromoalveolates) and Unikonts (Amebozoa, Fungi and Animals; [226, 228]). Though subgroup I of Nramp archetype comprises homologs found in monocots and eudicots plants, Nramp archetype subgroup II is shared by organisms from both Unikonta and Bikonta. Prototype Nramp display more restricted distribution (Amebozoa and Fungi, green and red Algae and lower plants, e.g., bryophytes), which seems to be the result of selective loss of this isoform in animals, higher plants (monocots, eudicots) as well as in Chromoalveolates; in contrast, most fungi lost archetype Nramp isoforms, except some species that diverged basally.

Four different approaches have been used to phylotype *PmNramp1* and other putative apicomplexan Nramp homologs (*Plasmodium falciparum*, *P. yoelii* and *Toxoplasma gondii*). It was indicated that *PmNramp1* and apicomplexan Nramp genes share a same archetype Nramp ancestor; while, apicomplexan Nramp, especially *Plasmodium* spp. Nramp, is obviously divergent from other archetype Nramp. It seems that the closest homologues of *PmNramp1* and apicomplexan Nramp are plant and *Dictyostelium discoideum* homologues [228]. With the identification of the extra two *PmNramp* isotypes, the phylogeny of *PmNramp* is revisited in this chapter. In addition, the evolution of the three *PmNramp* isotypes is proposed.

MATERIALS AND METHODS

Phylogenetic analysis

To phylotype the three *PmNramp*, a representative set of eukaryotic homologs was selected to generate multiple alignments using full-length amino acid sequences and the softwares Clustal X [229] or Muscle [230], which were edited manually and used

alternatively to compare phylogenies. Sets of parsimony-informative sites (corresponding to at least two different amino acids, and at least two of them occurring with a minimum frequency of two, [195]) were also examined as an alternative to full-length sequences to examine tree robustness. A consensus phylogenetic tree was established by implementing several approaches using different substitution models. The rate of amino acid variation among sites was modeled using the WAG amino acid substitution matrix [231] and a discrete Gamma distribution [232]. Phylogenies were inferred using three different types of calculations: i) changes probabilities along the tree branches were determined by Quartet Puzzling and Maximum Likelihood using Tree-Puzzle (Schmidt HA & A von Haeseler, 2007); ii) pairwise evolutionary distances (numbers of substitutions) were deduced by using the Minimum Evolution/Neighbor-Joining method [233] and allowing heterogeneous pattern of substitution across the lineages [234] as well as pairwise or complete deletion modes [195]; iii) Maximum Parsimony [235] was used to deduce the evolutionary transitions required to explain the observed amino acid distributions [195]. The consistency of each calculation was estimated by bootstrapping ([236]; 3000 replicates) and the confidence score of tree nodes was compared.

To evaluate the type of selective pressure exerted on *Perkinsus* gene sequences, Kumar's modification of the Pamilo-Bianchi-Li method was used to analyze the relative abundance of synonymous (*S*) and nonsynonymous (*N*) substitutions in codon-by-codon pairwise comparisons (Fig. 18 and 19) of the three aligned *PmNramp* nucleotide sequences [195, 237]. After estimating the number of synonymous substitutions per synonymous site (d_s) and the number of nonsynonymous substitutions per

nonsynonymous site (d_N) as well as their variances, $\text{Var}(d_S)$ and $\text{Var}(d_N)$, the level of significance at which the null hypothesis of neutral evolution ($H_0: d_N = d_S$) may be rejected was tested considering three alternative hypotheses (AH1: $d_N \neq d_S$, strict neutrality; AH2: $d_N > d_S$, positive selection; AH3: $d_N < d_S$, purifying selection). A two-tailed Z-test was used to determine the level of significance of the difference $d_N - d_S$ (AH1) and a one-tailed Z-test was applied to examine the other hypotheses (AH2,3). Both pairwise and complete site-deletion options were used to compare the results obtained; the variance of the difference $d_N - d_S$ was calculated by bootstrap resampling (3000 replicates).

Molecular evolutionary gene analyses

The molecular clock hypothesis was evaluated using Tajima's relative rate test, which implies equality of evolutionary rate between two sequences, irrespective of a substitution model and whether or not the substitution rate varies among sites [195, 238]. Pairs of PmNramp nucleotide or amino acid sequences were compared, using the third sequence as an outgroup. Tajima's method uses a chi-square (χ^2) test to estimate the independence of paired observations on two variables; a value of the corresponding probability ($p < 0.05$) was used to reject the molecular clock hypothesis.

Homogeneity of substitution patterns was derived from pairwise sequence comparisons using the Disparity Index test, which calculates the extent of differences in base or amino acid residue composition between sequences. The probability p of rejecting the null hypothesis that sequences evolved with the same pattern of substitution was determined using a Monte Carlo test and bootstrap resampling (3000 replicates; [194, 195]).

Tridimensional structural models were obtained for PmNramp 1 and 3 using the default parameters of the meta server I-Tasser [239] as previously described [240].

Fig. 18

```

                *           20           *           40           *           60           *           80           *           100
FmNramp1 : DGSESLFVVRTEKEKQVEIPIDPPGVKFSERTEFKYAGPGWLMSLAYLDPGNLEADLQAGAFITGFQLLWVLLLAHIVGLILQILSSRLAAVTGKHLAEHCR : 100
FmNramp2 : DEPGFL-IRDC--HQIDIPIDPPGVKFSIRTFKRYAGPGWLMSLAYLDPGNLEADLQAGAFITGFQLLWVLLLAHIAGLLLQICACRIGAAATGESLAENCR : 97
FmNramp3 : ---GRVVVCPVDSLDDISEKR-RTKFSMRTEFRYAGPGWLMSLAYLDPGNLEADLQSGVYTGFLSWVLLLAHAVGLLLQCLARLGFVTGKSLAQHCR : 96

                *           120          *           140          *           160          *           180          *           200
FmNramp1 : ARYFHWIATVLWIMTEIAIIGSDIQEVLGTAIAFKVLLNIEFLWAGTLITAVDTITFTITHLHIGIRVLEAFIFILILTMMACFFIDMAISAPPAVDIHRG : 200
FmNramp2 : RGYSTRVSNILWIMSEIAIIGSDIQEVLGTAIAFHVLFGLDMWVGLITAADTITFLFIQTHGMRVMEAFIFILIMTMGCFANMAITAPPAVEVARG : 197
FmNramp3 : QGYGORTGTILWILTEIAIIGSDIQEVLGSAVAFRLLEGLFLWMCVITADTFELAAQYHGTIRVLECFVVSVMIMCACFFANLIDIVREEFINVAIG : 196

                *           220          *           240          *           260          *           280          *           300
FmNramp1 : FIFVVA SYATMQVGLIGAVIMPHNLYLHSALTGS-RKIDRSEERNIQANKYEFIDSTSSISVSFLINIAMVSAFAHGMSSIQCATIECGPLACTVTFE : 299
FmNramp2 : FIFVNS SYAVMELVGIVGAVIMPHNLYLHSALTGS-RKIDRNNHEFVRQANMYLTVDACCSIIISFIINMAVVCSEFAYGMFSLHCARMPKGFACLSSEED : 296
FmNramp3 : FLPSVA SYAVVQVGVVAVIMPHNLYLHSALISSTRRIDRRNPRALEQANVYFSLDAVAVALISFFINTAIMTSFAQGFESPHCATNPSGTLGON-TAA : 295

                *           320          *           340          *           360          *           380          *           400
FmNramp1 : DWDRSVCSFSDAACCHPEGIAGVCSSTIGLENAGALAAVMYFG-AVKYIFAVGILAAGQASTLTGTLAGQYVMEGFMRWKIFMWERVLI TRTIALGPA : 398
FmNramp2 : DWSTSTCDEFLNPDCHCTTSYGETGVCAVGLENAEEALGAVISSD-AMKYIFAVGVLAAGQASTLTGTMTAGQYVMEGFMHIRTSMWVRVLLTRTIALGPA : 395
FmNramp3 : VVAITSECEL--AVCSOVNSMGCEGCTAIGLSNGGSALASLVGSSSEFAATLFAIGVLAAGQASTMTGSLAGQYVMEGFLGLRIELWLRLLVTRSIATVPA : 393

                *           420          *           440          *           460          *           480          *           500
FmNramp1 : LAFAILQGEIR-----AMNGVNAWLNILQSIQLPFALLPVLHFSMSREVLG-RFVIGRFWTAVMWILACLVIGVNFYLVIEITIIPLNWPVYVAIAIIVA : 492
FmNramp2 : LAIALVSEVSEV-----GMNGINAWLNILQSIQLPFALLPLLHYAMSKFVMG-TEFLNRWWSAGLWLLALILAINVYLIITTLVPLDWPVYVAIAIIGVVF : 489
FmNramp3 : LEVAVVQSSAAGESAASISAVNDWLNILQSVQLPFALLPLLHEVGDPRVMGHDWVIGRRLKIICWACALSLIVINAYLLHSQIANIQAGTFVVLVIGVAVF : 493

                *           520          *           540          *           560          *           580          *
FmNramp1 : CIYIWLCSVKEEDIMG-----AARKVFGK-----CAASIEVS----- : 525
FmNramp2 : YLYVSLCFYCVEDDLSRGCSNVKHDITFFLKPVIRGFRMLYGCCKRAEDKCIGRKDDDEVEDCEDTSSSSVDTPRCVVADVPSPPSSAIVEEGFKH : 585
FmNramp3 : CGYIVLMAIAYQSELKA-----FLFYIRSP-----WILWRATNYRR----- : 529

```

Fig. 18. Amino acid alignment of the three PmNramp isotypes

The alignment was generated using Mega 4.0 [195] and displayed with GeneDoc [196].

Identical residues are highlighted at three cutoffs (50, 75 and 100 %). The N-terminal sequences of PmNramp isotypes are omitted to avoid the variation caused by the potential signal peptides.

Fig. 19

```

                *           20           *           40           *           60           *           80           *           100
FmNr1 : ATGTCACACGTCCTCCCGATCCGCTCTACGGAGGAGTCTAACTCGACGCCTCTGGCTATCGACTCGAGTAGCATTTCAGCGGGCAAAGCGGTAGAATTAGTGC : 100
FmNr2 : -----G----- : 1
FmNr3 : ----- : -

                *           120          *           140          *           160          *           180          *           200
FmNr1 : ATGGGCCCTCAGAGTGCCTGTCGGAAGTGGCAAGGAGAGGCAACTCGAAATACCGATTGACCCGCCGGTGTAAAGTTCGCTTTCGGACATTTTGCAG : 200
FmNr2 : ATCAACCTTGGTCCTCTT--ATATAGAGACGGCT-----CATCAAAATTGATATACCAATTGACCCCTCGGGGTGTAAAGTTCCTATACGGACATTTTCAA : 92
FmNr3 : -----GGCAGAGTAGTGGTATGCCAGTGGCTCCCTACCGATGACCTCACTGAGAGAGCGG---CGGACAAAGTTCAGCAATGCCATACGTTTTCG : 89

                *           220          *           240          *           260          *           280          *           300
FmNr1 : GTATGCTGGTCCCTGGTGGCTTATGTCATTTGGCCTATCTCGATCCTGGTAATTTAGAGCCGATCTACAGGCTGGAGCCCTTCACAGGCTTCCAGTTGCTA : 300
FmNr2 : GTATGCTGGTCCCTGGTGGCTTATGTCATTTGGCCTATCTCGATCCTGGCAATCTCGAGGCCAGACCTTCAAGCTGGGGCATTCACAGGCTTCCAGTTACTA : 192
FmNr3 : TTACGCCGCCCGGGCATGGTTCATGTCCTTAGCCTACTTGTATCCGGCAATCTTGAAGCCGACTTGCATTCAGGGCTTTACACGGGTTTCAATTCCT : 189

                *           320          *           340          *           360          *           380          *           400
FmNr1 : TGGGTATTGCTTCTTGCTCATATAGTGGACTCCTTCCCTCAAAATTTTATCAAGCCGCTCTACCGGCAGTAACAGGGAGCCATTTGGCTGAGCATTGCCGGG : 400
FmNr2 : TGGGTATTGCTTCTTGCTCATATAGCAGGCTCTACTACTCAAAATTTGTCCTGTCTGATTTGGTGGCTCTAATCGGTGATAGTGTGGCAGAGATTGCCCTA : 292
FmNr3 : TGGGTATTGCTTCTTGCTCATATGAGTCCGCTCTTCTCCAGAGTGTCTCAGCGCAAGGCTCGGTTTGTATACAGGGAGAGTCTTGCATCAGCATTGCTCCAC : 289

                *           420          *           440          *           460          *           480          *           500
FmNr1 : CTAGATATCTCTAATGGACTGCAAGCTGCTATGGATAATGACTGAGATGCCCATTTATGGTTCGGATATTCAGGAGGTGTTGGAACTGCTATAGCATT : 500
FmNr2 : GAGGTACTCGAGGAGAGTGTCCAAATTAATCTATGGATAATGAGTGABATGCCCATCATCGGCATCGAGACATTGAGGAGGTCAATGGAACTGCTACTGCC : 392
FmNr3 : AAGGCTACGGACAGCGGACAGCAAAATATTGGGATACTTACGABATTTGCTATTTATCGGTTCTGACATTGAGGAGTATTTGGGTTCCGCAGTGGCTTT : 389

                *           520          *           540          *           560          *           580          *           600
FmNr1 : CAACTGTTTATAAATCATCCCTCTCTGGCGGGGACTCTCATTACTGGCTGGATACCCCTCACTTTTGTGACATTAATTTGCTGCAAGGATCAGAGTA : 600
FmNr2 : TCACGTGTTGTTCCGCTATTTGATATGTTGGGTTGGTGTCTTATCACAGCCGCTGATACCTCAGCTTTTGTTCATACAAATATCCATGGAAACCGGTGTT : 492
FmNr3 : CCGCTGTTGTTTGGCATTCCTCTCTGCAATGGGCTGCTTATAACAGCCGCTGATACCTTTCACATTTCTGGCAAGCCAGTATTTACATGGGACTCGAGTA : 489

                *           620          *           640          *           660          *           680          *           700
FmNr1 : CTGGAAAGCCTTTATATTCATACCTCATCTTAACGATGATGGCGTCTCTTTATAGACATGGCGGATTTGAGCGCCCCAGCTGTTGGACATCTTTAAAGGGT : 700
FmNr2 : ATGGAGCGCTTTATATTCATCCCTTATCATGACGATGATGGGGTGGCTTTTGGTCAATATGGGAATAAAGAGCCACCAGCAATAGAGGTTGCTAAAGGGT : 592
FmNr3 : TTGGAAAGGACTCGTACAGTCTCTTATAATGATATGTTGGCTTGGCTTCTTTGGCAAGCTGGACATCGTCAAAACGGGATCCGAAATCAATTTGGCACTTGGCT : 589

                *           720          *           740          *           760          *           780          *           800
FmNr1 : TCAATCCCTATGTTGGCTAGTATAGCGACTATGCAAAATGGTGGCTTATTTGGCGGAGTTATATGCGCCATAACCTTACCTTCACTCGGCATTGACAG : 800
FmNr2 : TTTATCCAAAGCTATCGACTATGCTGTTATGCAAGTGGTGGATTTGTTGGTGGCTGTTATATGCGCCATAAATCTTATCTCACTCGGCATTGACAG : 692
FmNr3 : TCCCTCCCTCTCGTGGCTTCAATATGCTGTTGTCAAAATGGTCCGAGTAACTGGAGCGTGTATATGTCCTCATAAATTTATCTCACTCGGCATTGACAG : 689

```

Figure continued

```

FmNr1 : C T C T -- C G C A A G A T A G A T A G A A C G G G G A G G A A C A T C C A G C A G G C T A A C A G T A C T T T T C A T C G A T T C A A C A T C A T C C T T A T C C G T A T C T T T C C T C : 897
FmNr2 : G T C T -- A G G A A A T C G A T A G A T A A T A T C A C G A C T T T G T A A G C A G G C T A A T A T G T A T T G A C C C T A G A T C C A T G T T G T C T A T C C T C A T A T C G T T C A T C : 789
FmNr3 : C T C G A C G G G C G T A T C G A C C G C C A A T C T C G G G C T T T G G A G C A G C C A A T G T A T T T C T C T T G G A T C T G C G G C C G C T C T T G C A A T T C A T T T T T C : 789

FmNr1 : A T C A A C C T A G C C A T G G T A T G G C A T T C G C C C A T G G G A T G T C T T C T C T C C A G T G C G C C A C T C C C T C A A G G A C C C T C G C C T G C C T A G T T A C T C C G A A G : 997
FmNr2 : A T C A A C A T C G C A G T G G T A T G C T C C T T T G C A T A T G G C A T G T T C T C A C T A C A C T G T G C G A G A A T G C C A A G G G A C C A T T T G C A T G C C T A G C A G T C C A G A T G : 889
FmNr3 : A T A A A T A C A G C G A T A T A G A C C A G C T T C G C C A G G G G T T T T T C T C T C C A C A T G T G G A G C A G A C C C T C C G G A A C C T C G C A T C T A A A --- A C T G C A G C T G : 886

FmNr1 : A T T G G G A A C G T T C G G T G T C G A G C C G A G T G T G C A G C T T G C C A T P G C C A T A C T C C T G A G G T A T T C C C G A G T A T G C G C A G C A T C G G C C T T G A C A A C G C : 1097
FmNr2 : A T T G G A G T A G G A G T A C G T C T G A T C C G C T A A C C C T G A T T C T C A C R G T A C A A C T T C G T A T G G T G A C A C A G G G G T C G T G C T A T G G T T G C A C T T G A A A T G G : 989
FmNr3 : T A G T A C C C A C C A G T G A G T G C G A G T T A --- G C G T C T C A G A T T G T G T C A A T T C A T A G G G C C A G G A A G G T T T C T G T A C A G C T A T T G G C T T A G T A G T G G : 980

FmNr1 : C G C G S G T G C A C T G C T G C A G T C A T C A T T T C C G T --- G C G S T G A A G T A C T C T T C G C T G T T G G C A T A T T T G C G G C T G G C A A G C A G T A C T C T T A C C G G T : 1194
FmNr2 : A G C A G A G G C C T T A G C G C A G T G A T T T C A T C G C A T --- G C T A T G A A G T A T A T C T T C G C T G T T G G T G T A T T G C A G C A G G C A A G C A G T A C C T T A C T G G C : 1086
FmNr3 : A G G T C G G C T C T C G C T T C G C T A G T T G G C T C A T C T G A G T T C C A G C C A C T C T C T T C G C A A T A G G C G T T T T A G C A G C T G G C A A G C A G C A C T A T A C A G C C : 1080

FmNr1 : A C T T T G G C T G G C C A A T A C G T G A T G G A A G G A T T C A T G A C G T G A A G A T T C C A A T S T G G T T C C G T G T C T C A T C A C T A G A C G A T T G C A C T A G G A C C G G C C : 1294
FmNr2 : A C C A T G G C T G G T C A A T A C G T A T A G G A G G G T T T A T G C A T A C C C T A T A C A A T S T G G G T A A G A G A C T A T A A C A C G T A C A T A G C T C T A G G G C C G G C C T : 1186
FmNr3 : T C G T C G C C G G T C A A T A C G T C A T G G A A G G T T T C T T G G C A C T G C C A T C C G C T C G G C T G G A T T G C T T G A C C A G A T C A A T A G G C C T C T C C C G C C T : 1180

FmNr1 : T A S C A T T C G C T A C C T G C A G G G T G A A A T C A G A --- G C C A T G A A T G G A C T A A A C G C G T G G T T G A A T A T T C T T C A G T C G A T T C A G C T T C C : 1379
FmNr2 : T G G C A T T C C T C A G T T C A G A G T G A A G G A T C G --- G G T A T G A A C C G C A T C A A T G C A T G G T T G A A T A T T C T G C A G T C T A T A C A G C T A C C : 1271
FmNr3 : T G T T T G T A C C C G T T T G G C A G A G T A G T C C C C T G G G G A G T C A G C G G C T T C C C T G T C A G C C G T C A A G A T T G G C T G A A T A T T C T C C A G T C C G T T C A C A C T A C C : 1280

FmNr1 : T T T G C T T T G T T C C A G T G C T G C A C T T C T C G A T G A C C G T G A A G T G T T G G G A --- A G A T T G C T C T C G C C G C T C T G G A C A G C C S T A A T G T G G A T T C T T : 1476
FmNr2 : C T T T G C G T T G T T A C C G T T A C T G C A C T A T C G G A T G A C A A G A A G G T A T T G G G C --- A C G T T T G C A T T G A A T A G A T G G T G G A G T G C T G G A C T G T G G T T G C T G : 1368
FmNr3 : A T T G C C C T G T T G C C G T T C T T G C A T T T C C T C G G G G A C C G A A A G T C A T G G G A C A T G A T T G G G T G T T G G A A G G A G G C T C A G A T A T C T G C T G G C C T G C : 1380

FmNr1 : G C E T C C A G T A A T T G G C T C A A C T T C T A T C T G G T A T T G A G A C T A T C A T C C C T C T G A A T T G G C C A T G G T A C G T T G G G T A A T C C T C G C C A T C G T G C A T : 1576
FmNr2 : G C A C C A T A T C C A C G C T A T T A A C S T T T A C C T T A T C A T C A C T A C T C T G S P C C C T T A G A T T G G C C T T G S T A T G C A T G G G C A A T T A T T G G T G T T G T A T T C T : 1468
FmNr3 : G C E A T T T C G C T C A T T G T C A T T A A C C G T A T C T C C T G C A C T C C A A C T C E C T A A A T A T A C A G C A G G A C T T T C G T G C T T G T T T T G G G A G T G C A G T G T T T : 1480

```

Figure continued

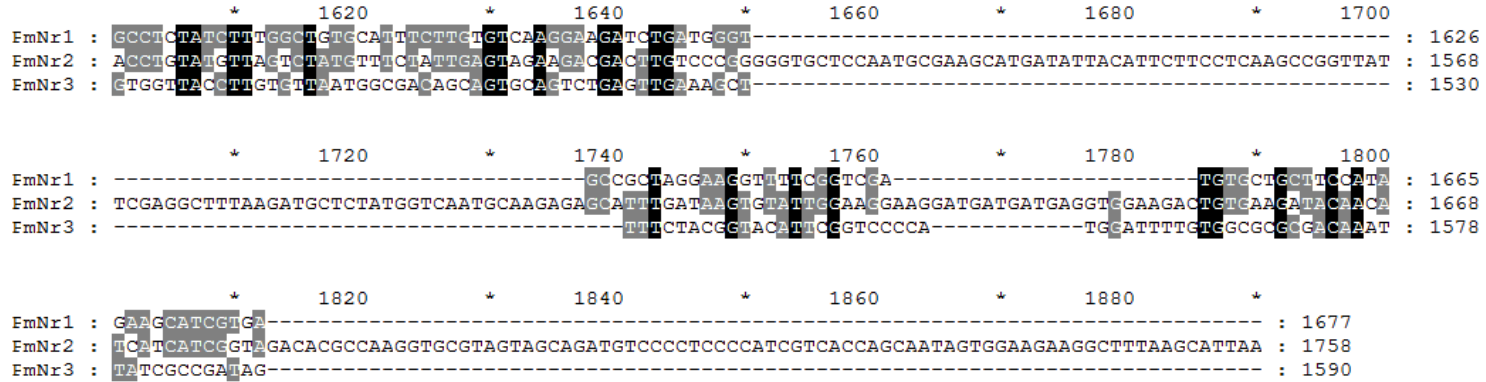


Fig. 19. Codon-by-codon cDNA alignment of PmNramp isotypes

The cDNA sequences of PmNramp isotypes are aligned codon-by-codon based on the amino acid alignments in Fig. 18. The alignment was generated using Mega 4.0 [195] and displayed with GeneDoc [196].

RESULTS AND DISCUSSION

Taxonomic distribution of Nramp in eukaryotes

A linearized phylogenetic tree showing key nodes supported by high bootstrap values obtained by different methods is presented in Fig. 20. The three *Perkinsus* Nramp sequences (PmNramp1-3) form a moderately tight set among other homologs that together constitute Nramp archetype subgroup II. The three PmNramp thus represent fairly close relatives of animal Nramp, similarly to the homologs found in most other Chromoalveolate genomes to date, including some *Stramenopile* spp. (e.g., PsoNR1a, Fig. 20 and Table 7), and to a lesser extent those from Apicomplexans and Ciliates, which appear more divergent (e.g., Tthe1-3, Fig. 20). Also, the diatom *Thalassiosira* possesses an Nramp homolog (TpseNR) resembling more the archetype I found in Plantae. Assuming a hypothetical common ancestry for Chromoalveolates and Plantae [241-243], this might suggest an ancient origin for Nramp archetype I and II paralogs in Bikonta, and selective loss of subgroup I in most Chromoalveolates.

The distribution of prototype and archetype Nramp in both Unikonta and Bikonta suggest an ancient origin/duplication corresponding to early stages in the emergence of eukaryotic cells. To verify this possibility a taxonomically broad database of expressed sequence tags (TBestDB, [244]) was searched by Blast analyses using prototype and archetype Nramp as queries; individual eukaryote databases of the DOE JGI genome portal were queried as well. The results presented in Table 10 show that archetype Nramp are present in several species of Chromoalveolates (Dinoflagellates; Apicomplexans: Hemisporozoans and Coccidians; Stramenopiles: Oomycetes and

Pelagophyceae; Haptophytes), as well as in Plantae (archetype I or II, Rhodophytae, Chlorophytae), Amoebozoa, basal Fungi (Mucoromycotina, Zygomycota) and Eumetazoa.

Regarding prototype Nramp, several DNA sequences found in Bikonta (Excavata: Jakobids and Euglenoids; Plantae: Glaucophytae and Chlorophytae) represent potential candidates, albeit derived from 3' mRNA ends, which encode parts of Slc11 transporters that are little conserved and thus yielding weakly supported relationships (Fig. 21 B). However, phylogenetic analyses performed with the 5' ESTs enable to distinguish Nramp prototype from archetype I with confidence (Fig. 21 A). Together with prior data obtained with full-length sequences, the present results thus support the conclusions that the duplication and divergence of proto- and archetype Nramp, and the later diversification of archetype Nramp in subgroups I and II, both predated the emergence of Unikonta and Bikonta. Subsequently, organisms independently conserved one type or another or both. In Alveolata, it is the Nramp archetype II that was selectively retained, and which was triplicated in both the Dinoflagellate *Perkinsus* and the Ciliate *Tetrahymena*.

Fig. 20

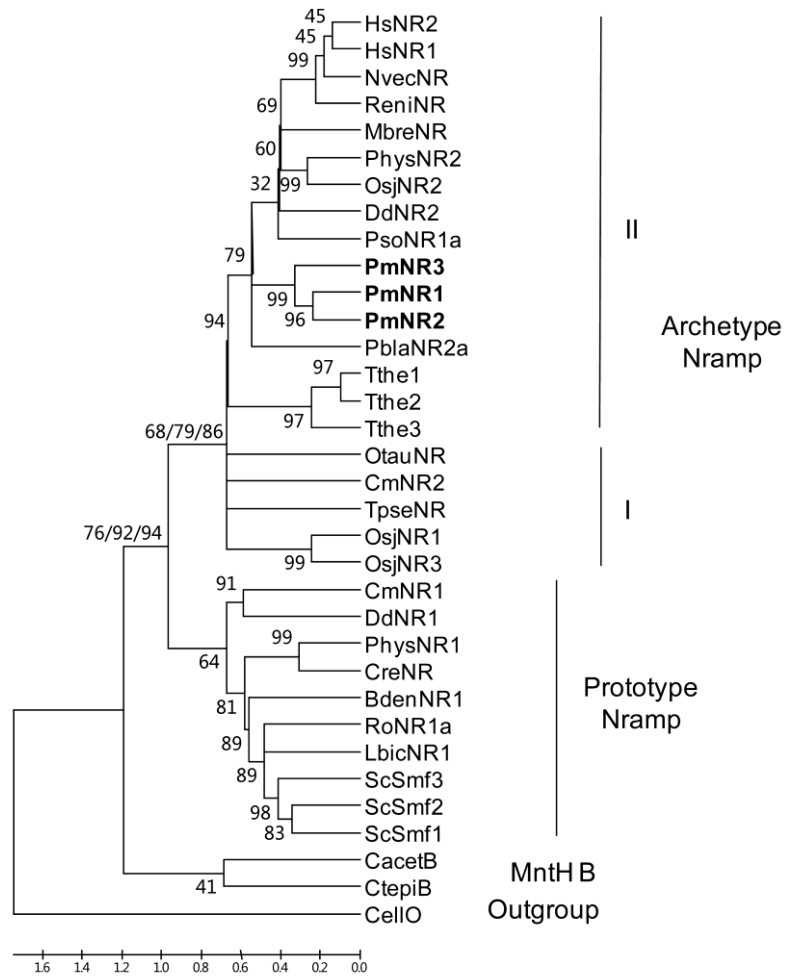


Fig. 20. Simplified phylogeny of PmNramp1-3

The consensus tree presented was obtained using Mega 4.0 [195]; it was linearized by assuming equal evolutionary rate among lineages [245] and drawn to scale by calibration using a time of divergence between Nramp1 and 2 of 350 million years ago [185].

Phylogeny was inferred using a set of 340 parsimony-informative sites derived from full-length sequence initially aligned with the Muscle algorithm; the Minimum Evolution method was implemented based on distances computed using the Equal Input amino acid substitution model [246] and considering both differences in the composition bias among sequences and rate variation among sites modeled with a gamma distribution (shape parameter = 1.41). The percentage (>50%) of replicate tree nodes inferred from 3,000 bootstrap samplings are indicated while less reproducible partitions were collapsed.

Percentage replicates of the main nodes (divergence of proto- and archetype Nramp; archetype I and II Nramp) obtained by other approaches are also indicated (Maximum Parsimony and Maximum Likelihood, Fig. 22 B & C). The non-linearized version of this phylogenetic reconstruction is presented in Fig. 24 A, together with those produced by other approaches (Fig. 22 B & C) as well as using full-length sequences (Fig. 22 D & E).

Following are indicated the SLC11 phylogroups (**bold**) and full names of the organisms (*italics*) included in this analysis: Outgroup: CellO, *Cellulophaga*; MntH B: CacetB, *Clostridium acetobutylicum*, CtepiB, *Chlorobium tepidum*; Prototype Nramp: ScSmf1-3, *Saccharomyces cerevisiae*, LbicNR1, *Laccaria bicolor*, RoNR1a, *Rhizopus oryzae*, BdenNR1, *Batrachochytrium dendrobatidis*, CreNR, *Chlamydomonas reinhardtii*, PhysNR1, *Physcomitrella patens*, DdNR1, *Dictyostelium discoideum*, CmNR1, *Cyanidioschyzon merolae*; Archetype Nramp, type I: OsjNR1,3, *Oryza sativa japonica*,

TpseNR, *Thalassiosira pseudoana*, CmNR2, *C. merolae*, OtauNR, *Ostreococcus tauri*;
Archetype Nramp, type II: TtheNR1-3, *Tetrahymena thermophila*, PblaNR2, *Phycomyces*
blakesleeanus, PmNramp1-3, *Perkinsus marinus*, PsoNR1a, *Phytophthora sojae*, DdNR2,
D. discoideum, OsjNR2, *O. sativa japonica*, PhysNR2, *P. patens*, MbreNR, *Monosiga*
brevicollis, ReniNR, *Reniera*, NvecNR, *Nematostella vectensis*, HsNR1,2, *Homo sapiens*.
The distribution of the taxa sampled is given in Table 7.

Table 7. Taxonomic distribution of known eukaryotic Nramp homologs

Taxa	Species	Prototype Nramp	Archetype Nramp	
			I	II
<i>Hemisporozoon</i>	<i>Plasmodium</i> (6)			1
	<i>Neospora</i>			1
<i>Coccidian</i>	<i>Toxoplasma</i>			1
<i>Apicomplexan</i>				
<i>Dinoflagellates</i>	<i>Perkinsus</i>			3
	<i>Ichthyophthirius</i>			2
<i>Ciliates</i>	<i>Tetrahymena</i>			3
<i>Alveolata</i>				
<i>Pelagophyceae</i>	<i>Aureococcus</i>			2
	<i>Hyaloperonospora</i>			1
	<i>Saprolegna</i>			1
<i>Oomyceta</i>	<i>Phytophthora</i> (2)			1-4
<i>Diatoms</i>	<i>Thalassiosira</i>		1	
<i>Stramenophiles</i>				
<i>Haptophyta</i>	<i>Emiliana</i>			1
<i>Chromoalveolata</i>				
<i>Spermatophytae</i>			1-2	2-4
<i>Embryophytae</i>	<i>Marchantia</i>	1	1-	
	<i>Physcomitrella</i>	1-		2-
	<i>Chlorella</i>			1
	<i>Micromonas</i>		1	
	<i>Ostreococcus</i> (2)		1	
	<i>Volvox</i>	1		
	<i>Chlamydomonas</i>	2		
<i>Chlorophytae</i>	<i>Scenedesmus</i>	2		
<i>Viridiplantae</i>				
<i>Rhodophytae</i>	<i>Cyanidioschyzon</i>	1	1	
	<i>Glaucocystis</i>	1		
<i>Glaucophyteae</i>	<i>Cyanidioschyzon</i>	1		
<i>Plantae</i>				
<i>Euglenoids</i>	<i>Euglena</i>	1		
	<i>Reclinomonas</i>	1		
<i>Jakobids</i>	<i>Seculamonas</i>	1		
<i>Excavata</i>				
<i>Bikonta</i>				
<i>Unikonta</i>				
<i>Amoebozoa</i>				
<i>Tubulinea</i>	<i>Hartmanella</i>		1	
<i>Mycetozoa</i>	<i>Dictyostelium</i> (2)	1		1
	<i>Physarum</i>	1		1
<i>Opisthokonta</i>				
<i>Fungi</i>				
<i>Mucoromycotina</i>	<i>Cunninghamella</i>			1
<i>Chytridiomycota</i>	<i>Spizellomyces</i>	1		
	<i>Batrachochytrium</i>	1		
<i>Zygomycota</i>	<i>Rhizopus</i>	2		2
	<i>Phycomyces</i>	2		2
<i>Basidiomycota</i>	<i>Ustilago</i>	1		
	<i>Cryptococcus</i>	1		
	<i>Phanerochaete</i>	2		
<i>Ascomycota</i>	<i>Neurospora</i>	1		
	<i>Candida</i>	4		
<i>Eumetazoa</i>				
<i>Porifera</i>	<i>Reniera</i>			1
<i>Cnidaria</i>	<i>Nematostella</i>			1
<i>Metazoa</i>	<i>Monosiga</i>			1
	<i>M. ovata</i>	1		
<i>Vertebrata</i>	<i>Homo sapiens</i>			2

Fig. 21

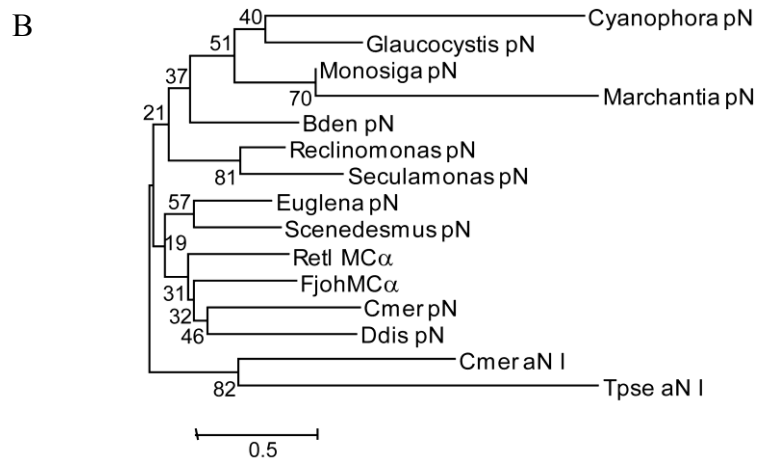
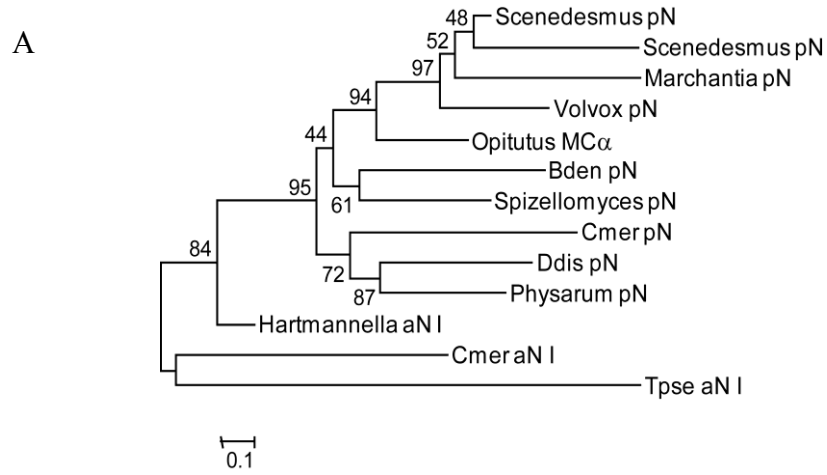


Fig. 21. Phylogenetic analyses of sequences derived from taxonomically diverse unicellular eukaryotes demonstrate prevalence of prototype Nramp (pN).

The taxonomic distribution of the species studied is indicated in Supp. Table 2. Amino acid sequences deduced from expressed sequence tags (TBestDB) [244] and corresponding to either 5' (A) or 3' (B) parts of suspected prototype *SLC11/Nramp* mRNAs were analyzed together with full-length control sequences of bacterial SLC11 homologs of eukaryotic origin [226], M α , MntH α ; *Opitutus terrae* (Verrucomicrobium), *Rhizobium etli* (α -proteobacterium), *F. johnsonii* (Flavobacterium) as well as Archetype I Nramp homologs (aN I) from the red alga *C. merolae* and the diatom *T. pseudoana*. These dendrograms were generated as described in Fig. 20 but without molecular clock assumption, and using the pairwise deletion option and a gamma distribution shape parameter of 1.5.

Phylogeny of *Perkinsus* Nramp1-3 proteins

Assessment of the Nramp protein phylogeny (Fig. 20 and 21), regarding in particular the level of sequence divergence among PmNramp homologs as well as between this set and other Nramp archetype II, indicates two main properties: i) compared to their Alveolatan relatives, in Apicomplexans and Ciliates, the PmNramp sequences did not diverge extensively from the other members of the archetype II group; and, ii) compared to other unicellular organisms that possess multiple genes, the extent of apparent divergence among PmNramp polypeptides (e.g., PmNramp3) appears significant.

First, the absence of the PmNramp sequence set from the cluster formed by the Nramp from Ciliates and Apicomplexans (Fig. 22 D & E) was unexpected, based on the commonly accepted phylogeny of Dinoflagellates as sister group of Apicomplexans, and the more basal divergence of Ciliates (Moore RB et al., 2008, Sanchez-Puerta & Delwiche, 2008, Nash EA et al., 2008); however this result may be a simple consequence of variations in DNA maintenance and overall GC percent, which is very low in both Ciliates and Apicomplexans. Secondly, PmNramp paralogs appeared consistently more divergent than *T. thermophila* paralogs in various phylogenetic trees (longer branches for PmNramp paralogs, Fig. 19 and Fig. 21); even though similar patterns were observed in both species, with two homologs relatively close and another more distant. The extent of sequence divergence among *Perkinsus* Nramp resembled more that existing between yeast Smfps, suggesting perhaps some functional significance.

Fig.22

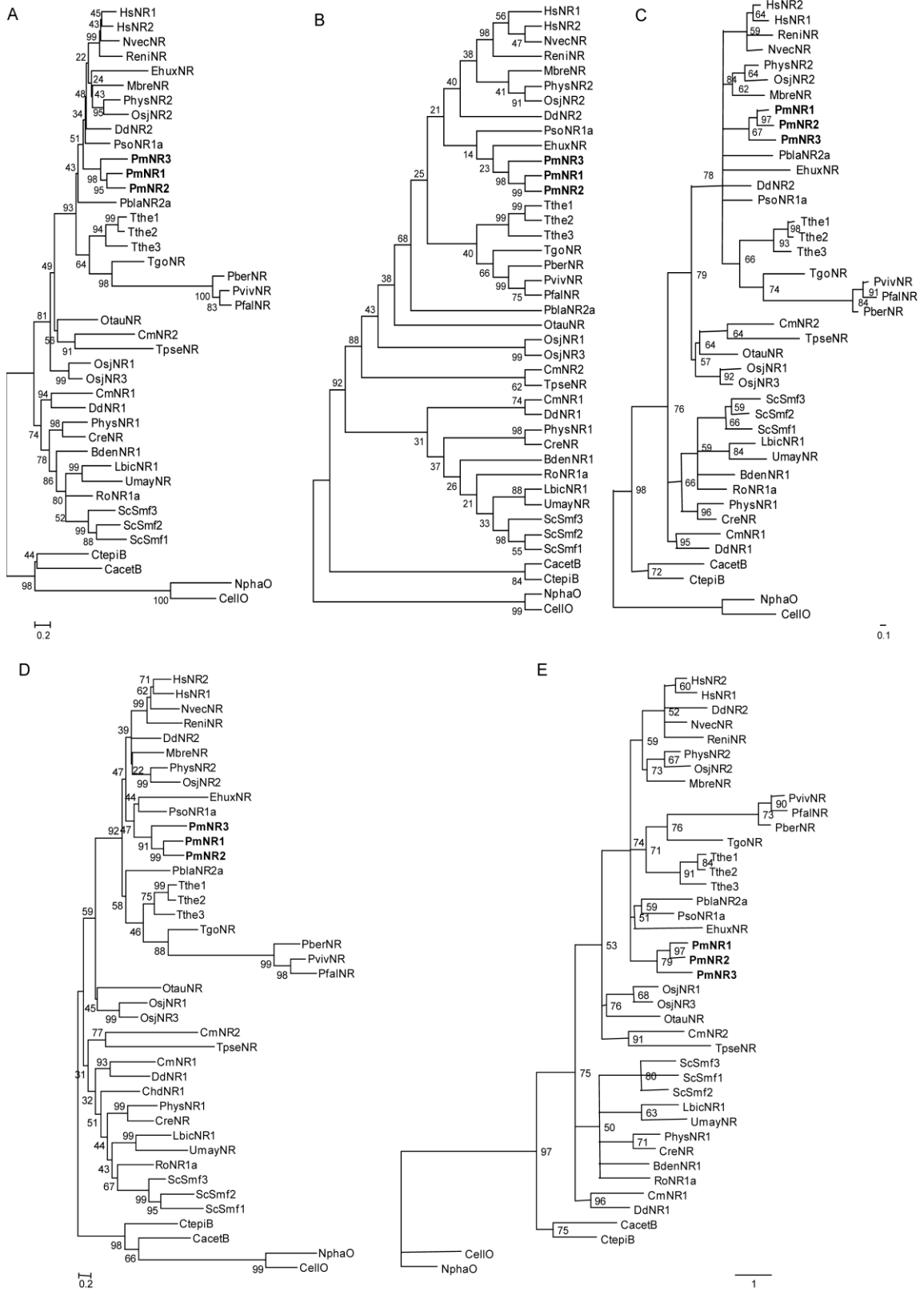


Fig. 22. Detailed phylogeny of *P. marinus* Nramp homologs (PmNramp1-3) demonstrates they belong to the Nramp Archetype II group.

A. The dendrogram presented was generated as described in Fig. 20 but without the molecular clock assumption, and using additional sequences which showed more significant disparity in amino acid composition bias (Archetype Nramp, type II: PfaNR, *Plasmodium falciparum*, PvivNR, *P. vivax*, PberNR, *P. berghei*, TgoNR, *Toxoplasma gondii*, EhuxNR, *Emiliana huxleyi*; Prototype Nramp: UmayNR, *Ustilago maydis*; Outgroup: NphaO). B & C. Dendrograms generated using the same set of sequences and parsimony-informative aligned sites as in (A), by implementation of Maximum Parsimony (B) and Maximum Likelihood (C) approaches. D & E. Dendrograms generated using full-length sequences (same set as (A-C), 1136 sites) and a gamma distribution shape parameter = 1.0; *D*, Minimal evolution; *E*, Maximum Likelihood. Scales indicate the number of amino acid substitutions per site.

Analysis of *Perkinsus* Nramp1-3 gene evolution

Closer examination of PmNramp sequence variation was undertaken to address specifically the possibility of functional divergence between PmNramp3 and PmNramp1 and/or 2. Regarding the closely related *PmNramp1* and *PmNramp2* genes, analyses of the relative abundance of synonymous and nonsynonymous substitutions in codon-by-codon pairwise sequence comparisons showed that the hypothesis of strict-neutrality could be rejected ($d_N - d_S = -5.554$, $p=0.000$ using pairwise deletion, and $d_N - d_S = -6.264$, $p=0.000$ for complete deletion) in favour of the alternative hypothesis of purifying selection ($d_S - d_N = 5.45$, $p=0.000$ for pairwise deletion and $d_S - d_N = 6.056$, $p=0.000$ for complete deletion). Second, Tajima's test of relative rate of exchange between aligned sequences supported the molecular clock hypothesis, i.e., similar evolutionary rates for *PmNramp1* and 2 genes (χ^2 test values of 0.89, $p = 0.346$, for nucleotide sequences, and χ^2 test values of 0.11, $p = 0.745$, for amino acid sequences). Third, estimation of the homogeneity of substitution pattern per site between aligned sequences indicated homogeneous protein sequences (Disparity index null), as well as homogeneous nucleotide sequences (Disparity index < 0.260 , with $p > 0.1$, excepted for the third position of the codons). Thus, *PmNramp1* and 2 gene sequences are homogeneous, evolving at similar rates under purifying selection that favors synonymous substitutions.

PmNramp3 sequence relationships with *PmNramp1* or 2 contrasted with the similarities between the two latter. Hence, the relative abundance of synonymous and nonsynonymous substitutions between *PmNramp3* and *PmNramp1* or 2 were similar, suggesting neutral evolution; Tajima's test of constancy of evolutionary rates between *PmNramp3* and *PmNramp1* or *PmNramp2* sequence yielded χ^2 test values respectively of

57.56, $p = 0.00000$ and 71.87, $p = 0.00000$ enabling to strongly reject the molecular clock hypothesis. In fact, *PmNramp3* sequence exhibited high counts of unique transitions and transversions (133 and 210) relatively to *PmNramp1* (86 and 85) or *PmNramp2* (77 and 77). Applying then Tajima's test to amino acid sequences confirmed different rates of evolution for *PmNramp3* compared to *PmNramp1* or 2 (χ^2 test values of 30.83, $p = 0.00000$ and 27.61, $p = 0.00000$). In addition, *PmNramp3* was distinguished from *PmNramp1* by measuring the heterogeneity of substitution pattern per site in pairwise sequence alignments with *PmNramp2*. The disparity index between *PmNramp3* and 2 was independent of the third codon position, and it was also significant using the protein sequences (0.449, $p = 0.019$), while borderline non-significant heterogeneity was detected between *PmNramp3* and *PmNramp1* protein sequences, or between the mRNA sequences when using only the two first codon positions.

Detailing evolutionary patterns of *Perkinsus* Nramp1-3 genes domains

These results obtained using full-length sequences suggested that purifying selection and more or less ancient gene duplications, yielding first *PmNramp2* and 3, and then *PmNramp1*, may explain the observed sequence relationships of *PmNrams*. To validate our interpretation, Tajima's rate test was employed to analyze less variable subsets of sites, spanning either the four TMS believed to constitute the transmembrane cations core conductive pathway (TMS1, 3, 6, 8) or the five successive TMS constituting a domain repeat (N-terminal: 1-5, and C-terminal: 6-10) but excluding the more variable extra-membranous regions (N- and C-termini as well as the extra-loop 7/8). These sets of sites differ by increasing sequence divergence, respectively ~ 25, 42 and 50 % and notably, in the proportion of sites divergent in all three sequences (~5, 9 and 19 %).

These amino acid data sets showed fairly constant proportions of isoform-specific sites, similar for *PmNramp1* and 2, and about two-fold more for *PmNramp3*.

Heterogeneous substitution patterns per site were found among *PmNramp1* and 2 (N-terminal domain, 0.232, $p = 0.036$) and between *PmNramp2* and 3 (C-terminal domain, borderline significance, 0.299, $p = 0.055$). Significant evolutionary rate variations were detected with the most divergent data sets (C-terminal domain) and involved *PmNramp3* and *PmNramp1* or 2 (χ^2 test values of 7.41, $p = 0.00649$ in both cases).

Corresponding nucleotide sequence analyses revealed for the most conserved data sets (predicted translocation pathway and N-terminal domain) homogeneous substitution patterns per site, and purifying selection between *PmNramp2* and 3 (respectively, $d_S - d_N = 2.272$, $p=0.012$ and $d_S - d_N = 2.042$, $p=0.022$, for pairwise deletion); purifying selection between *PmNramp1* and 2 was also confirmed with the three data sets (the predicted pore and both N- and C-domains, respectively, $d_S - d_N = 3.064$, $p=0.001$, $d_S - d_N = 2.357$, $p=0.010$ and $d_S - d_N = 2.128$, $p=0.018$) as expected from full-length sequence analyses. Lastly, Tajima's evolutionary rate tests showed significant pairwise differences with all data sets only when *PmNramp3* was tested (predicted pore: χ^2 test value of 9.56, $p = 0.00199$ vs. *PmNramp1* or 2; N-terminal domain: 10.64, $p = 0.00111$ vs. *PmNramp1* or 11.92, $p = 0.00055$ vs. *PmNramp2*; C-terminal domain: 16.56, $p = 0.00005$ vs. *PmNramp1* and of 14.3, $p = 0.00016$ vs. *PmNramp2*).

Overall the results of domain analyses enable us to conclude that the four TMS forming the predicted translocation pathway are submitted to strong purifying selection, which was detected by comparing *PmNramp2* and *PmNramp1* or *PmNramp3* coding sequences and demonstrating homogeneous substitution patterns per site between all

three gene and protein sequences; only *PmNramp3* nucleotide sequence showed differences in evolutionary rate compared to *PmNramp1* or *PmNramp2*. Regarding the continuous N-terminal domain that spans TMS 1-5, purifying selection was still detected in comparisons using *PmNramp2* coding sequence, but at the amino acid level, distinct substitution patterns per site were noted between PmNramp1 and 2 as well as almost significant evolutionary rate difference between PmNramp1 and 3. Considering the C-terminal domain without the extra-loop 7/8, significant variation in nucleotide substitution pattern was found between *PmNramp2* and the two other genes; the corresponding variation in amino acid disparity index between PmNramp2 and 3 was borderline significant, while PmNramp3 exhibited significantly different amino acid substitution rate, though the evolution of this protein sequence remained neutral.

We therefore conclude that the presence of three PmNramp genes is consistent with sequential gene duplications of PmNramp2 yielding first PmNramp3, and more recently PmNramp1. PmNramp3 is the most divergent homolog among the three PmNramp isotypes, but this divergence may not be related to functional diversification. The yeast complementation data are consistent with the phylogeny test since both PmNramp1 and PmNramp3 function as iron transporter. The functional data reinforce the proposed PmNramp1 homologous structural model, and together with the molecular evolutionary gene analyses indicating that the hydrophobic core of PmNramp paralogs remained constrained by purifying selection, suggest that PmNramps function as proton-dependent iron transporters.

CHAPTER 4 FUNCTIONAL CHARACTERIZATION OF THE PMNRAMP ISOTYPES

SUMMARY

Yeast mutant strain *fet3fet4* has defect in both high- (*fet3*) and low-affinity (*fet4*) iron transporters. Yeast complementation assay using *fet3fet4* indicates iron uptake activity of PmNramp1. PmNramp2 and PmNramp3 cannot complement *fet3fet4* growth in low iron conditions. Expression of PmNramp isotypes in yeast was investigated. It was found out that PmNramp2 cannot be transcribed in yeast. PmNramp3 protein was expressed in a much lower level compared to PmNramp1. Subcellular localization of PmNramp1 by IFA showed a cell peripheral localization, which is absent in PmNramp3 immunostaining. A PmNramp1 and PmNramp3 chimera made by substituting the predicted PmNramp3 N- and C-termini with the corresponding part of PmNramp1 was expressed in the peripheral of yeast cells as accessed by IFA. Chimeric PmNramp3 was able to complement *fet3fet4* growth in the medium without iron supplement, indicating iron transport function of PmNramp3.

INTRODUCTION

Knowledge about Nramp transport substrate comes from studies performed in different expression systems: 1) *Xenopus* oocyte expression system [247] 2) yeast complementation assay [247, 248] 3) mammalian cell lines [165, 249] 4) knockout or knockdown of endogenous genes [250]. There are pros and cons in the three different

methods. *Xenopus* oocyte electrophysiology studies are relatively expensive and require dedicated facilities to hold the animals. Demonstration of metal accumulation in the oocyte, in most of the case by measuring of radioactive isotope is needed after the electrophysiology studies. The advantage is that several metal substrates can be tested by exposing mRNA-injected oocytes to the substrate of interest. Yeast complementation is a low-cost one-step experiment compared to *Xenopus* oocyte electrophysiology study; however, a particular mutant strain is required for particular substrate at most cases. Mammalian cell lines are usually used in iron uptake study in virtue of fluorescence dye calcein that can get into the live cell and be quenched after binding to iron. It is possible that exogenous Nramp from another species cannot be expressed properly in heterologous systems, which make knockout/knockout of Nramp a valuable strategy if those molecular tools are available.

In this chapter, yeast complementation assays were performed to test the potential iron and manganese transport activity of PmNramp isotypes. The expression and function of PmNramp isotypes in yeast were investigated in details.

MATERIALS AND METHODS

Yeast strains and plasmid

Yeast mutant *fet3fet4* was kindly provided by Dr. Eide (University of Wisconsin-Madison, USA) and Dr. Jones (Queensland Institute of Medical Research, Australia).

This yeast strain grows poorly under iron-limiting conditions because it has mutated low-affinity and high-affinity iron transporters (MAT α ; *ura3*; *trp1*; *leu2*; *his3*; *can1*; *fet3*::HIS3; *fet4*::LEU2) [251, 252].

For the test of manganese transport activity, the yeast mutant *smf1smf2* was provided by Dr. Gros (McGill University, Canada). *Smf1smf2* mutant cannot survive EGTA challenge in submillimolar concentration under oxidative stress since the high-affinity manganese transporter is inactivated (MATa *ura3-52 leu2-3 -112 gal2 SMF1::LEU2, SMF2::LEU2*) [253]. It also grows poorly in alkaline medium.

To express PmNramp isotypes in yeast, the corresponding CDS with HA tag in C-terminus was cloned into the *NotI* site of the expression vector pFL61 (a gift from Dr. Jones, Queensland Institute of Medical Research, Australia), which has an active yeast GPK (glycogen phosphorylase kinase) promoter.

Culture and transformation of yeast cells

Fet3fet4 yeast cells were first streaked onto YPAD agar (10g/L Bacto yeast extract, 20g/L Bacto peptone, 20g/L D-glucose, 40mg/L adenine hemisulphate, 20g/L Bacto agar) supplemented 50 μ M FeCl₃. After 3 to 4 days of growth, yeast cells from the agar medium were inoculated into YPAD liquid medium with 50 μ M FeCl₃ and incubated over-night at 30°C with shaking (250 rpm). Yeast was transformed using lithium acetate method [254] and selected for growth on synthetic-defined (SD) medium (6.7 g/L yeast nitrogen base, 20g/L D-glucose, 20 mg/L L-tryptophan, 20 mg/L L-histidine, 30 mg/L L-leucine, 20 mg/L methionine, 20 mg/L adenine hemisulphate, 20 g/L Bacto agar, pH 5.6), which is appropriate auxotrophic requirements.

Transformation and expression of PmNramp isotypes in transformed yeast

Total DNA was extracted from transformed yeast cells using the QIAamp tissue kit (Qiagen) following the manufacturer's instructions. Extracted DNA was used for the

confirmation of the vector existence by PCR using PmNramp isotype specific primers and pFL61 vector primer (Table 8). Total RNA was extracted from the transformed yeast cells with the RNeasy Mini Kit (Qiagen). RT-PCR was performed to examine the expression of PmNramp mRNA in yeast using gene specific primers (Table 2). Yeast cells were ruptured by glass beads. The enriched membrane fraction of yeast protein was prepared by 1% Triton X100 in Tirs buffer and SDS sample buffer for Western blot to test the expression of PmNramp protein using monoclonal anti-HA antibody 3F10 conjugated with biotin (Roche Applied Science, Indianapolis, IN) and streptavidin-peroxidase (Sigma).

Table 8. Primers used in N- and C-terminus swapping and yeast complementation

Primers	Sequences	PCR reactions
pFL61F	5'- GTTTTTCAAGTTCTTAGATGC-3'	Screening for yeast transfectants
pFL61R	5'- AGCGTAAAGGATGGGG-3'	
<i>Bam</i> HI-PmNR3core	5'- GGATCCCGTTACGCCGGCCGGGATG-3'	Terminus swapping in PmNramp3
<i>Sph</i> I-PmNR3coreR	5'- GCATGCCAACTCAGACTGCACTGCTG-3'	
<i>Bam</i> HI-PmNR2core	5'- GCATGCCAACTCAGACTGCACTGCTG-3'	Terminus swapping in PmNramp2
<i>Msc</i> I-PmNR2coreR	5'- TGGCCAATCTAAGGGGACCAGTGTAG-3'	
<i>Bam</i> HI-PmNR1core	5'- GGATCCAAGTATGCTGGTCCTGGTTG-3'	Insertion of <i>Bam</i> HI site in PmNramp1
<i>Bam</i> HI-PmNR1coreR	5'- GGATCCCTTAGCACCGGGCGGGTCAA-3'	

Construction of chimeric PmNramp2 and PmNramp3

To test the metal transport capacity of PmNramp2 and PmNramp3, their N- and C-termini were swapped with counterparts of PmNramp1 (Fig.23). For N-terminus swapping, a *Bam*HI restriction site was introduced by PCR in the coding regions of all the three isotypes, using the primers indicated in Table 8. To verify that introducing of this restriction site dose not perturb PmNramp1 function, PmNramp1 with the *Bam*HI site was included as a control in yeast complementation assays. For C terminus swapping, an *Msc*II site was identified upstream of PmNramp1 TMS12, and was introduced to the corresponding positions in PmNramp2 by PCR with the primers listed in Table 8. An

SphI site was found in the same proximal region of PmNramp1. For the replacement of PmNramp3 C-terminus, the *SphI* site was added into PmNramp3 CDS. The graphic demonstrations about domain swapping are in Fig. 23. Despite the changes in amino acid sequence of PmNramp2 and PmNramp3 after domain swapping due to insertion of the restriction sites, the core structures from TMS1 to TMS10 were kept intact in both molecules (Fig. 23).

Fig. 23

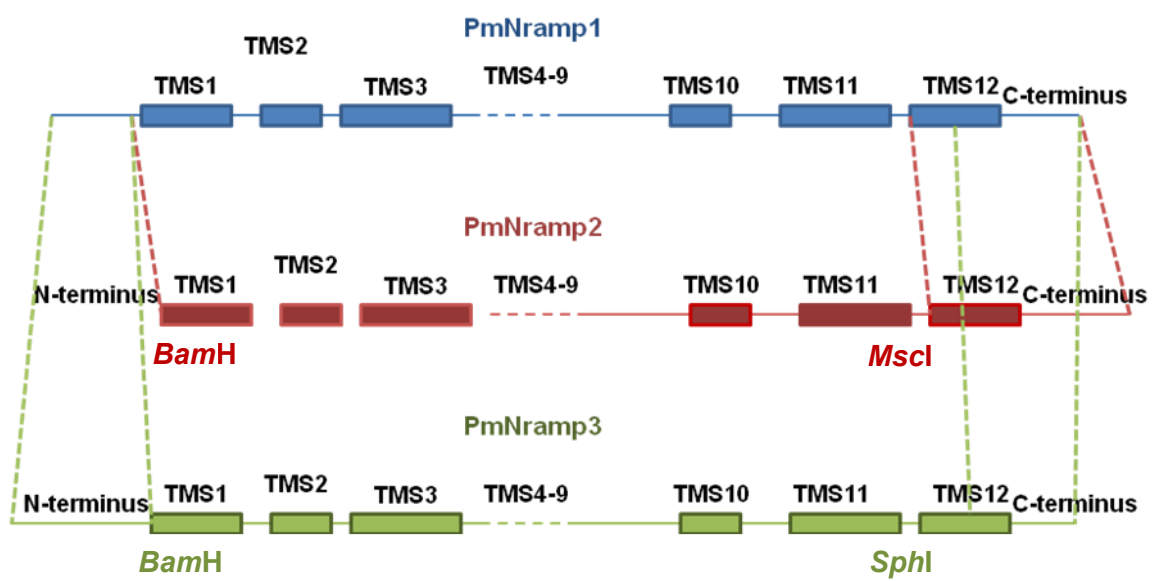


Fig. 23. N- and C-termini swapping of PmNramp1 to PmNramp2 and PmNramp3

A *Bam*HI site was introduced to PmNramp2 (PmNR2swap) and PmNramp3 (PmNR3swap) for N- terminal swapping. The same *Bam*HI site was introduced to PmNramp1 (PmNR1swap) to verify that the mutation does not perturb PmNramp1 activity. For C-terminal swapping, an *Msc*I site and an *Sph*I site in PmNramp1 was used for PmNramp2 and PmNramp3 domain swapping respectively. The core structures formed by TMS1 to TMS10 were kept intact.

IFAs to detect PmNramp protein expression in *fet3fet4*

Fet3fet4 yeast cells transformed with PmNramp1, PmNramp3 and chimeric PmNramp3 were harvested for IFAs. Cells were fixed in 4% formaldehyde in SD medium at room temperature for 30 minutes. After that, yeast cells were centrifuged at 3000 g for 5 minutes and washed three times in 0.1 M potassium phosphate buffer containing 1.2M sorbitol (pH 7.5). In the same buffer, yeast cell wall was digested by 50 µg/ml lyticase (Sigma) at 30°C for 5 hours. Cells were centrifuged, re-suspended in PBS with 3% BSA, applied to the slide wells (Thermo Scientific), and allowed to sediment for 40 minutes. Cell were dehydrated 6 minutes in cold methanol (-20 °C), washed in cold acetone (-20 °C) for 10 seconds, and dried at room temperature. IFA was performed as follows. Every sample is incubated with 3% PBS-BSA as blocking agent in room temperature for 1 h. Primary antibody mouse anti-HA, monoclonal 16B12 (Invitrogen) was added into 3% PBS-BSA in 1:100 dilution and incubated with every sample for 1 h at room temperature. After three washes in PBS for 5 minutes, secondary antibody (goat anti-mouse FITC conjugated) (Sigma) was added into 3% PBS-BSA in 1:1000 dilution and incubated in dark for 1h at room temperature. After three washes in PBS for 5 minutes, samples were stained with DAPI (Invitrogen, Carlsbad, CA) in 1:1000 dilution for 10 minutes followed by 3 washed in PBS. ProLong Gold antifade reagent (Invitrogen) was applied onto each sample as the mounting solution, and the slide was stored in dark at 4 °C. The samples were examined using Nikon Eclipse E800 fluorescence microscope, and images of the cells were taken with SPOT RT2540 camera (Diagnostic Instruments, INC., Sterling Heights, MI)

Yeast complementation assay of transformed *fet3fet4*

Complementation experiments in *fet3fet4* mutant were performed following methods of Eide and colleagues [252]. The *Arabidopsis thaliana* ferrous iron transporter (AtIRT1) [255] known from previous yeast complementation assays to be an efficient Fe²⁺ transporter [248], was incorporated into pFL61 vector (gift from Dr. Jones, Queensland Institute of Medical Research, Australia) and was used as positive control. As a negative control, yeast was transformed with pFL61 vector alone.

Transformed yeast was grown in SD medium supplemented with 50 µM FeCl₃ over night. Yeast cultures were adjusted to OD=1.0 measured by UV- Visible spectrophotometer (Shimadzu, UV-1601). 3 µl of yeast cultures diluted 1, 10, and 100 times was pipette onto SD agar medium supplemented with 50 µM, 20 µM and 0 µM FeCl₃, and incubated at 30 °C. After 5 days of incubation, the pictures of the agar plates were taken using Gel Logic 200 Imaging System (Kodak). For iron uptake assay in liquid medium, 100 µl yeast cultures with OD 1.0 were seeded into 30 ml fresh SD medium with 20 µM FeCl₃ and incubated at 30 °C with shaking (250 rpm). OD values were measured at different time points using UV-visible spectrophotometer in triplicates.

Complementation assay of yeast *smf1smf2*

The same expression vector pFL61 was used for expression of PmNramp isotypes in *smf1smf2*. The transfection procedures were the same as mentioned above. The yeast Nramp homolog Smf1 was incorporated into pFL61 vector and used as a positive control. Transformed cells were grown on YPD (2% bacto-peptone, 1% yeast extract, 2% dextrose) supplemented with 50 mM Na-Mes (pH 6), 0.5 mM methyl viologen (Sigma)

and 3mM EGTA. For complementation of the *sm1smf2* mutant on alkaline solid medium, transformed yeast cells were placed on YPD medium adjusted to pH 7.9 by 50 mM Tris-Cl.

RESULTS

Expression of PmNramp isotypes in *fet3fet4*

PCR of genomic DNA extracted from transformed *fet3fet4* showed amplification of PmNramp-containing pFL61 vectors (Fig. 24 A). RT-PCR using PmNramp isotypes specific primers confirmed the transcription of PmNramp1 and PmNramp3 mRNA (Fig. 24 B), but not PmNramp2 RNA. Western blot using anti-HA monoclonal antibody picked up expressed PmNramp1-HA and PmNramp3-HA (Fig. 24 C). As shown in the results, only PmNramp1 and PmNramp3 were expressed as protein, however, PmNramp1 protein was expressed in a higher level than PmNramp3. The predicated sizes for PmNramp1 and PmNramp3 are 60.7 KDa and 60.0 KDa respectively (http://expasy.org/cgi-bin/pi_tool). While the indicated sizes in Western blot (Fig. 24 C) for PmNramp3 is much bigger than 60.0 KDa, which can be the result of anomalous migration of membrane proteins in SDS-PAGE. The multiple bands and the smear in the blot for PmNramp1 can be also due to the anomalous migration and potential carbohydrate modification of the protein.

The expression of PmNramp proteins in yeast cells were tested by immunofluorescence assays (Fig. 24 D). Consistent with the western blot results, PmNramp3 is expressed, but not in a high level as PmNramp1. PmNramp1 is localized both inside the cell and also in the peripheral. PmNramp3 did not show a cell peripheral localization, but a diffusive pattern of localization.

Fig. 24

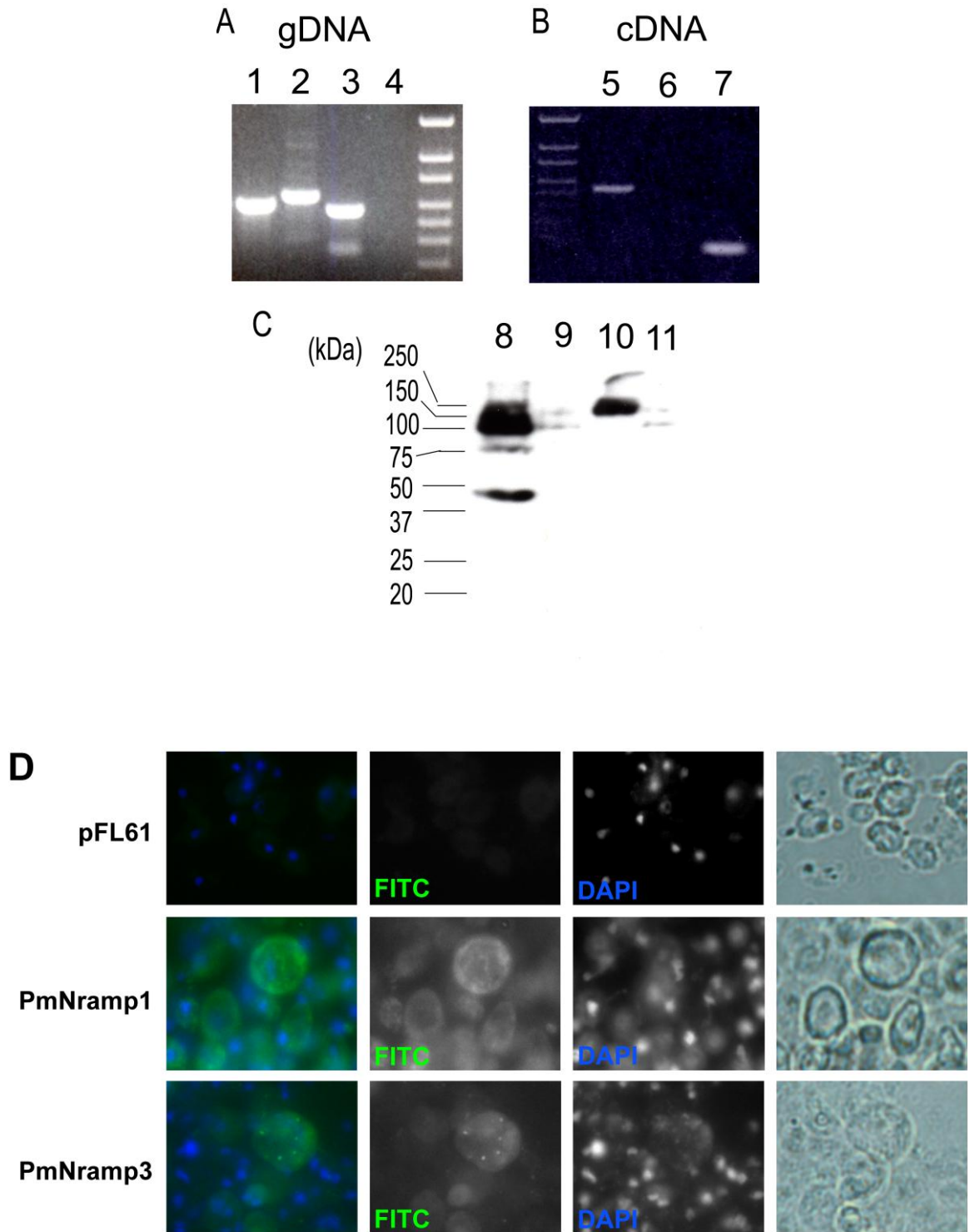


Fig. 24. Transformation and expression of PmNramp isotypes in *fet3fet4*.

A. Transformation of PmNramp isotypes in yeast. Genomic DNA (gDNA) extracted from yeast transformed with PmNramp1 (lane 1), PmNramp2 (lane 2), PmNramp3 (lane 3) full-length cDNA or pFL61 (lane 4) was used as template in PCR to confirm the presence of PmNramp containing vector in yeast cells

B. Transcription of PmNramp isotypes in yeast. RT-PCR was performed to check the expression of PmNramp1 (lane 5), PmNramp2 (lane 6) and PmNramp3 (lane 7) mRNA in yeast.

C. Western blot of PmNramp isotypes in yeast. Enriched membrane fractions were prepared from yeast transformed with PmNramp1 (lane 8), PmNramp2 (lane 9), PmNramp3 (lane 10) or pFL61 (lane 11), separated by 12% SDS-polyacrylamide gel electrophoresis, and probed by immunoblotting with the anti-HA high-affinity 3F10 antibody conjugated with biotin and streptavidin conjugated with horseradish peroxidase.

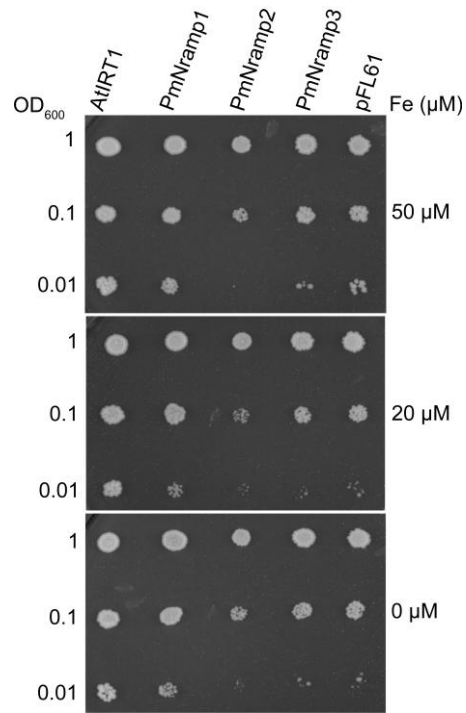
D. IFA of PmNramp1 and PmNramp3 in *fet3fet4* yeast cells. All the PmNramp isotypes were tagged with HA epitope. Monoclonal mouse anti-HA antibody and anti-mouse antibody conjugated with FITC were used to visualize PmNramp1 and PmNramp3 protein localizations in yeast cells. Nucleus positions were indicated by DAPI staining.

PmNramp1 complements the growth of *fet3fet4*

In SD agar medium supplemented with 0 and 20 μM FeCl_3 , *fet3fet4* expressing PmNramp1 grows better than yeast that contains the empty cloning vector (Fig. 25 A). The growth of yeast transformed with PmNramp1 entered the exponential growth much earlier than cells transformed with pFL61 vector alone (Fig. 25 B), thereby demonstrating the function of PmNramp1 as an iron-transporter.

Fig. 25

A



B

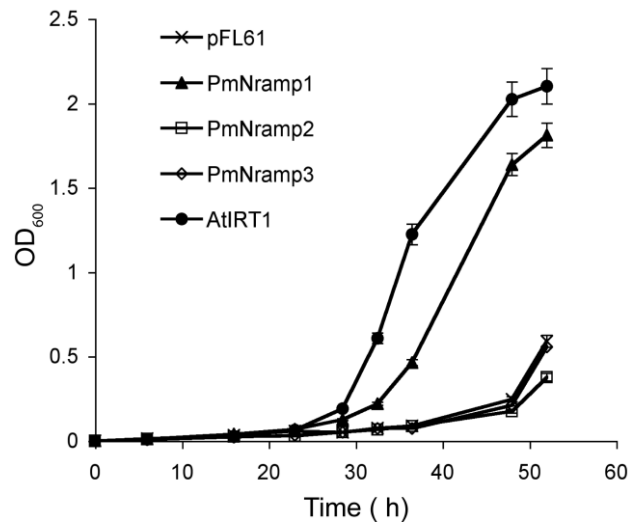


Fig. 25. Yeast complementation assay of PmNramp isotypes in *fet3fet4*

Fet3fet4 yeast cells were transformed with the three PmNramp isotypes or positive control AtIRT1, which were all inserted in the expression vector pFL61. Cells were also transformed with the empty expression vector as negative control. The transformed yeast cells were subjected to complementation assays in both agar and liquid medium. A, growth of serially diluted yeast cells after 5 days incubation at 30°C on SD medium supplemented with 50, 20, or 0 μM FeCl_3 . B, growth in liquid SD medium supplemented with 20 μM FeCl_3 as indicated by OD_{600} .

***Fet3fet4* complementation assay of chimeric PmNramp2 and PmNramp3**

Based on the previous study in Nramp protein family, the N- and C- termini of NRAMP could be closely related to the expression and localization of the protein in a heterologous system [256, 257]. Following the same line of thought, since PmNramp1 can be properly expressed in *fet3fet4*, the N- and C- termini of PmNramp1 was swapped to PmNramp2 and PmNramp3 without interrupting any of the predicted TMS1-10 (Fig. 23). The chimeric PmNramp3 was expressed in the yeast cell peripheral (Fig. 26 A), and PmNramp3 showed a significant complementation activity in both solid and liquid medium after domain swapping (Fig. 26 B, C). Chimeric PmNramp2 cannot be obtained in 4 independent transformation of yeast *fet3fet4*. The result implies that both PmNramp1 and PmNramp3 can function as iron transporters.

Fig. 26

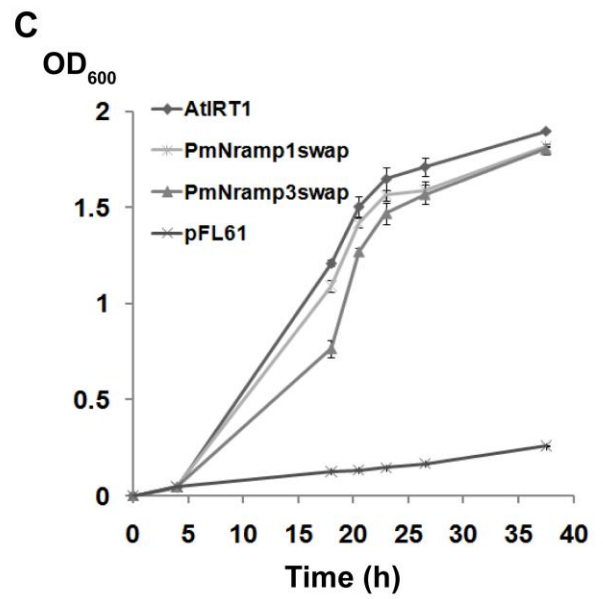
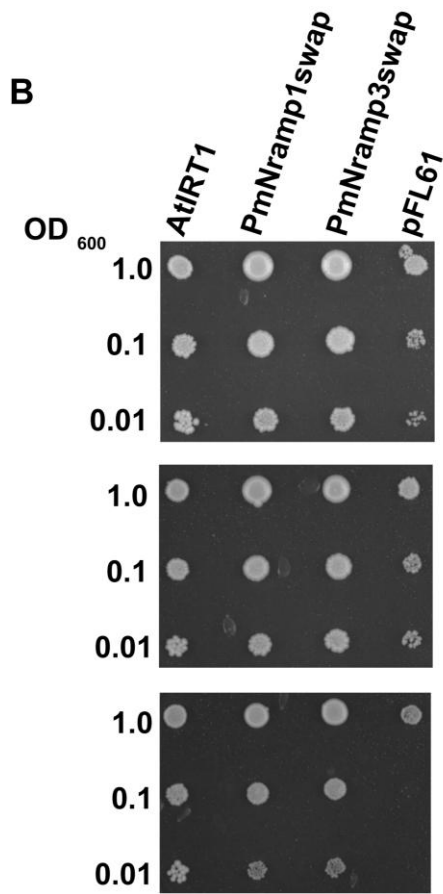
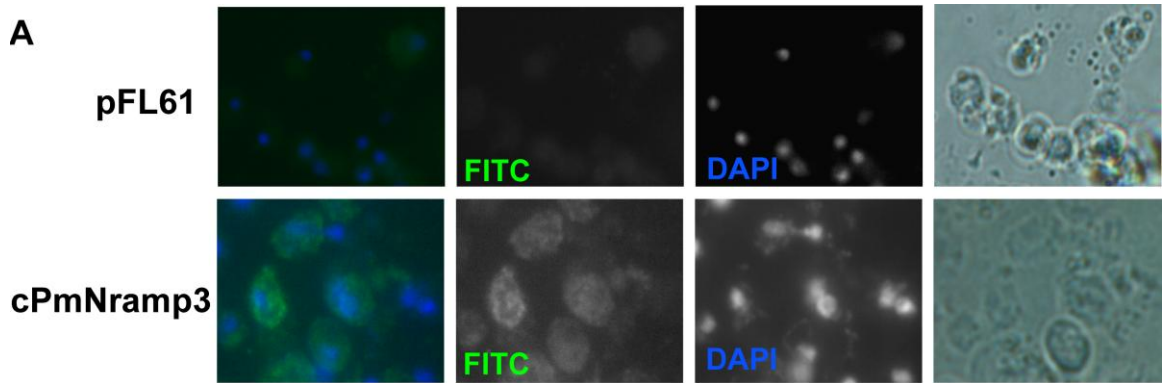


Fig. 26. Complementation of iron deficiency phenotype of yeast *fet3fet4* mutant by chimeric PmNramp3.

A, IFAs of chimeric PmNramp3. The chimeric PmNramp3 was tagged with HA epitope. Monoclonal mouse anti-HA antibody and anti-mouse antibody conjugated with FITC were used to visualize PmNramp1 and PmNramp3 protein localizations in yeast cells. Nucleus positions were indicated by DAPI staining. Yeast cells transformed with empty pFL61 vector was used as negative control.

B, Yeast complementation assays of chimeric PmNramp3 in solid medium. Serially diluted cells transformed with PmNramp1 and chimeric PmNramp3 after domain swapping (PmNramp1swap & PmNramp3swap) were incubated 5 days at 30°C on SD medium supplemented with 50, 20 or 0 μM FeCl_3 .

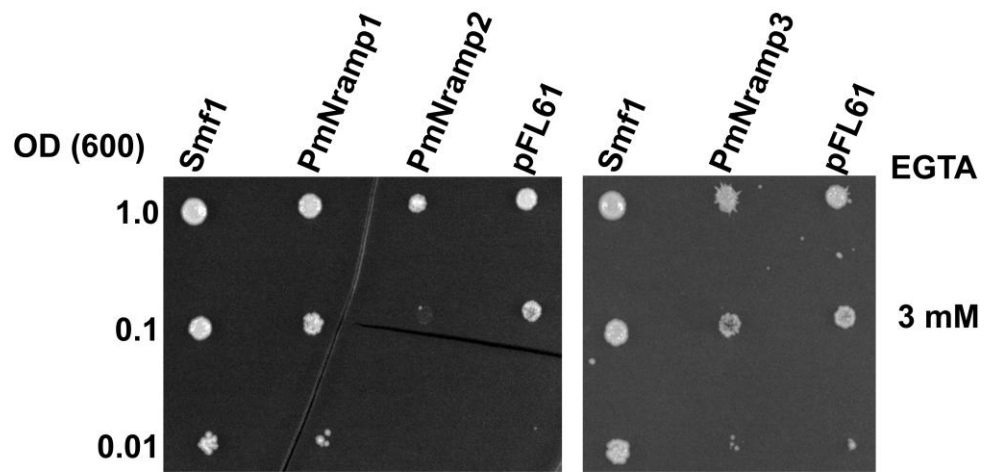
C, Yeast complementation assays of chimeric PmNramp3 in liquid medium. Yeast cells transformed with PmNramp1 and chimeric PmNramp3 were incubated in liquid SD medium supplemented with 20 μM FeCl_3 . The growth curve of the cells is indicated by OD_{600} .

Yeast complementation assay in *smf1smf2*

Under the treatment of EGTA and oxidative stress induced by methyl viologen, *smf1smf2* yeast cells transformed with PmNramp1 grow better than yeast cells transformed with empty vector, PmNramp2, and PmNramp3 (Fig. 27 A). However, there was not obvious complementation by PmNramp1 when yeast cells were grown under the alkaline condition (Fig. 27 B).

Fig. 27

A



B

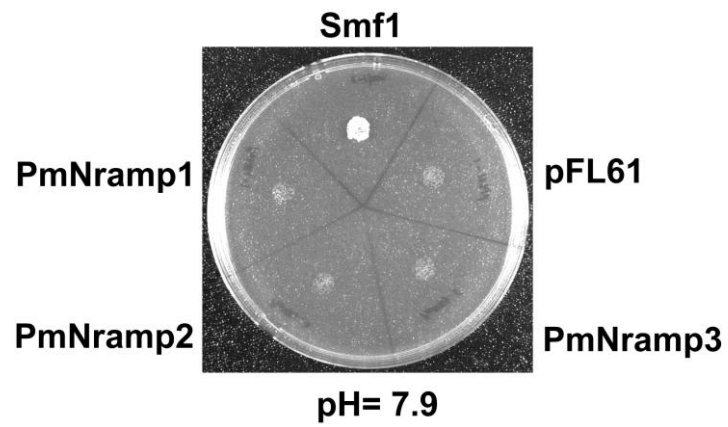


Fig. 27. Complementation assay of yeast strain *smf1smf2* in solid medium.

Smf1smf2 yeast were transformed with expression vector pFL61 containing Smf1, PmNramp1, PmNramp2 or PmNramp3 tagged with HA or pFL61 vector alone. A, Growth of serially diluted cells after 5 days at 30°C on SD medium containing 3mM EGTA. B, Growth of transformed yeast cells after 5 days at 30°C in YPD medium (pH 7.9) supplemented with 50mM Tris-Cl.

DISCUSSION

The data showing that PmNramp1 is able to complement iron transport activity in yeast constituted the first piece of information about iron uptake in *P. marinus*. The function of PmNramp1 as manganese transporter remains to be further investigated since the data in yeast complementation is not yet confirmative. Nramp homologs usually have a wide substrate range with high affinity to divalent iron and manganese [184]. Most of the Nramp homologs identified so far can transport both iron and manganese although some of them have a preferred substrate. Another heterologous expression system may be needed to further investigate manganese transport function of PmNramp1. If manganese is not a physiologically-related substrate for PmNramp1 in *P. marinus*, there are potential manganese uptake pathways. BLAST searches in *P. marinus* genome data base using amino acid sequences of yeast PHO84 and *A. thaliana* MTP11 suggest a potential low-affinity manganese transporter (GenBank Accession number XP_002781691) PHO84 [258] and a CDF (Cations Diffusion Facilitators) Metal Tolerance Proteins MTP11 (Accession number XP_002777192) that has a signature DXXXD domain for manganese transport [259].

Although PmNramp1 was able to complement iron uptake in *fet3fet4*, PmNramp2 and PmNramp3 indicate no complementation in yeast. The lack of complementation by PmNramp2 is caused by the problematic expression of the gene, and the failure of complementation by PmNramp3 is probably because the protein cannot be targeted to yeast cell surface (Fig. 24). In previous studies of Nramp function in heterologous systems, substitution of N- and C-termini with other Nramp homologs was key to improve the expression and change subcellular compartment localization. A chimera of

yeast *smf1* with mammalian Nramp2 termini was made to enable electrophysiology study in *Xenopus* oocytes [257, 260]. Based on the model of MntH [240], the hydrophobic core formed by TMS1-10 is closely related to substrate transport, and TMS11 and TMS12 may serve as anchors for the molecule. The N- and C-domain substitution strategy was adopted to circumvent the expression problem of PmNramp3. Since PmNramp1 can be expressed in yeast, a PmNramp1 and PmNramp3 chimera with an intact hydrophobic core formed by PmNramp3 TMS1-10 was generated. The chimera demonstrated an iron uptake function in *fet3fet4*. The results is consistent with the prediction by evolutionary studies (Chapter 3) that the protein sequence divergence among the three PmNramp isotypes is probably not related to the diversification of critical function elements, since PmNramp3 showing the greatest divergence in amino acid level can function as iron transporter as PmNramp1.

The functional studies in yeast systems implies the possibility that PmNramp1 may serve as the surface transporter for the uptake of environmental iron while PmNramp3 could be in charge of supply for downstream iron utilization inside the cells.

CHAPTER 5 STRUCTURAL AND MECHANISTIC STUDIES OF THE PMNRAMP ISOTYPES

SUMMARY

Homology modeling of PmNramp1 predicted the 12 transmembrane segments (TMS) typical of the archetype Nramp proteins, and showed symmetric organization of the conserved hydrophobic core (TMS1-10) in two repeated domains of inverted topology typical of several families of cation-driven transporters (including Slc5 and Slc6). The center position of the Slc11-specific triplets Asp-Pro-Gly (TMS1) and Met-Pro-His (TMS6) in a three-dimensional arrangement formed with TMS3 and TMS8 provides the mechanistic basis for iron acquisition via PmNramp1. Mutations of the residues in the central triplets located in TMS1 and TMS6 abolished the complementation of *fet3fet4* by PmNramp1. Mutants with mutations on TMS1 were expressed in a much lower level compared to wild-type PmNramp1 protein, and mutants with mutations on TMS6 showed a similar expression level. IFAs revealed that mutations on TMS6 did not change the protein localization as compared to the wild-type PmNramp1. Therefore, our data supported the critical functional roles played by the residues on TMS6.

INTRODUCTION

The function of transporters is intimately determined by their transmembrane arrangement, which enables them to carry solutes. Genetic studies using prokaryotic and

eukaryotic Slc11[♦] homologs and various topological reporters have yielded a consensus transmembrane topology placing both ends of the Slc11 hydrophobic core (TMS1-10) on the cytoplasmic side of the membrane, but some extra-membranous loops remain to be tested experimentally [188, 261-263]. The global Slc11 transmembrane topology also fits a predicted tridimensional fold, which is conserved among apparently distant families of Na⁺- and H⁺- dependent transporters showing less than 15% overall amino acid sequence identity, including Slc6, [264], Slc5, [265], Slc23, [240, 266], and Slc7 [267]. Obtaining consistent models by threading using structural templates unrelated by sequence may thus provide, even with moderate accuracy due to remote homology, good structural indication of functional significance.

Nramp homology modeling was performed by threading Slc11 sequences onto a structure representative of Na⁺-coupled amino acid transporters (Slc6), and it was tested both functionally and topologically using several Slc11-specific mutants of *E. coli* MntH [240]. Further threading using available resources and the ever expanding RCSB Protein Data Bank (PDB; <http://www.rcsb.org/>) confirmed this model, because three novel structures that were solved for members from apparently unrelated families of cation-driven transporters revealed a conserved architectural fold [265-267].

According to such conserved tridimensional structure, the Slc11 hydrophobic core comprises two domains that are direct repeats with inverted topology. The two specific triplets Asp-Pro-Gly (TMS1) and Met-Pro-His (TMS6) would occupy the central position

[♦]In topology, the terminology Slc11 is used instead of Nramp for convenient comparison to other Slc members.

and together with segments of TMS3 and TMS8, form a three-dimensional arrangement enabling directional cation symport [264-266]. The TMS1 Asp-Pro-Gly motif contributes to proton-binding and -motive force, shown by the loss of H⁺ uptake in *E. coli* MntH Asp³⁴ mutants, while the TMS6 Met-Pro-His motif mediates pH-dependent regulation consistent with requirement for *E. coli* MntH His²¹¹ for Cd²⁺ uptake at neutral pH. These two Slc11-invariant sites were accessible *in situ*, respectively to fluorescein-maleimide and N-ethylmaleimide, while three others were not, corresponding to transmembrane Asn residues that could mediate inter-helix interactions key for transport [240].

The similar structures solved for the transporters Mhp1, LeuT, vSGLT and ApcT appear to represent discrete steps in a ‘gated-pore’ transport cycle common to diverse families of cation-driven carriers, respectively open-to-out, open-to-out and ‘occluded’ by substrate and closure off from external bulk water, and open-to-in [264-267]. Hence, utilization of a cation-motive force to symport substrate may constitute the functional activity that preserved a common architecture among many families of solute carriers in absence of obvious sequence similarity. These structures also revealed an internal symmetry with two 5 TMS repeats assembled in inverted orientations placing the cosubstrates binding sites at the apex of a cavity formed in part by TMS 1, 3, 6 and 8.

In this chapter, 3D models of PmNramp1 protein were proposed by homology modeling. The 3D models provided a mechanistic basis for the iron transport activity of PmNramp1 as implied by the functional studies in Chapter 4. To test the accuracy of the models, the predicted central residues involved in substrate translocation were mutated by

site-directed mutagenesis, and the resulted mutants were tested by yeast complementation assays.

MATERIALS AND METHODS

Structural analysis of PmNramp1 by homology modeling

Tridimensional structural models were obtained as previously described [240] for the three PmNramp isotypes using either MODELLER with consensus restraints, or with the default parameters of the programs developed by the Zhang laboratory including iterative TASSER simulations (I-TASSER)[239], with the default parameters of the programs developed by the Zhang laboratory including the Local Meta-Threading-Server (LOMETS) [268], which generates 3D models by collecting consensus target-to-template alignments from 9 locally-installed threading programs, the MUlti-Sources ThreadER (MUSTER) [269], which combines sequence profile-profile alignment with multiple structural information. The PDB coordinates calculated by the different programs were used with the freeware viewer Pymol (DeLano WL: The PyMOL molecular graphics system, <http://www.pymol.org>) to visualize the 3D models.

Site-directed mutagenesis

To test the structural/functional value of the predicted model and the importance of the canonical triplets in TMS1 and TMS6 for PmNramp1 function, selected amino acid residues were mutated by site-directed mutagenesis using QuikChange II site-directed kit (Stratagene, Santa Clara, CA). The primers used for introducing the mutations are listed

in Table 9. All mutations were confirmed by sequencing the plasmids prior to the yeast complementation assay. Expression and subcellular localization of mutated PmNramp1 protein in *fet3fet4* was assessed by Western blot and IFAs

Yeast cells were ruptured by glass beads. The enriched membrane fraction of yeast protein was prepared by 1% Triton X100 in Tirs buffer and SDS sample buffer for Western blot to test the expression of PmNramp protein using monoclonal anti-HA antibody 3F10 conjugated with biotin (Roche Applied Science, Indianapolis, IN) and streptavidin-peroxidase (Sigma). IFAs were performed as described in Chapter 4.

Table 9. Site directed mutagenesis of PmNramp1

	TMS	Mutations	Primers
Mut1	TMS1	Asp76Glu	5'- CATTGGCCTATCTCGAACCTGGTAATTTAGAAGCCG -3'
Mut2	TMS1	Gly78Ala	5'- CATTGGCCTATCTCGATCCTGCTAATTTAGAAGCCG -3'
Mut1&2	TMS1	Asp76 Glu+ Gly78Ala	5'- CATTGGCCTATCTCGAACCTGCTAATTTAGAAGCCG -3'
Mut3	TMS6	Met250Ala	5'- GGC GCAGTTATTGCTCCGCATAACCTCTACCTGCAC -3'
Mut4	TMS6	His252Tyr	5'- GGC GCAGTTATTATGCCGTATAACCTCTACCTGCAC -3'
Mut3&4	TMS6	Met250Ala + His252Tyr	5'- GGC GCAGTTATTGCTCCGTATAACCTCTACCTGCAC -3'

RESULTS

Functional features predicted from protein sequence structural modeling analysis ♦

Multiple alignments of the sequences encoding the PmNramps and human Nramp2 proteins (Fig. 28) show residue conservation predominantly in the Slc11

♦ This part of result was generated through the collaboration with Dr. Mathieu F. M.

hydrophobic core and invariant residues forming clusters in areas corresponding to the TMS1-10. This conservation suggests that PmNramps may function as transporters which complete transmembrane (re)arrangements to carry solutes by using energy.

Fig. 29 shows the best models obtained by threading PmNramp1 sequence on available PDB templates, which detail alternating conformation states presumed to affect PmNramp1 TMS1, 3, 6, and 8 during metal uptake activity, based on the solved structures of Mhp1 [266] and vSGLT (*Vibrio parahaemolyticus* sodium/galactose symporter) [265]. An open-to-out conformation would allow cation cosubstrates to reach their translocation site, approximately in the middle of the plasma membrane and involving the Slc11-specific residues Asp-Pro-Gly (TMS1) and Met-Pro-His (TMS6) as well as other residues from TMS3 and 8. After the PmNramp1 isomerisation, an open-to-in conformation would enable the release on the other side of the membrane of the cation solutes. As shown in Fig. 28, clusters of residues invariant among PmNramps are found along these TMS predicted to line a central transmembrane aqueous translocation pathway (TMS1, 3, 6, 8) supporting their functional role.

The sequence of the “conserved transport motif” (indicated by dash line, Fig. 28) is now predicted as integral to TMS8 in the tridimensional Slc11 model structure obtained by threading [240, 263]. Such “conserved transport motif” was initially proposed to form a cytoplasmic re-entrant loop, situated immediately downstream of a shorter TMS8, and predicted to contribute to cations selection by analogy with the “pore region” of K⁺ channels and glutamate and GABA transporters [270]. This suggestion was re-evaluated because i) the “pore region” of the GABA and serotonin transporters corresponds in fact to the TMS8 in LeuT-based models [271, 272], and ii) indeed, the

GABA transporter “pore region” was demonstrated experimentally to form a transmembrane helix lining the aqueous translocation pathway [271].

Fig. 28

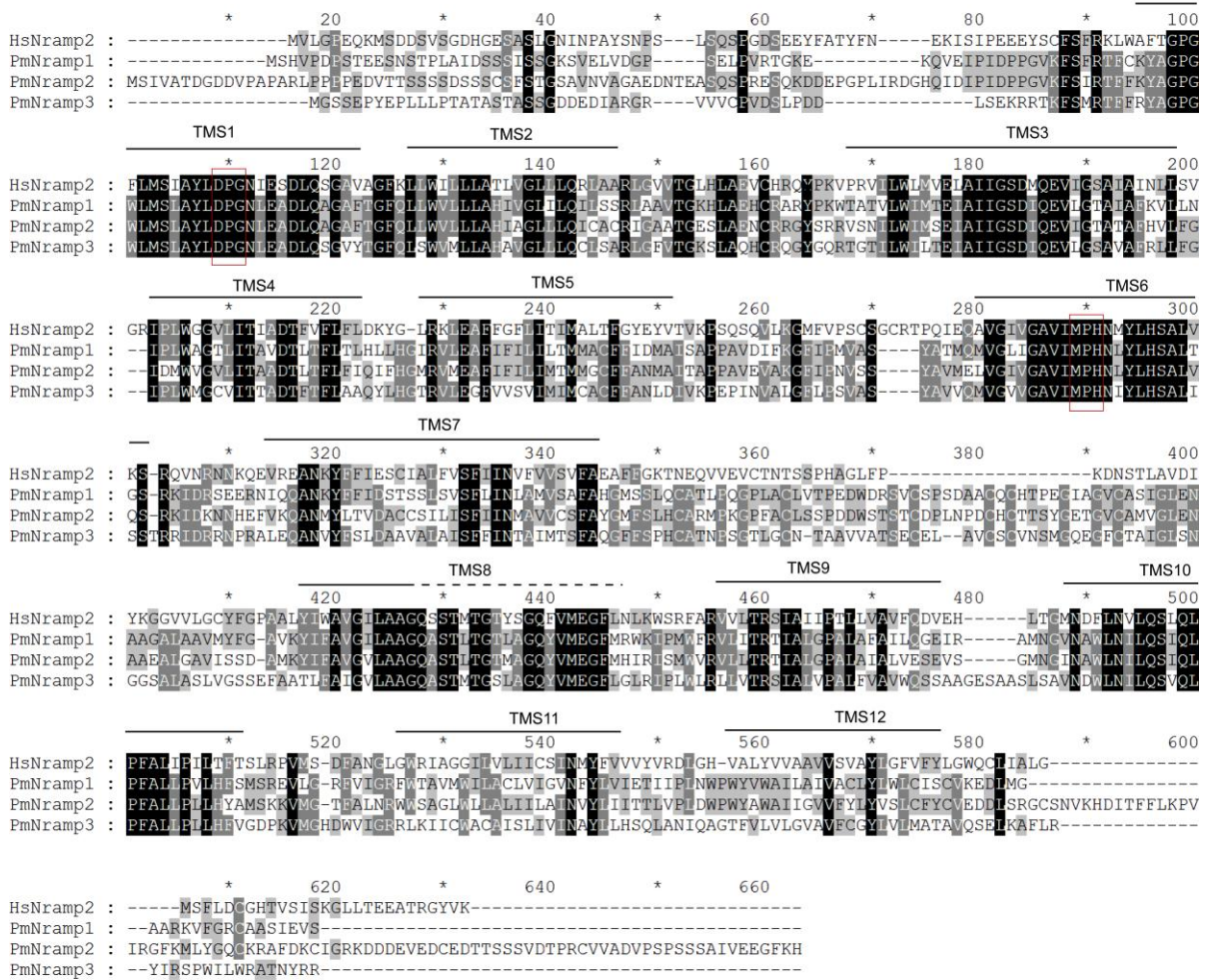


Fig. 28. Display of predicted structure by alignment of PmNramp isotypes with human NRAMP2.

Amino acid sequences alignment of human NRAMP2 with the three PmNRAMP isotypes. The predicted TMS are annotated. The conserved “transporter signature motif” is indicated by dash line. The triplets in TMS1 and TMS6 were indicated by red boxes. The alignment was generated using Mega 4.0 [194, 195] and displayed with GeneDoc [196]. Identical residues were highlighted at three cutoffs (50, 75 and 100 %).

Fig. 29

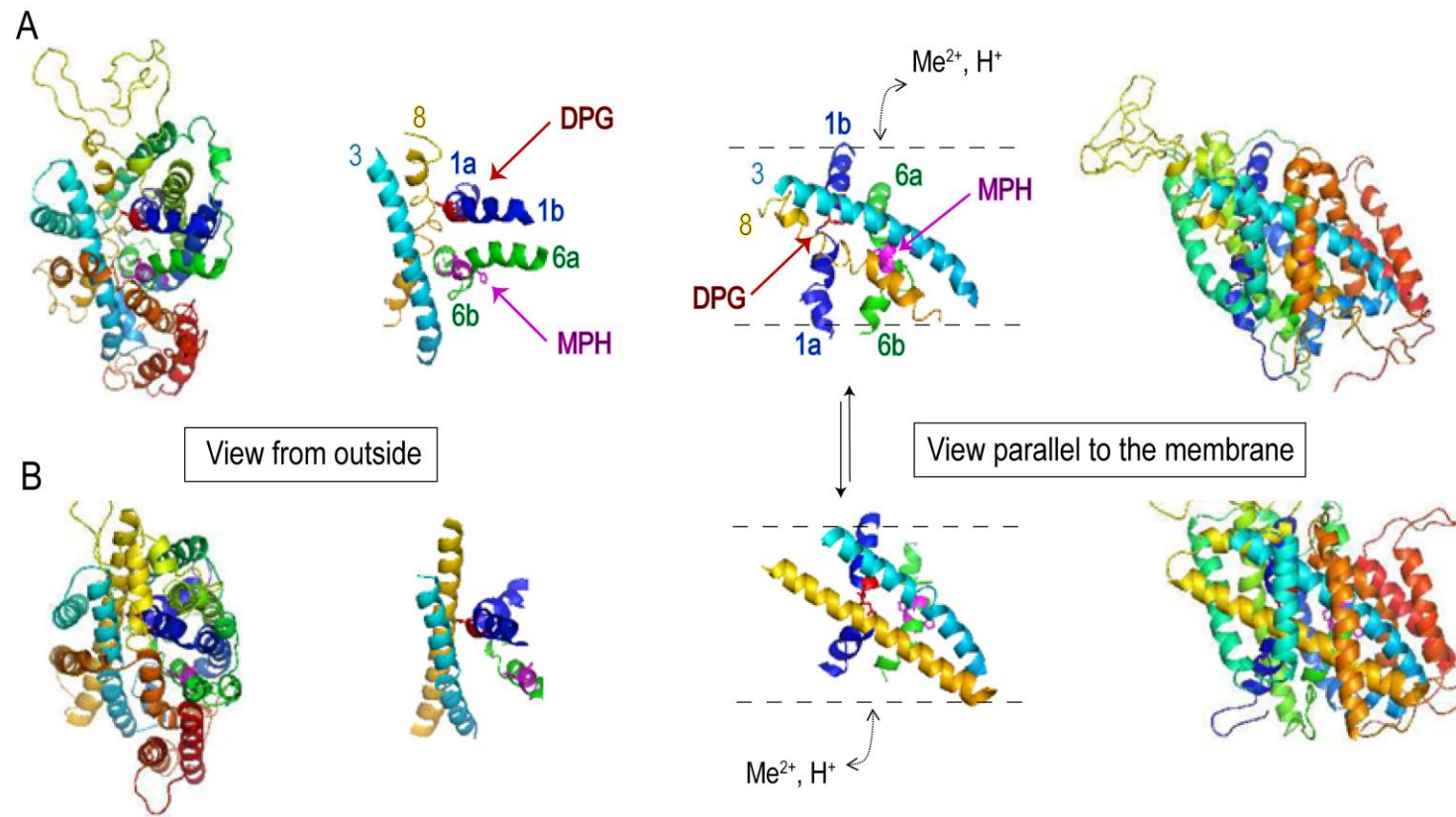


Fig. 29. Hypothetic model for transmembrane symport of divalent metals and protons via PmNramp1.

A short version of PmNramp1 (Pm1_NCD, 485 residues; VKFSF... EDLMG) was used to generate alignments that mapped PmNramp1 residues to homologous sites in candidate template crystal structures, using the parameters provided by the developers of multiple threading approaches, and models generated by two different approaches were compared. The models shown were derived either from *Microbacterium liquefaciens* nucleobase-cation- symport1 transporter, in open-to-out conformation (A), or from the *Vibrio parahaemolyticus* sodium/galactose symporter, in open-to-in conformation (B). Two views are presented for each model as indicated, one from the external surface (outside) and one parallel to the membrane with the TMS 4 and 9 in front. For each view, either the 485 residues structure is shown or only the residues that constitute the TMS1, 3, 6 and 8. A possible pathway of metal and proton symport is outlined.

Site-directed mutagenesis of PmNramp1 predicted functional residues

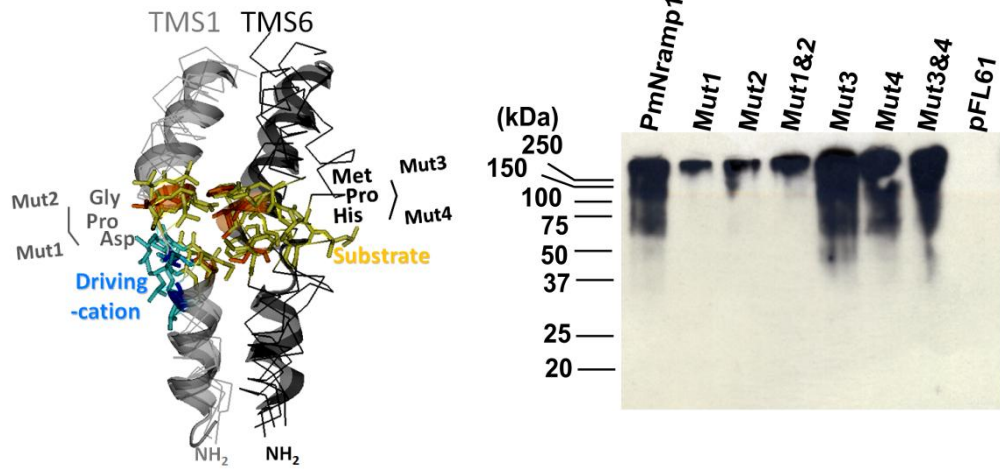
A multiple alignment allowing flexibilities was obtained for the X-ray structures of 5 cation-driven transporters with inverted symmetry, which represent distinct intermediates in a conserved transporter cycle: 2 open to out, one occluded from both sides and 2 open to in (respectively, Mhp1, LeuT, BetP, SGLT1 and ApcT). Though these X-ray structures represent distant families of transporters, superposition demonstrates remarkable spatial conservation: a common core spanning ~200 equivalent positions (e.p.) and 3.4 Å overall Root Mean Square Deviation (RMSD). The RMSD is not distributed homogeneously along the 10TMS hydrophobic core and for instance, TMS1 exhibits remarkable 3D conservation while the structure of TMS6 apparently evolved with less constraint (Fig. 30 A, left panel). It seems there is a functional correlate as LeuT (Slc6) TMS1 interacts with both the driving cation (dark blue sticks) and substrate (orange sticks) and TMS6 only binds the substrate (orange sticks). One speculation is that TMS6 evolved more in relation to different substrate geometries and TMS1 coupled of the cation-driving force and substrate translocation pathway. The triplets targeted for mutagenesis represent candidate substrate binding contacts both on TMS1 (DPG, Mut1, 2) and TMS6 (MPH, Mut3, 4).

Mutation of the targeted amino acids in TMS1 and TMS6 abrogate PmNramp1 iron uptake activity in the yeast mutant *fet3fet4*. The loss of complementation resulted from both single and double mutations on each of the TMS (Fig. 30 C, D). Inspection of protein expression levels of the mutants tested showed that mutations in TMS1 impaired PmNramp1 expression in yeast, while mutations in TMS6 preserved PmNramp1 heterologous expression levels (Fig. 30 A, right panel). Therefore, because the TMS1

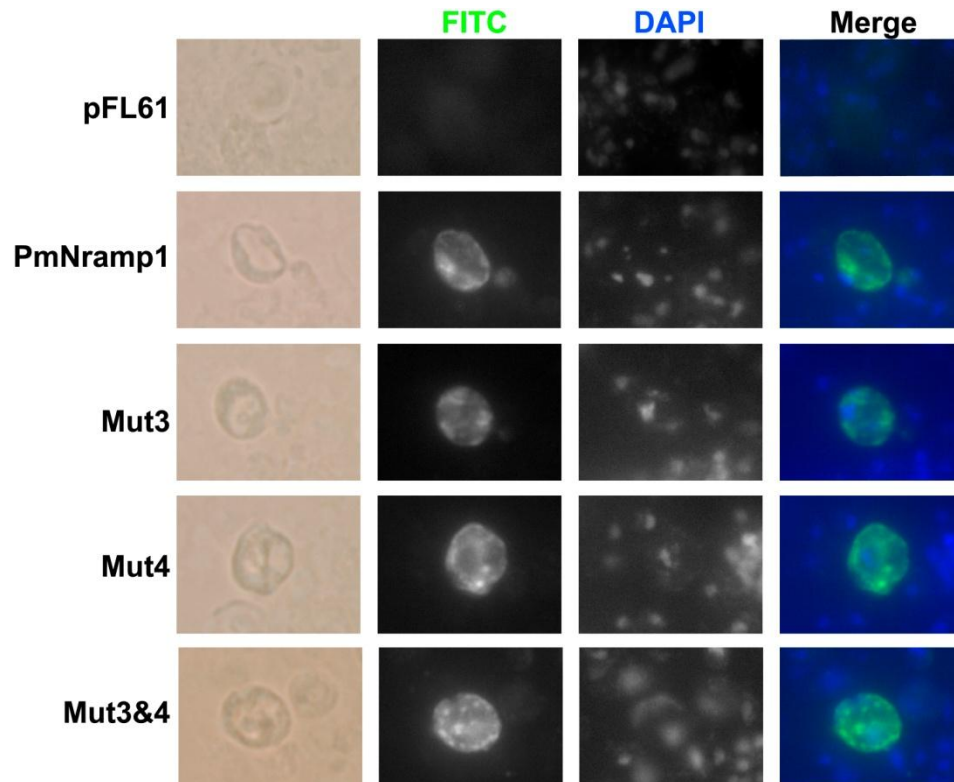
mutant protein was expressed in a much lower level than the wild type, it is not possible at this time to establish a strong correlation between the losses of complementation by TMS1 mutants to the functional roles of the mutated residues in iron uptake. In contrast, in addition of showing similar expression levels, IFAs revealed that mutants in TMS6 showed a similar localization in yeast cells as compared to the wild type PmNramp1 protein. Therefore, the failure of complementation by TMS6 mutants is likely to result from the disruption of the iron transport mechanism caused by the mutation of those specific function-related residues.

Fig. 30

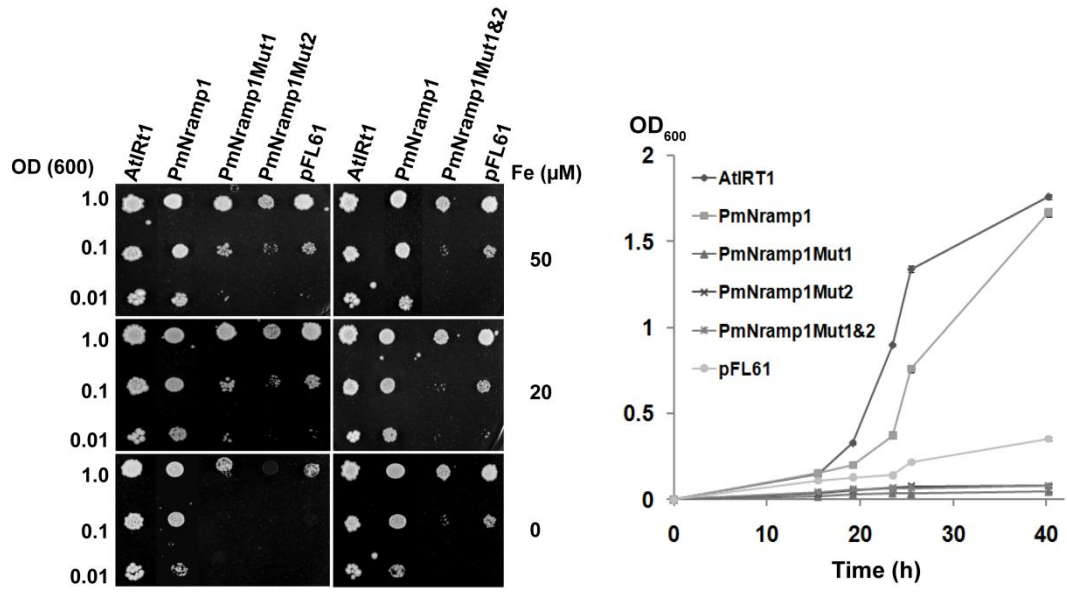
A



B



C



D

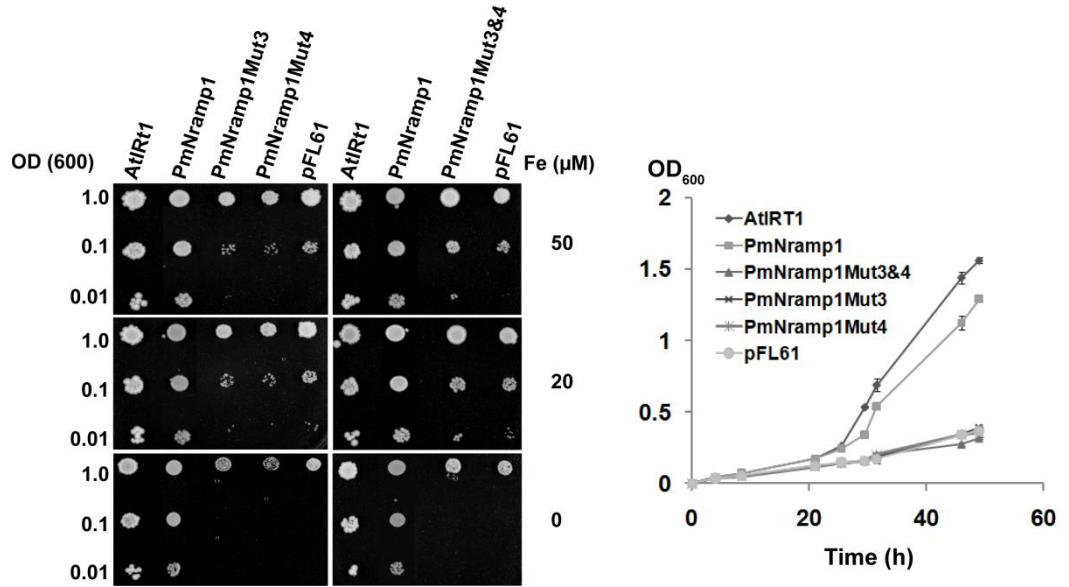


Fig. 30. Complementation assays of yeast *fet3fet4* mutant after mutations of key residues in PmNramp1.

A, Left panel, view of superimposed TMS1 and TMS6 of carriers from 5 evolutionary distant families (Mhp1, LeuT, BetP, SGLT1 and ApcT) showing LeuT residues engaged in substrate binding (orange sticks) and those interacting with the driving-cation (Na² site, dark blue sticks); the corresponding sites in other transporters are represented with yellow and light blue sticks, respectively. The areas targeted for mutagenesis are indicated. Right panel, western blot of the membrane-enriched extract from yeast cells transformed with mutated PmNramp1.

B, IFAs of yeast cells transformed with TMS6 mutants. All the PmNramp1 mutants were tagged with HA epitope. Monoclonal mouse anti-HA antibody and anti-mouse antibody conjugated with FITC were used to visualize protein localizations in yeast cells. Nucleus positions were indicated by DAPI staining.

C, Left panel, growth of serially diluted cells transformed with PmNramp1 with mutations at TMS1 after 5 days at 30°C on SD medium supplemented with 50, 20 or 0 μM FeCl₃. Right panel, growth of TMS1 mutants in liquid SD medium supplemented with 20 μM FeCl₃.

D, Left panel, growth of serially diluted cells transformed with PmNramp1 with mutations at TMS6 after 5 days at 30°C on SD medium supplemented with 50, 20 or 0 μM FeCl₃. Right panel, growth of TMS6 mutants in liquid medium supplemented with 20 μM FeCl₃.

DISCUSSION

Yeast complementation assay suggested the iron uptake function in PmNramp1 and PmNramp3. Following the concept that protein function is the reflection of protein structure, we modeled PmNramp1 3D structure by homologous threading (Fig. 29). The 3D model of PmNramp1 fits the iron complementation activity in the yeast. As a further confirmation of the model, mutations on the central triplets Asp-Pro-Gly (TMS1) and Met-Pro-His (TMS6) of PmNramp1 abolished the complementation. It turned out that mutants with mutated TMS1 triplet were not expressed properly compared to wild-type PmNramp1; while mutants with mutated TMS6 triplet were expressed as normally as intact PmNramp1. Therefore, the failure of complementation may be due to the structure interference while the interruption of complementation by mutants in TMS6 is probably due to the functional damage. It seems that mutations in TMS1 have a greater impact on PmNramp structure. Although the equivalent TMS1 mutants in the *E. coli* MntH or mouse Nramp2 are efficiently expressed in the homologous cells, causing significantly impaired transport activity; when transformed into yeast, the mouse Nramp2 D86A mutant exhibits a noticeable reduced expression [273]. These observations suggest that although the mutation in TMS1 does not affect Nramp expression in the homologous cells, it can severely impair expression in the heterologous system. Mutation in TMS6 seems to have little impact in Nramp homolog expression in either homologous or heterologous expression system. In a recent study on *E. coli* MntH, site-directed mutagenesis of several highly-conserved residues in TMS6, including those tested here, kept endogenous expression in a moderate to normal level compared to wild type [274].

Mouse Nramp2 with mutated TMS6 tripeptide could be stably expressed in *smf1smf2* yeast and CHO (Chinese hamster ovary) cells [256].

Substitution of Asp³⁴ in MntH with Gly or more conservative Asn can abolish both Me²⁺ and H⁺ transport [275, 276]. Equivalent mutant Asp86Ala in mouse Nramp2 failed to complement yeast strain *smf1smf2*; the same mutant showed no metal transport activity in CHO cells [273]. Consistent with those reports, our result about PmNramp1 mutant Asp76Glu supported the key role of the Asp residue in Nramp function. The other residue Gly78 in PmNramp1 TMS1 was indicated to be necessary in this site. The equivalent mutation was tested in *E. coli* MntH [276] and mouse Nramp2 [256]. Regardless of the nature of the substitution, mutation in the corresponding Gly site resulted in the loss of function. In TMS6 triplet, the Met residue seems to be indispensable. Substitution of this residue with Ala in PmNramp1 abrogated the complementation function as iron transporter. Substitution of the corresponding Met residue in *E. coli* MntH with either Ile or Lys demolished transport activity despite the similar side chain volumes of Met and Ile [274]. Site-directed mutagenesis of His residue in TMS6 triplet seems to have a mild effect on transport function, and the nature of the substitution can have different impact. The choices of amino acid for substitution of the targeted residue could be made on different basis. Some of the substitutions that appeared in the literature were chosen based on the evolutionary analysis and the others were based on the biochemical features of the amino acid residues. Chaloupka et al. made the His211 residue to Tyr mutation in *E. coli* MntH that is equivalent to PmNramp1 His252 substitution in this study, since tyrosine is the most prevalent substitution for this residue in the phylogenetic outgroup [275]. This mutation significantly reduced the sensitivity of

E. coli growth under toxic concentration of metals. Proton uptake of H211Y mutant was detected only with the substrate Cd^{2+} . Substitution of H211A imposed a milder effect on MntH function. *E. coli* carrying this mutation showed a higher sensitivity to toxic metal compared to H211Y mutant, albeit at a reduced level compared to wild type; the co-transport of proton and metal were restored [275]. Tyr possesses an acid side chain while His exposes a basic imidazole group, and therefore, mutation of His to Ala is more neutral compared to substitution with Tyr. In mouse Nramp2, the equivalent residue His²⁶⁷ was characterized to be highly mutation sensitive. Substitution with Ala, Cys and Arg all resulted in severe or complete loss of function. Lower pH conditions seem to restore the transport activity of mutant His267A, while decreasing pH has little effect on the function of wild type mouse Nramp2. Therefore, the hypothesis was raised that His²¹¹ might involve in pH-dependent regulation of MntH transport activity [273]. While Haemig and colleagues argued that their result did not support the pH regulation function of the equivalent His residue in *E. coli* MntH. They pointed out that His²¹¹ did not play a critical role in Mn^{2+} binding because substitution at this site kept K_m values similar to wild type. In addition, lower pH did not give obvious advantage to the mutant H211Q in transport activity as seen in mouse Nramp2 mutant H267A [274]. The divergence in results can be caused by the difference in the nature of substitution (H267A, H267C, and H267R by Lam-Yuk-Tseung *et al.*; H211A, H211Y by Chaloupka *et al.*; H211Q by Haemig *et al.*). Secondly, the data on mouse Nramp2 were generated in heterologous expression systems, including yeast and CHO cells. Despite the difficulty in judgment of the actual function of His residue in TMS6 triplet, it can still be concluded that this residue is closely involved in Nramp homolog function.

In summary, the results from our functional studies buttress the relevance of the TMS 1 and 6 predicted to exert pseudo-symmetric roles in substrate transport, and support a possible direct role of TMS6 residues in iron uptake. These results provide novel evidence consistent with the 3D model for the Slc11 family that is based on remote homology with cation-driven transporters with inverted symmetry. Sequence divergence among PmNramp homologs correspond predominantly to regions predicted extra-membranous (Fig. 22), which can nevertheless harbor site-specific signals for protein localization and/or turnover. Distinct Lys residues in yeast Smf1p N-terminal hydrophilic sequence are targeted for Rsp5p dependent ubiquitination to promote endocytosis in response to external cadmium [277] and to toxic manganese [278]. These observations suggest that divergent sequences amongst PmNramp extra-membranous regions may still contain residues useful for post-translational regulation of expression, subcellular localization and trafficking of PmNrams in response to environmental metals. Although PmNramp1 failed to transport manganese, because most Slc11 homologs show relatively low selectivity for divalent metals it is possible that PmNrams can transport other metals. Constitutive mRNA expression of *PmNramp1-3* in trophozoites *in vitro*, and extensive protein sequence variation in extra-membranous regions raise a possibility for dynamic post-translational control of expression, location and turnover of PmNrams. One possible scenario is that PmNramp1 might function as the prominent isotype for uptake of exogenous iron into the parasite cells, whereas PmNramp2 and PmNramp3 could function downstream of PmNramp1 for intracellular iron trafficking in relocation and storage. The key finding that PmNramp1 functions in uptake of exogenous iron in yeast provides the molecular and biochemical basis for prior observations on the effect of

environmental iron in enhancing infection prevalence and intensity, promoting parasite proliferation. The identification of PmNramp1 as a potential mediator of parasite virulence opens new avenues for exploring novel strategies of intervention.

CHAPTER 6 SUBCELLULAR LOCALIZATION OF THE PMNRAMP ISOTYPES

SUMMARY

The subcellular localization of PmNramp isotypes was investigated via IFA. Anti-serum against selected antigenic peptides from PmNramp isotypes was raised in rabbits. The IgG fraction was purified from the serum and tested for specificity by Western blot. Based on the Western blot result, PmNramp1 and PmNramp3 were expressed in cultured *P. marinus* while PmNramp2 expression was not detected.

IFAs of PmNramp isotypes in *P. marinus* trophozoites are still in progress. The IFAs of PmNramp3 in log-phase trophozoites, showed a cell surface staining when the parasite proliferates by binary fission. These data indicated potential roles of PmNramp3 in parasite growth.

INTRODUCTION

A number of organisms are known to have multiple Nramp genes. Three Nramp isotypes have been identified in the ciliate protozoan *Tetrahymena thermophila*, the baker yeast *Saccharomyces cerevisiae*, and the nematode *Caenorhabditis elegans*. The three *T. thermophila* Nramp homologs were annotated in the genome database. In *S. cerevisiae*, Nramp homologs Smf1p and Smf2p perform non-redundant roles as manganese transporters, with Smf1p mediating rapid massive influx at the plasma

membrane and Smf2p in charge of down-stream manganese utilization. Differently, Smf3 in *S. cerevisiae* plays a role in iron homeostasis [188]. Three *C. elegans* Nramp homologs are identified and Smf1 and Smf3 are expressed in intestine, functioning as manganese transporters and as part of innate immunity in the nematode [250]. Based on previous data, two of the three *P. marinus* Nramp homologs, PmNramp1 and PmNramp3 can function as iron transporters (Chapter 3). Information about PmNramp1 and PmNramp3 localization in the parasite can shed some light on the *in vivo* function of the transporters.

The detailed life cycle of *P. marinus* is not yet clearly documented. Ultrastructural features of *in vitro* *P. marinus* culture were studied by Sunila, *et al.* (2004) [279]. During vegetative cell cycles, *P. marinus* cells divide either by schizogony or binary fission with the former one being the common way of proliferation [279]. A graph about different cell types during *P. marinus* schizogony was presented in Fig. 31. Different cell types can be distinguished based on morphology and size. Large log-phase trophozoites (16 μm in diameter) are characterized by eccentric nuclei. Large log-phase trophozoites then develop to young log-phase schizonts with subdividing cytoplasm compartmentalized by daughter cell walls. After completion of schizogony, young log-phase schizonts turn to mature log-phase schizonts (20 μm in diameter), characterized by clear vacuoles and spherical nuclei. Despite the completion of division, the daughter cells are still bounded by the common schizont cell wall. After 24h, these daughter cells are released and become small log-phase trophozoites (5 μm in diameter) that develop to large log-phase trophozoites when there is plenty of nutrition in the medium. When the parasite population is large, the nutrients in the culture medium are depleted and metabolites from

the log-phase growth are built up. *P. marinus* growth enters the stationary phase. Mature log-phase schizonts become stationary-phase schizonts (10 μm in diameter) and small-log phase trophozoites turn into stationary-phase trophozoites [279].

In this chapter, subcellular localizations of PmNramp homologs were examined. Parasite cell from both exponential and stationary growth phases are investigated to test the possible life-stage dependent change in protein trafficking. In *C. elegans*, Smf1 has different expression patterns in embryo and adult nematodes [250]. Since both PmNramp1 and PmNramp3 can potentially function as iron transporters (Chapter 4) and iron is an essential element for *P. marinus* growth [10, 11], DFO chelation challenge is also included in the experiments.

Fig. 31

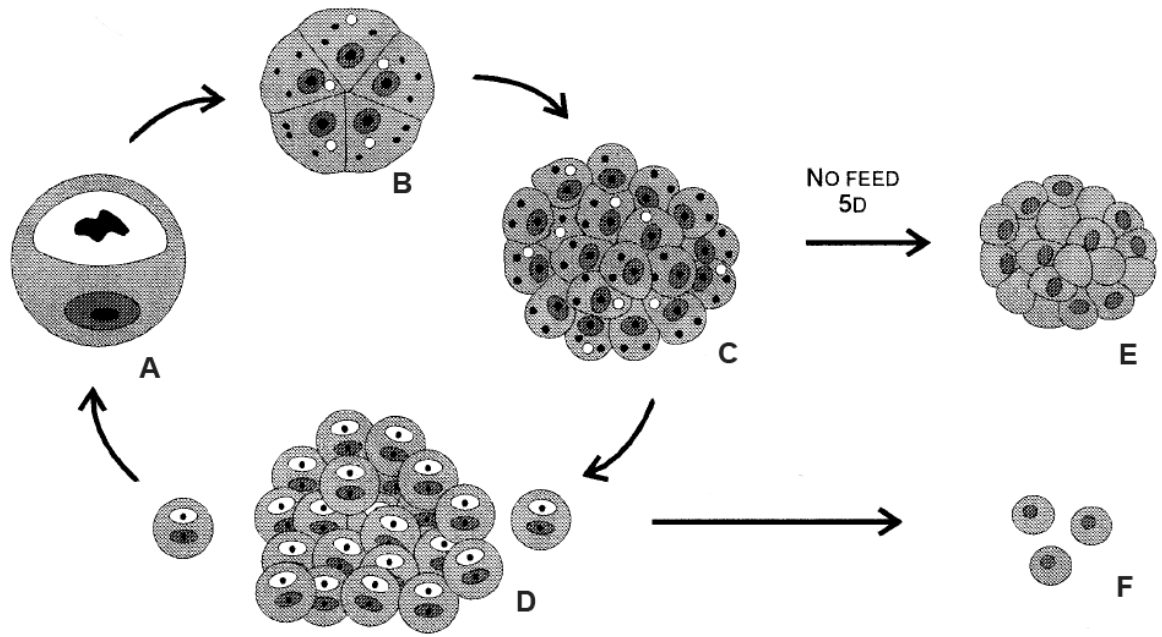


Fig. 31. A diagrammatic drawing of cell cycle of cultured *P. marinus*.

A. Large log-phase trophozoites in DME/F12 based medium. B. Young log-phase schizonts or internally subdividing mother cells containing daughter cells. C. Mature log-phase schizonts with daughter cells in a common schizont cell wall. D. Small log-phase trophozoites ready for the next division cycle. E. Stationary-phase schizonts limited by scarce nutrients. F. Stationary-phase trophozoites (modified from Sunila *et al.*, 2001).

MATERIALS AND METHODS

Generation of PmNramp antibodies

Rabbit antiserum (Open biosystems, Huntsville, AL) was raised against selected peptides on all the three PmNramp isotypes. The selected peptides are predicted to be part of the topological loop between TMS7 and TMS8 as indicated in Fig. 32. IgG subgroups were purified from both anti-serum and pre-immune serum using Protein A sepharose 4B (Sigma) and stored in PBS containing 0.02% NaN₃. The purified IgG antibodies were tested in Western blot by comparing the results from anti-serum IgG and pre-immune IgG. Because the pre-immune serum for PmNramp1 was missing, membrane extract from yeast cell *fet3fet4* transformed with HA-tag PmNramp1 was used to test purified PmNramp1 IgG. Monoclonal anti-HA antibody was used as a reference to detect PmNramp1 protein as described in Chapter 3. All the Western blots were performed using chemiluminescent detection (Pierce Biotechnologies, Rockford, IL) of HRP-conjugated goat anti-rabbit IgG antibodies (Bio-Rad, Hercules, CA).

Fig. 32

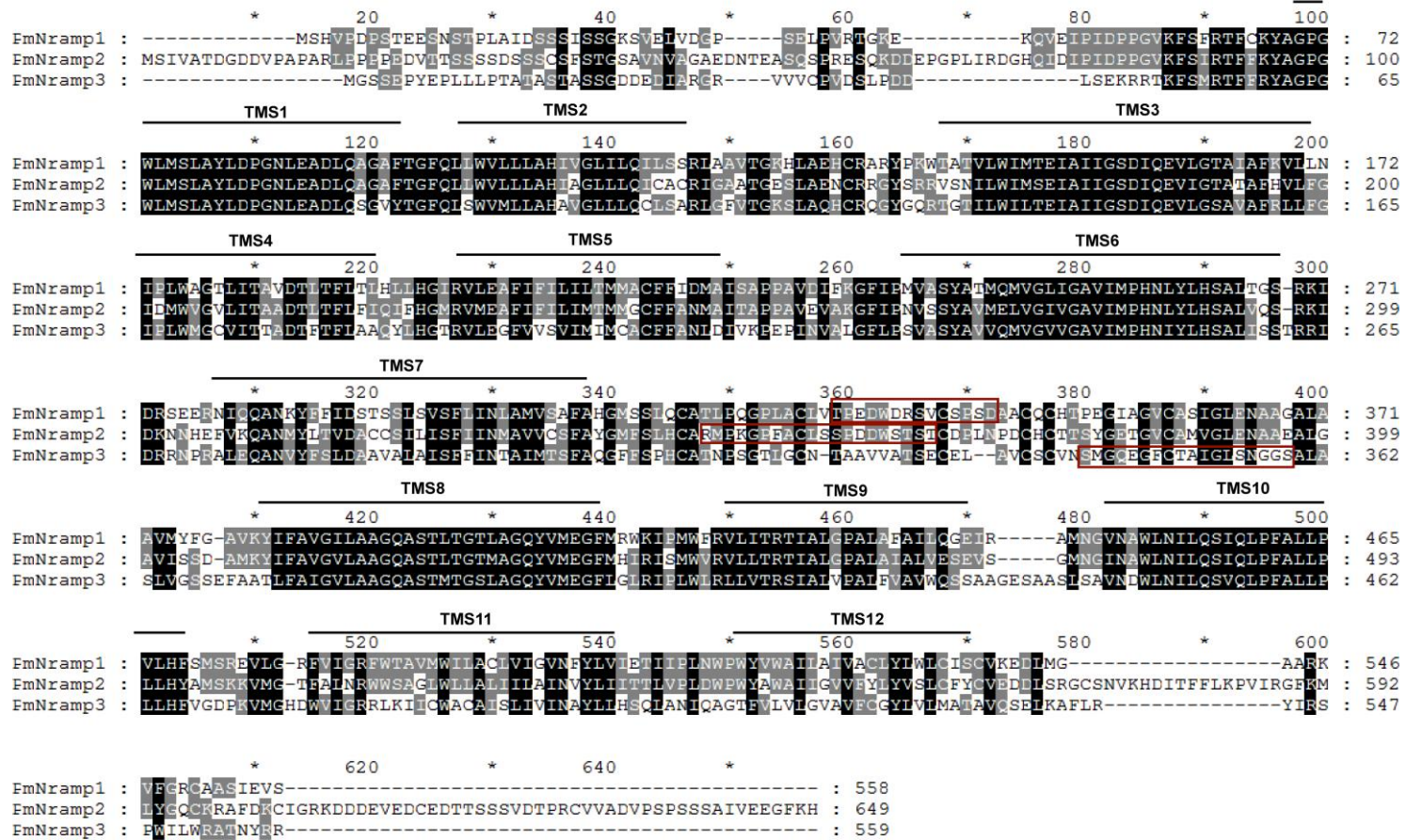


Fig. 32. Rabbit antiserum was raised against peptides predicted to be the loops between TMS7 and TMS8.

Amino acid sequences of PmNramp isotypes aligned using MEGA 4.1 and displayed by GeneDoc. The peptides selected to raise antiserum are indicated in red box. The positions of TMS based on the 3D model (Chapter 5) were indicated by lines. The selected peptides are part of the loop between TMS7 and TMS8.

Western blot analysis of PmNramp isotypes

Both the water soluble and the membrane-bound proteins from *P. marinus* were used in Western blot. The parasite cells are ruptured by vortexing together with glass beads. The soluble phase is stored in 50 mM Tris-HCl, pH 7.4 and the membrane enriched section was dissolved first in the same Tris buffer containing 1% Triton X-100, and then SDS sample buffer. The amount of protein used in Western blot is normalized to cell number. *P. marinus* cells were cultured in standard culture medium [191] and the cell number used in protein extraction is calculated based on OD₆₀₀ as described in Chapter 2. For water soluble fraction, 1 ml buffer was used to extract protein from 12 x 10⁸ cells; for membrane-bound fraction, 1 ml buffer was used to dissolve membrane protein from 30 x 10⁸ cells. 27 µl protein extracts were loaded for PmNramp1 and PmNramp2 western blot, and 18 µl extracts were loaded for PmNramp3 Western blot.

IFAs in *P. marinus* cells

After confirming the specificity of the IgG, IFAs were performed in *P. marinus* cells at exponential growth and stationary phase. At both stages, parasite cells were challenged with 0.02 mg/ml DFO for one day before the cells were harvested for IFAs. *P. marinus* cells were fixed in culture medium with 3% formaldehyde for 40 min at room temperature, then washed with PBS twice, followed by permeabilization in PBS containing 0.1% Triton X-100 for 30 min. Cells were washed in PBS before blocked with 3% BSA in PBS for 1 hour at room temperature. Cells were incubated with purified IgG in PBS containing 3% BSA in 1:50 dilution for 1h at room temperature. After three washes with PBS for 5 minutes, cells were incubated with FITC-conjugated donkey anti-rabbit IgG (Invitrogen, Carlsbad, CA) in PBS containing 3% BSA in 1:1000 dilution for

1 h at room temperature. Cells were washed three times with PBS for 5 minutes. After the nucleus staining with DAPI (Invitrogen, Carlsbad, CA) in 1:1000 dilution for 10 minutes followed by 3 washed in PBS, the cells were mounted on immunofluorescence slides (Thermo Scientific). The slides were examined using Nikon Eclipse E800 fluorescence microscope, and images of the cells were taken with SPOT RT2540 camera (Diagnostic Instruments, INC., Sterling Heights, MI).

RESULTS

Western blot on parasite lysates using purified PmNramp IgG

Western blot analysis using IgG purified from anti-serum against selected PmNramp1 peptides recognize a single band in *P. marinus* membrane-bound protein fraction (Fig. 33 A). No specific bands were detected in soluble fraction of the protein. In order to test the specificity of the IgG against the PmNramp1 peptide, membrane-bound protein from yeast cell *fet3fet4* transformed with PmNramp1-HA was used as a reference. Both the IgG and anti-HA antibody show a smear signal in the same position.

For PmNramp2 western blot, no bands were detected in western blot using purified IgG in both the soluble and the detergent phase. A dot blot using the antigen peptide showed signals with different intensities consistent with the amount of peptide applied. BSA serves as negative controls in the dot blot (Fig. 33 B). The negative result in detection of PmNramp2 in western blot, together with the detection of PmNramp2 peptide by the IgG, indicated that PmNramp2 may not be expressed as protein in trophozoites under this condition.

For PmNramp3 IgG western blot, a series of bands were detected for the membrane-fraction protein extract. It is known that Nramp proteins can be carbohydrate modified. The bands with different sizes can be the isomers during the carbohydrate modification process. No bands were detected using pre-immune serum and in the soluble fraction of the protein (Fig. 33 C). The amount of the protein loaded for PmNramp3 is half of that in PmNramp1 and PmNramp2 western blot, but the PmNramp3 bands shows a higher intensity compared to PmNramp1. Therefore, PmNramp3 is expressed in the highest level. The predicted size for PmNramp3 protein is 60 KDa, which is much smaller than the indicated size in the Western blot. The carbohydrate modification and the highly hydrophobic character of the membrane protein may cause the anomalous migration of the protein in SDS-PAGE.

Fig. 33

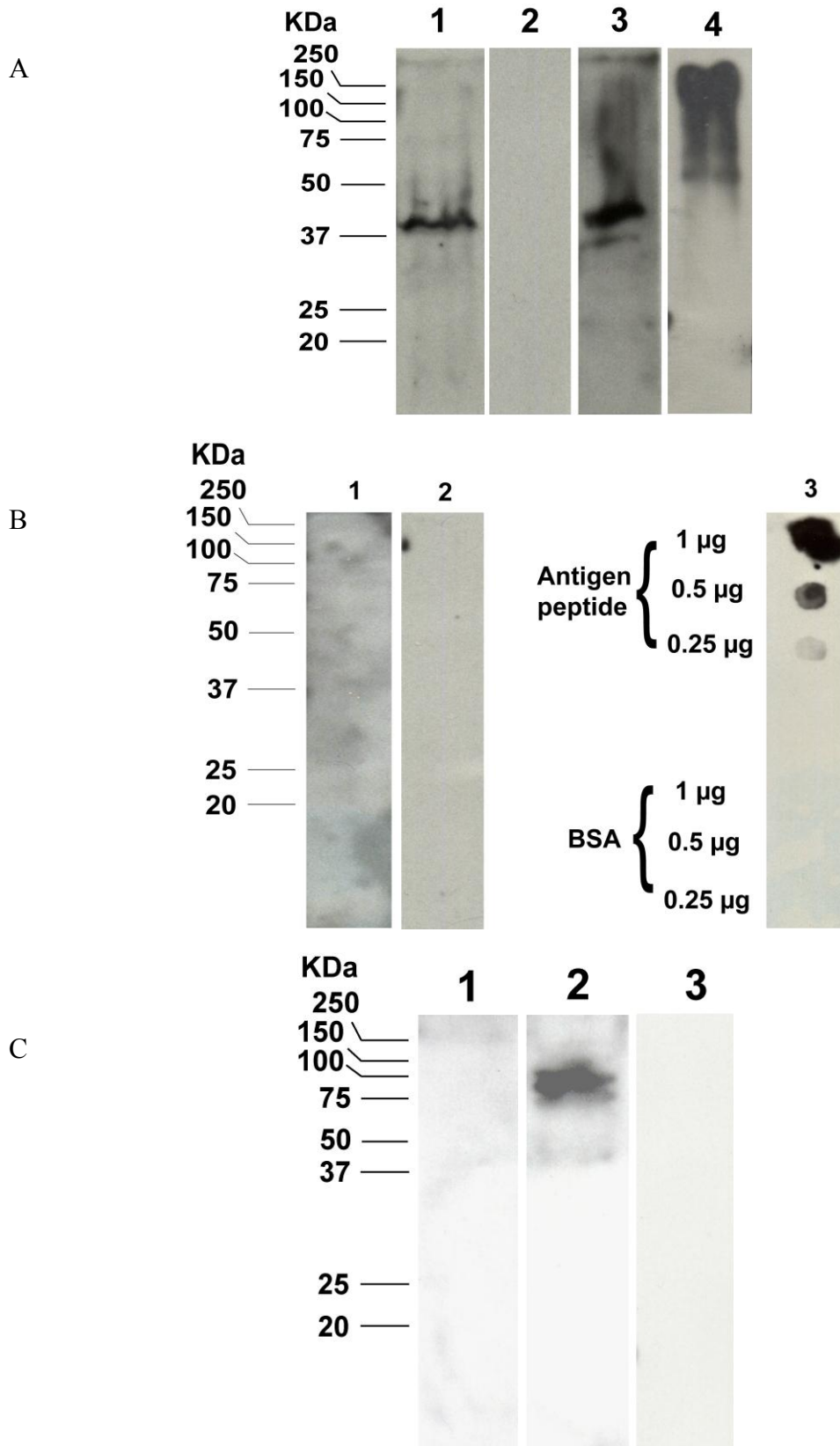


Fig. 33. Western blot analysis of PmNramp isotypes using purified IgG

A. Western blots of PmNramp1. Lane 1, detergent extraction of *P. marinus* protein; lane 2, water-soluble protein from *P. marinus*; lane 3, membrane protein extracted from *fet3fet4* transformed with HA-tagged PmNramp1, probed with PmNramp1 IgG; lane 4, same as lane 3 but probed with anti-HA antibody.

B. Western blots of PmNramp2. Lane 1, detergent extraction of *P. marinus* protein; lane 2, water-soluble protein from *P. marinus*; lane 3, dot blot with PmNramp2 antigen peptide and BSA as negative control.

C. Western blots of PmNramp3. Lane 1, detergent extraction of *P. marinus* protein probed with pre-immune IgG; lane 2, same as lane 1, but probed with purified PmNramp3 IgG; lane 3, water-soluble protein from *P. marinus*.

Localization of PmNramp3 in log-phase *P. marinus* trophozoites

In large log-phase trophozoites, when the parasite underwent schizogony, PmNramp3 seemed to localize on the dividing boundary of the cell; when the parasite proliferate by binary fission (indicated by two nuclei stained with DAPI), the protein appeared to be on the cell surface (Fig. 34).

Fig. 34

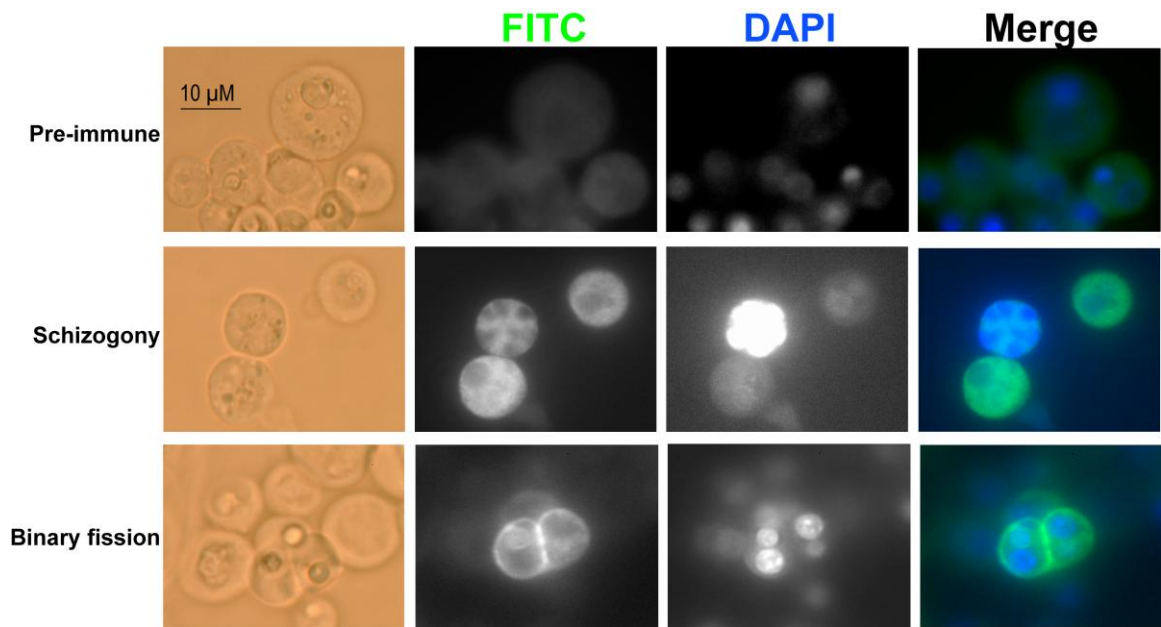


Fig. 34. Localization of PmNramp3 in log-phase *P. marinus* by fluorescence microscopy.

IFAs in extracellular *P. marinus* cells at the exponential growing stage using purified anti-PmNramp3 rabbit IgG as primary antibodies and FITC-conjugated anti-rabbit IgG as secondary antibodies. Nucleic dye DAPI was used to reveal the location of nuclei. In non-permeabilized parasite cells dividing by schizogony, PmNramp3 seemed to be on the dividing boundary. For log-phase parasites in the process of binary fission, PmNramp3 protein appeared to be targeted to the cell surface.

DISCUSSION

The western blot of PmNramp1 using purified anti-PmNramp1 IgG detected a band corresponding to a protein with a molecular weight much smaller than expected. To examine the possibility that other protein different from PmNramp might contain a similar peptide that justified cross-reactivity in *P. marinus*, a search for a protein with a similar antigenic peptide was performed. In the *P. marinus* genome archive, the NCBI tBLASTn program (Search translated nucleotide database using a protein query, http://blast.ncbi.nlm.nih.gov/Blast.cgi?PROGRAM=tblastn&BLAST_PROGRAMS=tblastn&PAGE_TYPE=BlastSearch&SHOW_DEFAULTS=on&LINK_LOC=blasthome) was launched using the PmNramp1 antigenic peptide as query. Two hits were obtained, and one of them is PmNramp1. The other one is PmNramp2 that has a stretch of peptide sharing 50% identity to the query. Therefore, we concluded that the higher mobility (apparent smaller size) of the protein as indicated by the western blot, could be the result of anomalous protein migration due to the particularly high number of hydrophobic domains. Alternatively, the PmNramp1 protein could have been degraded in the parasite, and the band detected was actually part of the protein. However, it may be worthwhile to validate the specificity of anti-PmNramp1 antibody by using the antibody against other potential epitopes in the recombinant protein.

In yeast, the PmNramp3 protein was not targeted to cell peripheral before the domain swapping (Chapter 4). The subcellular localization of PmNramp3 also showed a different pattern in *P. marinus* trophozoites as compared to the transformed yeast cells. In our preliminary study, PmNramp3, which was expressed poorly in yeast, was localized in parasite cell periphery during binary fission. The reason(s) for the discrepancy in the

subcellular localizations in the trophozoite and yeast are unclear, and but it becomes clear that *P. marinus* is very different from yeast in the various aspects of its complex life stages. As an intracellular parasite, *P. marinus* has co-evolved with its host, which is not the case for *S. cerevisiae*. Besides, the multiple modes of proliferation are also distinct between the two organisms. *S. cerevisiae* divides mostly by budding, but not schizogony or binary fission as *P. marinus*. Therefore, the protein regulation and targeting systems in the two organisms may be also very different, and the functional studies in an heterologous system such as yeast might not fully reflect the actual mechanisms that take place in the parasite.

The function of PmNramp2 remains unresolved. No functional data about PmNramp2 could be obtained by yeast complementation, because no PmNramp2 transcript was detected in yeast cells. Previous data showed a constitutive transcription of PmNramp2 RNA in *P. marinus*, while western blot indicated PmNramp2 is not translated under this particular life stage. It is noteworthy that the PmNramp2 RNA has a 3'UTR over 1000bp long (Chapter 2), and it become an interesting question whether this extensive 3'UTR might be involved in translational regulation. In addition, the PmNramp2 protein sequence was predicted to have a signal peptide targeted to chloroplasts (Chapter 2). Several lines of evidence supported the existence of a putative plastid in *Perkinsus* spp. [280-282] and several plastid-related pathways were identified in *P. marinus* EST database [217], however, it still not clear yet if *P. marinus* trophozoites do have plastid, and if this organelle only appear in certain life stage(s).

Localization of PmNramp1 and PmNramp3 remained unchanged upon DFO exposure, despite the fact that it can cause growth inhibition [11]. It may implies that

other redundant iron uptake pathways are up-regulated, or alternatively that from an energy consumption standpoint the inhibition in growth (up to 10%) at the DFO concentration tested is not dramatic enough to alter PmNramp trafficking. Thus, a higher concentration of DFO should be tested in future studies to examine this possibility, and investigate the impact of iron starvation on the subcellular localization of the PmNramp proteins.

In a non-synchronized *P. marinus* culture in the exponential growth phase, the parasite displays multiple cell division mechanisms, including schizogony and binary fission [3, 279]. Our observations are consistent with the report that schizogony is the most common way of proliferation. Our preliminary data on subcellular localization of Nramp isotypes suggests a role of PmNramp3 in the cell division process, and therefore, the targeting of PmNramp3 protein should be tightly controlled. During proliferation, parasite cells undergo an active process in which a number of enzymes are involved and numerous metabolites are generated. One of the enzymes is the ribonucleotide reductase (RR), an iron-dependent enzyme that converts ribonucleotides (NTPs) into deoxyribonucleotides (dNTPs) for DNA synthesis [283]. Therefore, iron is highly demanded during DNA duplication. On the other hand, abundant ROS are generated during the cell proliferation process and in addition to damage to DNA, membrane structures, and proteins, ROS can also interfere with the cell cycle [284]. Therefore, the activity of the antioxidant pathway has to be maintained and even enhanced during this process, and it is noteworthy that *P. marinus* trophozoites express several anti-oxidative pathway components [217], among which two SOD isotypes are iron-containing enzymes [14, 16, 285]. Thus, it is possible that PmNramp3 localizes on the cell membrane

during binary fission to facilitate rapid iron acquisition for both the nutrient supply and antioxidant protection. Another connection between iron transporters and cell division in protozoan parasites can be seen in *Leishmania*. The ferrous iron transporter LIT is an important player for iron acquisition by *Leishmania* amastigotes. The LIT knockout parasite has no significant effect on differentiation of promastigotes into amastigotes, but it abolishes amastigote division and the parasite virulence, indicating that LIT has a critical role at the intracellular stage [106]. The exact localization of PmNramp isotypes awaits further investigation. Nevertheless, the data in PmNramp3 localization is consistent with the importance of iron for *P. marinus* survival and growth.

CHAPTER 7 SUMMARY AND FUTURE DIRECTIONS

Functional studies of PmNramp isotypes

P. marinus has three Nramp isotypes with distinct gene organizations. All the PmNramp RNA is trans-spliced with a splicing leader sharing a high similarity with dinoflagellates (Chapter 2). PmNramp1, but not PmNramp2 and PmNramp3 can complement iron uptake activity in the yeast mutant *fet3fet4*. The failure of complementation of PmNramp2 and PmNramp3 in the complementation assay could result from difficulties in their expression in a heterologous system. However, the chimeric PmNramp3 with PmNramp1 N- and C- termini was able to complement iron uptake in the mutant yeast. The proposed 3D structure of PmNramp1 provides a mechanistic basis for iron acquisition via PmNramp1 (Chapter 5). A phylogenetic analysis suggested that all the three PmNramp isotypes are archetype. The protein sequence divergence among PmNramp isotypes was not related to diversification of critical functional elements, which remained constrained by purifying selection. Therefore, the function indicated by yeast complementation as iron transporter for both PmNramp1 and PmNramp3 is consistent with the phylogeny prediction (Chapter 3). The IFAs in *P. marinus* is ongoing, but a preliminary study showed distinct localization of the PmNramp isotypes in the cultured trophozoites, which appeared to relate to the cell division mode. Further, this study showed a plasma membrane localization of PmNramp3 during parasite binary fission (Chapter 6).

It has been reported that *P. marinus* requires iron for *in vitro* cell growth [11] and *in vivo* infection [Gauthier and Vasta, unpublished; [10]]; however, no information about *P. marinus* iron acquisition pathways was available until the demonstration of iron uptake

activity of PmNramp1 and chimeric PmNramp3 by yeast complementation (Chapter 4) in this study. The results obtained in this study contributed to the renewal of NSF grant that supported it, and the continuing financial support will enable the completion of the functional study in PmNramp isotypes.

Based on the literature, Nramp homologs are able to transport a wide range of divalent metals, with a high affinity to iron and manganese [286]. In this study, however, we were unable to confirm manganese transport by the PmNramp isotypes by complementation of the *smf1smf2* yeast mutant. In the future, the yeast mutant *smf1Δsmf2Δsod2Δ* could be used to test the potential manganese transport by PmNramp1, since the triple mutant has a higher demand for manganese as compared to the double mutant *smf1smf2* [253]. Alternatively, the metal (iron and manganese) accumulation in yeast transformed with PmNramp isotypes can be examined by inductively coupled plasma-MS (ICP-MS). No data about PmNramp2 transport substrate was obtained, since PmNramp2 could not be expressed in yeast cells. Electrophysiology studies in *Xenopus* oocytes may be able to enable the identification of the transport substrate(s) of PmNramp isotypes, including PmNramp2.

The subcellular localization of PmNramp3 in *P. marinus* during parasite binary fission indicated important roles of the transport during cell division. The hypothesis can be PmNramp3 is trafficked to the plasma membrane for the uptake of exogenous iron. For better understanding of PmNramp isotype localization, new antibodies directly conjugated with FITC can be generated against selected portions of the PmNramp isotypes produced as recombinant proteins. Another approach to test if the PmNramp isotypes are critical for parasite division is by monitoring parasite growth after knock-

down or knock-out of PmNramp genes. Despite the fact that the knock-down or knock-out techniques for *P. marinus* are not yet available, the developed transfection system [190] and the success in gene knockdown in *Giardia* using morpholinos [287] may open the new avenues to the development of new molecular tools for research in *P. marinus*.

Domain swapping as a novel approach for functional studies of protozoan Nramp in heterologous systems

Heterologous expression systems have long been the methodology for functional study of Nramp homologs. However, expression of Nramp homologs in heterologous systems can be problematic. To overcome this technical problem, substitution of Nramp N- and C-termini has been applied to facilitate the expression [257, 260]. Based on the data in Chapter 3, domain swapping can have an impact on both Nramp protein expression efficiency and protein trafficking. The success of PmNramp1 expression in yeast indicated that N- and C-termini of PmNramp1 may serve as the substitutions in other protozoan Nramp homologs that cannot be properly expressed in yeast complementation assays.

***P. marinus* and oyster hemocyte interaction: the “tug-of-war” for iron**

Our preliminary data indicated that Eastern oyster *C. virginica* can express two different Nramp isotypes, and one of which is up-regulated in oyster hemocytes when the oyster is challenged by LPS. With the findings of PmNramp isotypes as iron transporters, *P. marinus* and oyster hemocytes may serve as a model to study the “tug-of-war” for iron between host and protozoan parasites. As mentioned before, in *Leishmania* amastigotes, LIT knockout abolishes amastigote division and the parasite virulence, and LIT

expression is accelerated under iron depletion conditions, such as expression of host Nramp1 [106], suggesting competition for iron between LIT and host Nramp. The function of LIT seems to potentially overlap with the function of PmNamp3 in the aspect of parasite proliferation. In order to test the function of PmNramp isotypes in *P. marinus* and oyster hemocyte interaction, immunostaining of PmNramp3 and other PmNramp isotypes after phagocytosis of *P. marinus* by oyster hemocytes may be performed. The identification of PmNramp isotypes as iron transporters and the presence of host Nramp after detection of infection suggested that *P. marinus* trophozoites and oyster hemocyte may serve as a model system for the study of tug-off-war for iron between host and intracellular parasites.

Other potential iron uptake pathways in *P. marinus*

Besides further investigation of PmNramp functions, the data included in the dissertation also raised a number of other questions. It seemed that DFO challenge did not seem to change the trafficking of PmNramp isotypes despite the obvious inhibition in parasite growth. This observation led to the hypothesis that there other iron uptake pathways might be functional in *P. marinus*. It is worth to mention that the defined culture medium is rich in iron (1.7 mg/ml ferritin), and when there is no increased need for iron, a potential low-affinity iron transporter may be enough for the iron supply in the parasite. In addition, two homologs of facilitator of iron transport (Accession number XM_002764818 and XM_002781371) were annotated in *P. marinus* genome data base.

***P. marinus* genomic organization and post-transcription regulations**

The identification of SL in *P. marinus* and the lack of transcriptional regulation in the tested genes opened some interesting questions about *P. marinus* genomic organization. The presence of SL and the lack of transcription regulation suggest polycistronic transcription in *P. marinus*, which means genes are organized in different units and the genes in the same unit are transcribed into polycistronic RNA precursors. The identification of the transcription starting sites in *P. marinus* chromosomes, and a rigorous investigation of *P. marinus* genome organization may provide a detailed picture about the biology of the parasite. Noticeably, transcriptional regulation in *P. marinus* was shown in a trans-spliced gene. Transcript of *P. marinus* cyclins isotypes Pmacyclin1 was significantly increased when the cells were actively dividing [288]. There are two hypothetic explanations for the increased transcript: (a) upregulation of transcription, and (b) increased RNA stability as a post-transcriptional regulation. For genes lack of transcriptional regulation, the importance of post-transcriptional regulation that including RNA processing and export, RNAi, RNA stability and translation regulation [289] becomes obvious. No annotation of a complete RNAi machinery in the *P. marinus* genome. Our data in PmNramp2 provided a potential example of translational regulation. In cultured *P. marinus* trophozoites, PmNramp2 is transcribed, but no protein expression was detected by Western blot. The PmNramp2 gene structure has one unique feature compared to PmNramp1 and PmNramp3. The PmNramp2 transcript has a 3'-UTR about 1k bps, much longer than the PmNramp1 and PmNramp3 3'-UTRs, and it could be possible that the PmNramp2 3'UTR plays a role in translation. In *Leishmania* and trypanosomes, 3'-UTRs seemed to be the origination site of translation regulation, and

the change in the secondary structures of 3'-UTR may directly influence translation efficiency [289].

BIBLIOGRAPHY

1. Harvell CD, Kim K, Burkholder JM, Colwell RR, Epstein PR, Grimes DJ, Hofmann EE, Lipp EK, Osterhaus AD, Overstreet RM *et al*: **Emerging marine diseases--climate links and anthropogenic factors**. *Science* 1999, **285**(5433):1505-1510.
2. Villalba A, Reece KS, Ordas MC, Casas MC, Figueras A: **Perkinsosis in molluscs: A review**. *Aquatic living resources/Ressources vivantes aquatiques* 2004, **17**(4):411-432.
3. Perkins FO: **The structure of *Perkinsus marinus* (Mackin, Owen and Collier, 1950) Levine, 1978 with comments on taxonomy and phylogeny of *Perkinsus* spp.** *J Shellfish Res* 1996, **15**(1):67-87.
4. Ford SE: **Range extension by the oyster parasite *Perkinsus marinus* into the northeastern United States: Response to climate change?** *J Shellfish Res* 1996, **15**(1):45-56.
5. Ford SE, Chintala MM: **Northward expansion of a marine parasite: Testing the role of temperature adaptation**. *J Exp Mar Biol Ecol* 2006, **339**(2):226-235.
6. Pecher WT, Alavi MR, Schott EJ, Fernandez-Robledo JA, Roth L, Berg ST, Vasta GR: **Assessment of the northern distribution range of selected *Perkinsus* species in eastern oysters (*Crassostrea virginica*) and hard clams (*Mercenaria mercenaria*) with the use of PCR-based detection assays**. *J Parasitol* 2008, **94**(2):410-422.
7. Andrews JD: **History of *Perkinsus marinus*, a pathogen of oysters in Chesapeake Bay 1950-1984**. *J Shellfish Res* 1996, **15**(1):13-16.
8. Tasumi S, Vasta GR: **A galectin of unique domain organization from hemocytes of the Eastern oyster (*Crassostrea virginica*) is a receptor for the protistan parasite *Perkinsus marinus***. *J Immunol* 2007, **179**(5):3086-3098.
9. Chu F-LE: **Laboratory investigations of susceptibility, infectivity, and transmission of *Perkinsus marinus* in oysters**. *J Shellfish Res* 1996, **15**(1):57-66.
10. Lin Z, Fernández-Robledo J-A, Cellier MFM, Vasta GR: **Metals and membrane metal transporters in biological systems: The role(s) of Nramp in host-parasite interactions**. *J the Argentine Chemical Society* 2009, **97**(1):210-225.
11. Gauthier JD, Vasta GR: **Inhibition of *in vitro* replication of the oyster parasite *Perkinsus marinus* by the natural iron chelators transferrin, lactoferrin, and desferrioxamine**. *Devel Comp Imm* 1994, **18**(4):277-286.
12. Voley AK, Chu FL: **Suppression of chemiluminescence of eastern oyster (*Crassostrea virginica*) hemocytes by the protozoan parasite *Perkinsus marinus***. *Dev Comp Immunol* 1995, **19**(2):135-142.
13. Schott EJ, Pecher WT, Okafor F, Vasta GR: **The protistan parasite *Perkinsus marinus* is resistant to selected reactive oxygen species**. *Exp Parasitol* 2003, **105**(3-4):232-240.
14. Schott EJ, Robledo JAF, Wright AC, Silva AM, Vasta GR: **Gene organization and homology modeling of two iron superoxide dismutases of the early branching protist *Perkinsus marinus***. *Gene* 2003, **309**(1):1-9.

15. Schott EJ, Vasta GR: **The PmSOD1 Gene of the protistan parasite *Perkinsus marinus* complements the *sod2*Δ mutant of *Saccharomyces cerevisiae*, and directs an iron superoxide dismutase to mitochondria.** *Molecular and Biochemical Parasitology* 2003, **126**(1):81-92.
16. Asojo OA, Schott EJ, Vasta GR, Silva AM: **Structures of PmSOD1 and PmSOD2, two superoxide dismutases from the protozoan parasite *Perkinsus marinus*.** *Acta Crystallograph Sect F Struct Biol Cryst Commun* 2006, **62**(Pt 11):1072-1075.
17. Tsiftoglou AS, Vizirianakis IS, Strouboulis J: **Erythropoiesis: model systems, molecular regulators, and developmental programs.** *IUBMB Life* 2009, **61**(8):800-830.
18. Nishiya K: **Stimulation of human synovial cell DNA synthesis by iron.** *J Rheumatol* 1994, **21**(10):1802-1807.
19. Hirst J: **Towards the molecular mechanism of respiratory complex I.** *Biochem J* 2009, **425**(2):327-339.
20. Anderson GJ, Vulpe CD: **Mammalian iron transport.** *Cell Mol Life Sci* 2009, **66**(20):3241-3261.
21. Beisel WR: **Magnitude of the host nutritional responses to infection.** *Am J Clin Nutr* 1977, **30**(8):1236-1247.
22. Schaible UE, Kaufmann SH: **A nutritive view on the host-pathogen interplay.** *Trends Microbiol* 2005, **13**(8):373-380.
23. Ganz T: **Iron in innate immunity: starve the invaders.** *Curr Opin Immunol* 2009, **21**(1):63-67.
24. Lopez-Soto F, Leon-Sicairos N, Reyes-Lopez M, Serrano-Luna J, Ordaz-Pichardo C, Pina-Vazquez C, Ortiz-Estrada G, de la Garza M: **Use and endocytosis of iron-containing proteins by *Entamoeba histolytica* trophozoites.** *Infect Genet Evol* 2009, **9**(6):1038-1050.
25. Theurl I, Fritsche G, Ludwiczek S, Garimorth K, Bellmann-Weiler R, Weiss G: **The macrophage: a cellular factory at the interphase between iron and immunity for the control of infections.** *Biomaterials* 2005, **18**(4):359-367.
26. Lambe T, Simpson RJ, Dawson S, Bouriez-Jones T, Crockford TL, Lephert M, Latunde-Dada GO, Robinson H, Raja KB, Campagna DR *et al*: **Identification of a Steap3 endosomal targeting motif essential for normal iron metabolism.** *Blood* 2009, **113**(8):1805-1808.
27. Ohgami RS, Campagna DR, Greer EL, Antiochos B, McDonald A, Chen J, Sharp JJ, Fujiwara Y, Barker JE, Fleming MD: **Identification of a ferrireductase required for efficient transferrin-dependent iron uptake in erythroid cells.** *Nat Genet* 2005, **37**(11):1264-1269.
28. Gunshin H, Fujiwara Y, Custodio AO, Drenth C, Robine S, Andrews NC: **Slc11a2 is required for intestinal iron absorption and erythropoiesis but dispensable in placenta and liver.** *J Clin Invest* 2005, **115**(5):1258-1266.
29. Recalcati S, Invernizzi P, Arosio P, Cairo G: **New functions for an iron storage protein: the role of ferritin in immunity and autoimmunity.** *J Autoimmun* 2008, **30**(1-2):84-89.

30. Li JY, Paragas N, Ned RM, Qiu A, Viltard M, Leete T, Drexler IR, Chen X, Sanna-Cherchi S, Mohammed F *et al*: **Scara5 is a ferritin receptor mediating non-transferrin iron delivery**. *Dev Cell* 2009, **16**(1):35-46.
31. Liuzzi JP, Aydemir F, Nam H, Knutson MD, Cousins RJ: **Zip14 (Slc39a14) mediates non-transferrin-bound iron uptake into cells**. *Proc Natl Acad Sci U S A* 2006, **103**(37):13612-13617.
32. Huang ML, Becker EM, Whitnall M, Rahmanto YS, Ponka P, Richardson DR: **Elucidation of the mechanism of mitochondrial iron loading in Friedreich's ataxia by analysis of a mouse mutant**. *Proc Natl Acad Sci U S A* 2009, **106**(38):16381-16386.
33. Lim JE, Jin O, Bennett C, Morgan K, Wang F, Trenor CC, 3rd, Fleming MD, Andrews NC: **A mutation in Sec15l1 causes anemia in hemoglobin deficit (hbd) mice**. *Nat Genet* 2005, **37**(11):1270-1273.
34. White RA, Boydston LA, Brookshier TR, McNulty SG, Nsumu NN, Brewer BP, Blackmore K: **Iron metabolism mutant hbd mice have a deletion in Sec15l1, which has homology to a yeast gene for vesicle docking**. *Genomics* 2005, **86**(6):668-673.
35. Zhang AS, Sheftel AD, Ponka P: **The anemia of "haemoglobin-deficit" (hbd/hbd) mice is caused by a defect in transferrin cycling**. *Exp Hematol* 2006, **34**(5):593-598.
36. Chen W, Paradkar PN, Li L, Pierce EL, Langer NB, Takahashi-Makise N, Hyde BB, Shirihai OS, Ward DM, Kaplan J *et al*: **Abcb10 physically interacts with mitoferrin-1 (Slc25a37) to enhance its stability and function in the erythroid mitochondria**. *Proc Natl Acad Sci U S A* 2009, **106**(38):16263-16268.
37. Shaw GC, Cope JJ, Li L, Corson K, Hersey C, Ackermann GE, Gwynn B, Lambert AJ, Wingert RA, Traver D *et al*: **Mitoferrin is essential for erythroid iron assimilation**. *Nature* 2006, **440**(7080):96-100.
38. Ye H, Rouault TA: **Human iron-sulfur cluster assembly, cellular iron homeostasis, and disease**. *Biochemistry*, **49**(24):4945-4956.
39. Keel SB, Doty RT, Yang Z, Quigley JG, Chen J, Knoblauch S, Kingsley PD, De Domenico I, Vaughn MB, Kaplan J *et al*: **A heme export protein is required for red blood cell differentiation and iron homeostasis**. *Science* 2008, **319**(5864):825-828.
40. Quigley JG, Yang Z, Worthington MT, Phillips JD, Sabo KM, Sabath DE, Berg CL, Sassa S, Wood BL, Abkowitz JL: **Identification of a human heme exporter that is essential for erythropoiesis**. *Cell* 2004, **118**(6):757-766.
41. Kabanova S, Kleinbongard P, Volkmer J, Andree B, Kelm M, Jax TW: **Gene expression analysis of human red blood cells**. *Int J Med Sci* 2009, **6**(4):156-159.
42. Crouch SP, Slater KJ, Fletcher J: **Regulation of cytokine release from mononuclear cells by the iron-binding protein lactoferrin**. *Blood* 1992, **80**(1):235-240.
43. Boretti FS, Buehler PW, D'Agnillo F, Kluge K, Glaus T, Butt OI, Jia Y, Goede J, Pereira CP, Maggiorini M *et al*: **Sequestration of extracellular hemoglobin within a haptoglobin complex decreases its hypertensive and oxidative effects in dogs and guinea pigs**. *J Clin Invest* 2009, **119**(8):2271-2280.

44. Buehler PW, Abraham B, Vallelian F, Linnemayr C, Pereira CP, Cipollo JF, Jia Y, Mikolajczyk M, Boretti FS, Schoedon G *et al*: **Haptoglobin preserves the CD163 hemoglobin scavenger pathway by shielding hemoglobin from peroxidative modification.** *Blood* 2009, **113**(11):2578-2586.
45. Schaer DJ, Schaer CA, Buehler PW, Boykins RA, Schoedon G, Alayash AI, Schaffner A: **CD163 is the macrophage scavenger receptor for native and chemically modified hemoglobins in the absence of haptoglobin.** *Blood* 2006, **107**(1):373-380.
46. Corna G, Campana L, Pignatti E, Castiglioni A, Tagliafico E, Bosurgi L, Campanella A, Brunelli S, Manfredi A, Apostoli P *et al*: **Polarization dictates iron handling by inflammatory and alternatively activated macrophages.** *Haematologica* 2010.
47. Recalcatti S, Locati M, Marini A, Santambrogio P, Zaninotto F, De Pizzol M, Zammataro L, Girelli D, Cairo G: **Differential regulation of iron homeostasis during human macrophage polarized activation.** *Eur J Immunol* 2010, **40**(3):824-835.
48. Mantovani A, Sozzani S, Locati M, Allavena P, Sica A: **Macrophage polarization: tumor-associated macrophages as a paradigm for polarized M2 mononuclear phagocytes.** *Trends Immunol* 2002, **23**(11):549-555.
49. Majai G, Sarang Z, Csomos K, Zahuczky G, Fesus L: **PPARgamma-dependent regulation of human macrophages in phagocytosis of apoptotic cells.** *Eur J Immunol* 2007, **37**(5):1343-1354.
50. Mukundan L, Odegaard JI, Morel CR, Heredia JE, Mwangi JW, Ricardo-Gonzalez RR, Goh YP, Eagle AR, Dunn SE, Awakuni JU *et al*: **PPAR-delta senses and orchestrates clearance of apoptotic cells to promote tolerance.** *Nat Med* 2009, **15**(11):1266-1272.
51. N A-G, Bensinger SJ, Hong C, Beceiro S, Bradley MN, Zelcer N, Deniz J, Ramirez C, Diaz M, Gallardo G *et al*: **Apoptotic cells promote their own clearance and immune tolerance through activation of the nuclear receptor LXR.** *Immunity* 2009, **31**(2):245-258.
52. Freeman GJ, Casasnovas JM, Umetsu DT, DeKruyff RH: **TIM genes: a family of cell surface phosphatidylserine receptors that regulate innate and adaptive immunity.** *Immunol Rev* 2010, **235**(1):172-189.
53. Park SY, Jung MY, Kim HJ, Lee SJ, Kim SY, Lee BH, Kwon TH, Park RW, Kim IS: **Rapid cell corpse clearance by stabilin-2, a membrane phosphatidylserine receptor.** *Cell Death Differ* 2008, **15**(1):192-201.
54. Porta C, Rimoldi M, Raes G, Brys L, Ghezzi P, Di Liberto D, Dieli F, Ghisletti S, Natoli G, De Baetselier P *et al*: **Tolerance and M2 (alternative) macrophage polarization are related processes orchestrated by p50 nuclear factor kappaB.** *Proc Natl Acad Sci U S A* 2009, **106**(35):14978-14983.
55. Gunshin H, Starr CN, Drenzo C, Fleming MD, Jin J, Greer EL, Sellers VM, Galica SM, Andrews NC: **Cybrd1 (duodenal cytochrome b) is not necessary for dietary iron absorption in mice.** *Blood* 2005, **106**(8):2879-2883.
56. Shah YM, Matsubara T, Ito S, Yim SH, Gonzalez FJ: **Intestinal hypoxia-inducible transcription factors are essential for iron absorption following iron deficiency.** *Cell Metab* 2009, **9**(2):152-164.

57. Nunez MT: **Regulatory mechanisms of intestinal iron absorption-Uncovering of a fast-response mechanism based on DMT1 and ferroportin endocytosis.** *Biofactors*.
58. Shayeghi M, Latunde-Dada GO, Oakhill JS, Laftah AH, Takeuchi K, Halliday N, Khan Y, Warley A, McCann FE, Hider RC *et al*: **Identification of an intestinal heme transporter.** *Cell* 2005, **122**(5):789-801.
59. Donovan A, Lima CA, Pinkus JL, Pinkus GS, Zon LI, Robine S, Andrews NC: **The iron exporter ferroportin/Slc40a1 is essential for iron homeostasis.** *Cell Metab* 2005, **1**(3):191-200.
60. Oates PS: **The role of hepcidin and ferroportin in iron absorption.** *Histol Histopathol* 2007, **22**(7):791-804.
61. Darshan D, Anderson GJ: **Interacting signals in the control of hepcidin expression.** *Biometals* 2009, **22**(1):77-87.
62. Zhang AS, Enns CA: **Molecular mechanisms of normal iron homeostasis.** *Hematology Am Soc Hematol Educ Program* 2009:207-214.
63. Lesbordes-Brion JC, Viatte L, Bennoun M, Lou DQ, Ramey G, Houbron C, Hamard G, Kahn A, Vaulont S: **Targeted disruption of the hepcidin 1 gene results in severe hemochromatosis.** *Blood* 2006, **108**(4):1402-1405.
64. Lipinski P, Starzynski RR: **[Regulation of body iron homeostasis by hepcidin].** *Postepy Hig Med Dosw (Online)* 2004, **58**:65-73.
65. Nemeth E, Tuttle MS, Powelson J, Vaughn MB, Donovan A, Ward DM, Ganz T, Kaplan J: **Hepcidin regulates cellular iron efflux by binding to ferroportin and inducing its internalization.** *Science* 2004, **306**(5704):2090-2093.
66. Ramey G, Deschemin JC, Durel B, Canonne-Hergaux F, Nicolas G, Vaulont S: **Hepcidin targets ferroportin for degradation in hepatocytes.** *Haematologica*, **95**(3):501-504.
67. Knutson MD, Oukka M, Koss LM, Aydemir F, Wessling-Resnick M: **Iron release from macrophages after erythrophagocytosis is up-regulated by ferroportin 1 overexpression and down-regulated by hepcidin.** *Proc Natl Acad Sci U S A* 2005, **102**(5):1324-1328.
68. De Domenico I, Zhang TY, Koening CL, Branch RW, London N, Lo E, Daynes RA, Kushner JP, Li D, Ward DM *et al*: **Hepcidin mediates transcriptional changes that modulate acute cytokine-induced inflammatory responses in mice.** *J Clin Invest* 2010.
69. Gao J, Chen J, Kramer M, Tsukamoto H, Zhang AS, Enns CA: **Interaction of the hereditary hemochromatosis protein HFE with transferrin receptor 2 is required for transferrin-induced hepcidin expression.** *Cell Metab* 2009, **9**(3):217-227.
70. Wang RH, Li C, Xu X, Zheng Y, Xiao C, Zerfas P, Cooperman S, Eckhaus M, Rouault T, Mishra L *et al*: **A role of SMAD4 in iron metabolism through the positive regulation of hepcidin expression.** *Cell Metab* 2005, **2**(6):399-409.
71. Tanno T, Bhanu NV, Oneal PA, Goh SH, Staker P, Lee YT, Moroney JW, Reed CH, Luban NL, Wang RH *et al*: **High levels of GDF15 in thalassemia suppress expression of the iron regulatory protein hepcidin.** *Nat Med* 2007, **13**(9):1096-1101.

72. Shi J, Camus AC: **Hepcidins in amphibians and fishes: Antimicrobial peptides or iron-regulatory hormones?** *Dev Comp Immunol* 2006, **30**(9):746-755.
73. Theurl I, Theurl M, Seifert M, Mair S, Nairz M, Rumpold H, Zoller H, Bellmann-Weiler R, Niederegger H, Talasz H *et al*: **Autocrine formation of hepcidin induces iron retention in human monocytes.** *Blood* 2008, **111**(4):2392-2399.
74. Theurl M, Theurl I, Hochegger K, Obrist P, Subramaniam N, van Rooijen N, Schuemann K, Weiss G: **Kupffer cells modulate iron homeostasis in mice via regulation of hepcidin expression.** *J Mol Med* 2008, **86**(7):825-835.
75. Sow FB, Florence WC, Satoskar AR, Schlesinger LS, Zwilling BS, Lafuse WP: **Expression and localization of hepcidin in macrophages: a role in host defense against tuberculosis.** *J Leukoc Biol* 2007, **82**(4):934-945.
76. Nemeth E, Rivera S, Gabayan V, Keller C, Taudorf S, Pedersen BK, Ganz T: **IL-6 mediates hypoferrremia of inflammation by inducing the synthesis of the iron regulatory hormone hepcidin.** *J Clin Invest* 2004, **113**(9):1271-1276.
77. Mena NP, Esparza A, Tapia V, Valdes P, Nunez MT: **Hepcidin inhibits apical iron uptake in intestinal cells.** *Am J Physiol Gastrointest Liver Physiol* 2008, **294**(1):G192-198.
78. Mena NP, Esparza AL, Nunez MT: **Regulation of transepithelial transport of iron by hepcidin.** *Biol Res* 2006, **39**(1):191-193.
79. Ludwiczek S, Aigner E, Theurl I, Weiss G: **Cytokine-mediated regulation of iron transport in human monocytic cells.** *Blood* 2003, **101**(10):4148-4154.
80. Yang F, Liu XB, Quinones M, Melby PC, Ghio A, Haile DJ: **Regulation of reticuloendothelial iron transporter MTP1 (Slc11a3) by inflammation.** *J Biol Chem* 2002, **277**(42):39786-39791.
81. Ganz T: **Hepcidin and its role in regulating systemic iron metabolism.** *Hematology Am Soc Hematol Educ Program* 2006:29-35, 507.
82. Graversen JH, Madsen M, Moestrup SK: **CD163: a signal receptor scavenging haptoglobin-hemoglobin complexes from plasma.** *Int J Biochem Cell Biol* 2002, **34**(4):309-314.
83. Haas H, Eisendle M, Turgeon BG: **Siderophores in fungal physiology and virulence.** *Annu Rev Phytopathol* 2008, **46**:149-187.
84. Ratledge C: **Iron metabolism and infection.** *Food Nutr Bull* 2007, **28**(4 Suppl):S515-523.
85. Sutak R, Lesuisse E, Tachezy J, Richardson DR: **Crusade for iron: iron uptake in unicellular eukaryotes and its significance for virulence.** *Trends Microbiol* 2008, **16**(6):261-268.
86. Ballouche M, Cornelis P, Baysse C: **Iron metabolism: a promising target for antibacterial strategies.** *Recent Pat Antiinfect Drug Discov* 2009, **4**(3):190-205.
87. Frederick RE, Mayfield JA, DuBois JL: **Iron trafficking as an antimicrobial target.** *Biometals* 2009, **22**(4):583-593.
88. Weinberg ED: **Iron availability and infection.** *Biochim Biophys Acta* 2009, **1790**(7):600-605.
89. Kornitzer D: **Fungal mechanisms for host iron acquisition.** *Curr Opin Microbiol* 2009, **12**(4):377-383.
90. Weinberg ED: **The role of iron in protozoan and fungal infectious diseases.** *J Eukaryot Microbiol* 1999, **46**(3):231-238.

91. Golenser J, Waknine JH, Krugliak M, Hunt NH, Grau GE: **Current perspectives on the mechanism of action of artemisinins.** *Int J Parasitol* 2006, **36**(14):1427-1441.
92. Wang J, Huang W, Li L, Cheng J: **[Microchip electrochromatography: the latest developments and applications].** *Se Pu* 2010, **28**(3):264-272.
93. Golenser J, Domb A, Mordechai-Daniel T, Leshem B, Luty A, Kremsner P: **Iron chelators: correlation between effects on Plasmodium spp. and immune functions.** *J Parasitol* 2006, **92**(1):170-177.
94. Smith HJ, Meremikwu M: **Iron chelating agents for treating malaria.** *Cochrane Database Syst Rev* 2003(2):CD001474.
95. Zhang S, Kim CC, Batra S, McKerrow JH, Loke P: **Delineation of diverse macrophage activation programs in response to intracellular parasites and cytokines.** *PLoS Negl Trop Dis* 2010, **4**(3):e648.
96. Scharton-Kersten T, Afonso LC, Wysocka M, Trinchieri G, Scott P: **IL-12 is required for natural killer cell activation and subsequent T helper 1 cell development in experimental leishmaniasis.** *J Immunol* 1995, **154**(10):5320-5330.
97. Trinchieri G: **Interleukin-12 and the regulation of innate resistance and adaptive immunity.** *Nat Rev Immunol* 2003, **3**(2):133-146.
98. Liese J, Schleicher U, Bogdan C: **The innate immune response against Leishmania parasites.** *Immunobiology* 2008, **213**(3-4):377-387.
99. Chessler AD, Unnikrishnan M, Bei AK, Daily JP, Burleigh BA: **Trypanosoma cruzi triggers an early type I IFN response in vivo at the site of intradermal infection.** *J Immunol* 2009, **182**(4):2288-2296.
100. Leng J, Butcher BA, Denkers EY: **Dysregulation of macrophage signal transduction by Toxoplasma gondii: past progress and recent advances.** *Parasite Immunol* 2009, **31**(12):717-728.
101. Doherty CP: **Host-pathogen interactions: the role of iron.** *J Nutr* 2007, **137**(5):1341-1344.
102. Wilson ME, Vorhies RW, Andersen KA, Britigan BE: **Acquisition of iron from transferrin and lactoferrin by the protozoan Leishmania chagasi.** *Infect Immun* 1994, **62**(8):3262-3269.
103. Jacobson ES, Goodner AP, Nyhus KJ: **Ferrous iron uptake in Cryptococcus neoformans.** *Infect Immun* 1998, **66**(9):4169-4175.
104. Radisky D, Kaplan J: **Regulation of transition metal transport across the yeast plasma membrane.** *J Biol Chem* 1999, **274**(8):4481-4484.
105. Timmerman MM, Woods JP: **Ferric reduction is a potential iron acquisition mechanism for Histoplasma capsulatum.** *Infect Immun* 1999, **67**(12):6403-6408.
106. Huynh C, Sacks DL, Andrews NW: **A Leishmania amazonensis ZIP family iron transporter is essential for parasite replication within macrophage phagolysosomes.** *J Exp Med* 2006, **203**(10):2363-2375.
107. Sengupta S, Tripathi J, Tandon R, Raje M, Roy RP, Basu SK, Mukhopadhyay A: **Hemoglobin endocytosis in Leishmania is mediated through a 46-kDa protein located in the flagellar pocket.** *J Biol Chem* 1999, **274**(5):2758-2765.
108. Singh SB, Tandon R, Krishnamurthy G, Vikram R, Sharma N, Basu SK, Mukhopadhyay A: **Rab5-mediated endosome-endosome fusion regulates**

- hemoglobin endocytosis in *Leishmania donovani*.** *EMBO J* 2003, **22**(21):5712-5722.
109. Steverding D: **The transferrin receptor of *Trypanosoma brucei*.** *Parasitol Int* 2000, **48**(3):191-198.
110. Bitter W, Gerrits H, Kieft R, Borst P: **The role of transferrin-receptor variation in the host range of *Trypanosoma brucei*.** *Nature* 1998, **391**(6666):499-502.
111. Steverding D: **On the significance of host antibody response to the *Trypanosoma brucei* transferrin receptor during chronic infection.** *Microbes Infect* 2006, **8**(12-13):2777-2782.
112. Mussmann R, Engstler M, Gerrits H, Kieft R, Toaldo CB, Onderwater J, Koerten H, van Luenen HG, Borst P: **Factors affecting the level and localization of the transferrin receptor in *Trypanosoma brucei*.** *J Biol Chem* 2004, **279**(39):40690-40698.
113. Bruchhaus I, Tannich E: **Induction of the iron-containing superoxide dismutase in *Entamoeba histolytica* by a superoxide anion-generating system or by iron chelation.** *Mol Biochem Parasitol* 1994, **67**(2):281-288.
114. Lee J, Park SJ, Yong TS: **Effect of iron on adherence and cytotoxicity of *Entamoeba histolytica* to CHO cell monolayers.** *Korean J Parasitol* 2008, **46**(1):37-40.
115. Tsutsumi V, Martinez-Palomo A, Tanikawa K: **Scanning electron microscopy of erythrophagocytosis by *Entamoeba histolytica* trophozoites.** *Arch Med Res* 1992, **23**(2):173-175.
116. Das P, Debnath A, Munoz ML: **Molecular mechanisms of pathogenesis in amebiasis.** *Indian J Gastroenterol* 1999, **18**(4):161-166.
117. Reyes-Lopez M, Serrano-Luna JJ, Negrete-Abascal E, Leon-Sicairos N, Guerrero-Barrera AL, de la Garza M: ***Entamoeba histolytica*: transferrin binding proteins.** *Exp Parasitol* 2001, **99**(3):132-140.
118. Mundodi V, Kucknoor AS, Chang TH, Alderete JF: **A novel surface protein of *Trichomonas vaginalis* is regulated independently by low iron and contact with vaginal epithelial cells.** *BMC Microbiol* 2006, **6**:6.
119. Petropolis DB, Fernandes Rodrigues JC, da Rocha-Azevedo B, Costa e Silva-Filho F: **The binding of *Tritrichomonas foetus* to immobilized laminin-1 and its role in the cytotoxicity exerted by the parasite.** *Microbiology* 2008, **154**(Pt 8):2283-2290.
120. Suchan P, Vyoral D, Petrak J, Sut'ak R, Rasoloson D, Nohynkova E, Dolezal P, Tachezy J: **Incorporation of iron into *Tritrichomonas foetus* cell compartments reveals ferredoxin as a major iron-binding protein in hydrogenosomes.** *Microbiology* 2003, **149**(Pt 7):1911-1921.
121. Kim YS, Song HO, Choi IH, Park SJ, Ryu JS: **Hydrogenosomal activity of *Trichomonas vaginalis* cultivated under different iron conditions.** *Korean J Parasitol* 2006, **44**(4):373-378.
122. Sutak R, Chamot C, Tachezy J, Camadro JM, Lesuisse E: **Siderophore and haem iron use by *Tritrichomonas foetus*.** *Microbiology* 2004, **150**(Pt 12):3979-3987.

123. Tachezy J, Kulda J, Bahnikova I, Suchan P, Razga J, Schrevel J: **Tritrichomonas foetus: iron acquisition from lactoferrin and transferrin.** *Exp Parasitol* 1996, **83**(2):216-228.
124. Affonso AL, Benchimol M, Ribeiro KC, Lins U, De Souza W: **Further studies on the endocytic activity of Tritrichomonas foetus.** *Parasitol Res* 1994, **80**(5):403-413.
125. Tachezy J, Suchan P, Schrevel J, Kulda J: **The host-protein-independent iron uptake by Tritrichomonas foetus.** *Exp Parasitol* 1998, **90**(2):155-163.
126. Ardalan S, Lee BC, Garber GE: **Trichomonas vaginalis: the adhesins AP51 and AP65 bind heme and hemoglobin.** *Exp Parasitol* 2009, **121**(4):300-306.
127. Torres-Romero JC, Arroyo R: **Responsiveness of Trichomonas vaginalis to iron concentrations: evidence for a post-transcriptional iron regulation by an IRE/IRP-like system.** *Infect Genet Evol* 2009, **9**(6):1065-1074.
128. Solano-Gonzalez E, Burrola-Barraza E, Leon-Sicairos C, Avila-Gonzalez L, Gutierrez-Escolano L, Ortega-Lopez J, Arroyo R: **The trichomonad cysteine proteinase TVCP4 transcript contains an iron-responsive element.** *FEBS Lett* 2007, **581**(16):2919-2928.
129. Lehker MW, Alderete JF: **Iron regulates growth of Trichomonas vaginalis and the expression of immunogenic trichomonad proteins.** *Mol Microbiol* 1992, **6**(1):123-132.
130. Lehker MW, Chang TH, Dailey DC, Alderete JF: **Specific erythrocyte binding is an additional nutrient acquisition system for Trichomonas vaginalis.** *J Exp Med* 1990, **171**(6):2165-2170.
131. Newsome AL, Wilhelm WE: **Inhibition of Naegleria fowleri by microbial iron-chelating agents: ecological implications.** *Appl Environ Microbiol* 1983, **45**(2):665-668.
132. Kang JM, Cheun HI, Kim J, Moon SU, Park SJ, Kim TS, Sohn WM, Na BK: **Identification and characterization of a mitochondrial iron-superoxide dismutase of Cryptosporidium parvum.** *Parasitol Res* 2008, **103**(4):787-795.
133. Benitez AJ, Arrowood MJ, Mead JR: **Functional characterization of the nucleotide binding domain of the Cryptosporidium parvum CpABC4 transporter: an iron-sulfur cluster transporter homolog.** *Mol Biochem Parasitol* 2009, **165**(2):103-110.
134. Carvalho S, Cruz T, Santarem N, Castro H, Costa V, Tomas AM: **Heme as a source of iron to Leishmania infantum amastigotes.** *Acta Trop* 2009, **109**(2):131-135.
135. Borges VM, Vannier-Santos MA, de Souza W: **Subverted transferrin trafficking in Leishmania-infected macrophages.** *Parasitol Res* 1998, **84**(10):811-822.
136. Das NK, Biswas S, Solanki S, Mukhopadhyay CK: **Leishmania donovani depletes labile iron pool to exploit iron uptake capacity of macrophage for its intracellular growth.** *Cell Microbiol* 2009, **11**(1):83-94.
137. Meehan HA, Lundberg RA, Connell GJ: **A trypanosomatid protein specifically interacts with a mammalian iron-responsive element.** *Parasitol Res* 2000, **86**(2):109-114.

138. Pollack S, Schnelle V: **Inability to detect transferrin receptors on *P. falciparum* parasitized red cells.** *Br J Haematol* 1988, **68**(1):125-129.
139. Fry M: **Diferic transferrin reductase in *Plasmodium falciparum*-infected erythrocytes.** *Biochem Biophys Res Commun* 1989, **158**(2):469-473.
140. Sanchez-Lopez R, Haldar K: **A transferrin-independent iron uptake activity in *Plasmodium falciparum*-infected and uninfected erythrocytes.** *Mol Biochem Parasitol* 1992, **55**(1-2):9-20.
141. Goma J, Renia L, Miltgen F, Mazier D: **Effects of iron deficiency on the hepatic development of *Plasmodium yoelii*.** *Parasite* 1995, **2**(4):351-356.
142. Okada K: **The novel heme oxygenase-like protein from *Plasmodium falciparum* converts heme to bilirubin IXalpha in the apicoplast.** *FEBS Lett* 2009, **583**(2):313-319.
143. Dziadek B, Dziadek J, Dlugonska H: **Identification of *Toxoplasma gondii* proteins binding human lactoferrin: a new aspect of rhoptry proteins function.** *Exp Parasitol* 2007, **115**(3):277-282.
144. King AE, Kelly RW, Sallenave JM, Bocking AD, Challis JR: **Innate immune defences in the human uterus during pregnancy.** *Placenta* 2007, **28**(11-12):1099-1106.
145. Fuchs R, Ellinger I: **Endocytic and transcytotic processes in villous syncytiotrophoblast: role in nutrient transport to the human fetus.** *Traffic* 2004, **5**(10):725-738.
146. Barbosa BF, Silva DA, Costa IN, Mineo JR, Ferro EA: **BeWo trophoblast cell susceptibility to *Toxoplasma gondii* is increased by interferon-gamma, interleukin-10 and transforming growth factor-beta1.** *Clin Exp Immunol* 2008, **151**(3):536-545.
147. Ascenzi P, Bocedi A, Gradoni L: **Do neuroglobin and myoglobin protect *Toxoplasma gondii* from nitrosative stress?** *IUBMB Life* 2005, **57**(10):689-691.
148. Ascenzi P, Fasano M, Gradoni L: **Do hemoglobin and hemocyanin impair schistosoma killing by NO?** *IUBMB Life* 2002, **53**(6):287-288.
149. Ascenzi P, Salvati L, Brunori M: **Does myoglobin protect *Trypanosoma cruzi* from the antiparasitic effects of nitric oxide?** *FEBS Lett* 2001, **501**(2-3):103-105.
150. Plant J, Glynn AA: **Genetics of resistance to infection with *Salmonella typhimurium* in mice.** *J Infect Dis* 1976, **133**(1):72-78.
151. Bradley DJ: **Letter: Genetic control of natural resistance to *Leishmania donovani*.** *Nature* 1974, **250**(464):353-354.
152. Vidal SM, Malo D, Vogan K, Skamene E, Gros P: **Natural resistance to infection with intracellular parasites: isolation of a candidate for Bcg.** *Cell* 1993, **73**(3):469-485.
153. Vidal S, Belouchi AM, Cellier M, Beatty B, Gros P: **Cloning and characterization of a second human NRAMP gene on chromosome 12q13.** *Mamm Genome* 1995, **6**(4):224-230.
154. Vidal SM, Pinner E, Lepage P, Gauthier S, Gros P: **Natural resistance to intracellular infections: Nramp1 encodes a membrane phosphoglycoprotein absent in macrophages from susceptible (Nramp1 D169) mouse strains.** *J Immunol* 1996, **157**(8):3559-3568.

155. Feng J, Li Y, Hashad M, Schurr E, Gros P, Adams LG, Templeton JW: **Bovine natural resistance associated macrophage protein 1 (Nramp1) gene.** *Genome Res* 1996, **6**(10):956-964.
156. Hu J, Bumstead N, Barrow P, Sebastiani G, Olien L, Morgan K, Malo D: **Resistance to salmonellosis in the chicken is linked to NRAMP1 and TNC.** *Genome Res* 1997, **7**(7):693-704.
157. Hu J, Bumstead N, Skamene E, Gros P, Malo D: **Structural organization, sequence, and expression of the chicken NRAMP1 gene encoding the natural resistance-associated macrophage protein 1.** *DNA Cell Biol* 1996, **15**(2):113-123.
158. Chen SL, Wang ZJ, Xu MY, Gui JF: **Molecular identification and expression analysis of natural resistance associated macrophage protein (Nramp) cDNA from Japanese flounder (*Paralichthys olivaceus*).** *Fish Shellfish Immunol* 2006, **20**(3):365-373.
159. Chen SL, Zhang YX, Xu JY, Meng L, Sha ZX, Ren GC: **Molecular cloning, characterization and expression analysis of natural resistance associated macrophage protein (Nramp) cDNA from turbot (*Scophthalmus maximus*).** *Comp Biochem Physiol B Biochem Mol Biol* 2007, **147**(1):29-37.
160. Dorschner MO, Phillips RB: **Comparative analysis of two Nramp loci from rainbow trout.** *DNA Cell Biol* 1999, **18**(7):573-583.
161. Karsi A, Wolters WR, Waldbieser GC: **Assignment of immune-related genes to the channel catfish, *Ictalurus punctatus*, genetic map.** *Anim Genet* 2005, **36**(6):502-506.
162. Saeij JP, Wiegertjes GF, Stet RJ: **Identification and characterization of a fish natural resistance-associated macrophage protein (NRAMP) cDNA.** *Immunogenetics* 1999, **50**(1-2):60-66.
163. Sibthorpe D, Baker AM, Gilmartin BJ, Blackwell JM, White JK: **Comparative analysis of two slc11 (Nramp) loci in *Takifugu rubripes*.** *DNA Cell Biol* 2004, **23**(1):45-58.
164. Gunshin H, Mackenzie B, Berger UV, Gunshin Y, Romero MF, Boron WF, Nussberger S, Gollan JL, Hediger MA: **Cloning and characterization of a mammalian proton-coupled metal-ion transporter.** *Nature* 1997, **388**(6641):482-488.
165. Picard V, Govoni G, Jabado N, Gros P: **Nramp 2 (DCT1/DMT1) expressed at the plasma membrane transports iron and other divalent cations into a calcein-accessible cytoplasmic pool.** *J Biol Chem* 2000, **275**(46):35738-35745.
166. Portnoy ME, Jensen LT, Culotta VC: **The distinct methods by which manganese and iron regulate the Nramp transporters in yeast.** *Biochem J* 2002, **362**(Pt 1):119-124.
167. Toyohara H, Yamamoto S, Hosoi M, Takagi M, Hayashi I, Nakao K, Kaneko S: **Scallop DMT functions as a Ca²⁺ transporter.** *FEBS Lett* 2005, **579**(12):2727-2730.
168. Gruenheid S, Cellier M, Vidal S, Gros P: **Identification and characterization of a second mouse Nramp gene.** *Genomics* 1995, **25**(2):514-525.
169. Fleming MD, Romano MA, Su MA, Garrick LM, Garrick MD, Andrews NC: **Nramp2 is mutated in the anemic Belgrade (b) rat: evidence of a role for**

- Nramp2 in endosomal iron transport.** *Proc Natl Acad Sci U S A* 1998, **95**(3):1148-1153.
170. Fleming MD, Trenor CC, 3rd, Su MA, Foernzler D, Beier DR, Dietrich WF, Andrews NC: **Microcytic anaemia mice have a mutation in Nramp2, a candidate iron transporter gene.** *Nat Genet* 1997, **16**(4):383-386.
171. Mims MP, Prchal JT: **Divalent metal transporter 1.** *Hematology* 2005, **10**(4):339-345.
172. D'Souza J, Cheah PY, Gros P, Chia W, Rodrigues V: **Functional complementation of the malvolio mutation in the taste pathway of *Drosophila melanogaster* by the human natural resistance-associated macrophage protein 1 (Nramp-1).** *J Exp Biol* 1999, **202**(Pt 14):1909-1915.
173. Smyth DJ, Glanfield A, McManus DP, Hacker E, Blair D, Anderson GJ, Jones MK: **Two isoforms of a divalent metal transporter (DMT1) in *Schistosoma mansoni* suggest a surface-associated pathway for iron absorption in schistosomes.** *J Biol Chem* 2006, **281**(4):2242-2248.
174. Papp-Wallace KM, Maguire ME: **Manganese transport and the role of manganese in virulence.** *Annu Rev Microbiol* 2006, **60**:187-209.
175. Kehres DG, Zaharik ML, Finlay BB, Maguire ME: **The NRAMP proteins of *Salmonella typhimurium* and *Escherichia coli* are selective manganese transporters involved in the response to reactive oxygen.** *Mol Microbiol* 2000, **36**(5):1085-1100.
176. Makui H, Roig E, Cole ST, Helmann JD, Gros P, Cellier MF: **Identification of the *Escherichia coli* K-12 Nramp orthologue (MntH) as a selective divalent metal ion transporter.** *Mol Microbiol* 2000, **35**(5):1065-1078.
177. Herman C, Lecat S, D'Ari R, Boulloc P: **Regulation of the heat-shock response depends on divalent metal ions in an hflB mutant of *Escherichia coli*.** *Mol Microbiol* 1995, **18**(2):247-255.
178. Agranoff D, Monahan IM, Mangan JA, Butcher PD, Krishna S: **Mycobacterium tuberculosis expresses a novel pH-dependent divalent cation transporter belonging to the Nramp family.** *J Exp Med* 1999, **190**(5):717-724.
179. Reeve I, Hummel D, Nelson N, Voss J: **Overexpression, purification, and site-directed spin labeling of the Nramp metal transporter from *Mycobacterium leprae*.** *Proc Natl Acad Sci U S A* 2002, **99**(13):8608-8613.
180. Kuhn DE, Baker BD, Lafuse WP, Zwilling BS: **Differential iron transport into phagosomes isolated from the RAW264.7 macrophage cell lines transfected with Nramp1Gly169 or Nramp1Asp169.** *J Leukoc Biol* 1999, **66**(1):113-119.
181. Zwilling BS, Kuhn DE, Wikoff L, Brown D, Lafuse W: **Role of iron in Nramp1-mediated inhibition of mycobacterial growth.** *Infect Immun* 1999, **67**(3):1386-1392.
182. Abramson J, Smirnova I, Kasho V, Verner G, Kaback HR, Iwata S: **Structure and mechanism of the lactose permease of *Escherichia coli*.** *Science* 2003, **301**(5633):610-615.
183. Barton CH, Biggs TE, Baker ST, Bowen H, Atkinson PG: **Nramp1: a link between intracellular iron transport and innate resistance to intracellular pathogens.** *J Leukoc Biol* 1999, **66**(5):757-762.

184. Jabado N, Lam-Yuk-Tseung S, Forbes JR, Gros P: **Mouse Nramp1 resistance associated macrophage protein 1 (Nramp1): a key player in host innate immunity against infections.** New York, NY: Landes Bioscience/Kluwer Academic; 2004.
185. Cellier MF, Courville P, Campion C: **Nramp1 phagocyte intracellular metal withdrawal defense.** *Microbes Infect* 2007, **9**(14-15):1662-1670.
186. Fernández-Robledo JA, Courville P, Cellier MF, Vasta GR: **Gene organization and expression of the divalent cation transporter Nramp in the protistan parasite *Perkinsus marinus*.** *J Parasitol* 2004, **90**(5):1004-1014.
187. Kishi F: **Isolation and characterization of human Nramp cDNA.** *Biochem Biophys Res Commun* 1994, **204**(3):1074-1080.
188. Luk E, Jensen L, Culotta V: **The Nramp family.** New York, NY: Kluwer Academic/ Landes; 2004.
189. Portnoy ME, Liu XF, Culotta VC: ***Saccharomyces cerevisiae* expresses three functionally distinct homologues of the Nramp family of metal transporters.** *Mol Cell Biol* 2000, **20**(21):7893-7902.
190. Fernández-Robledo JA, Lin Z, Vasta GR: **Transfection of the protozoan parasite *Perkinsus marinus*.** *Mol Biochem Parasitol* 2008, **157**(1):44-53.
191. Gauthier JD, Vasta GR: **In vitro culture of the eastern oyster parasite *Perkinsus marinus*: Optimization of the methodology.** *J Invertebrate Pathology* 1995, **66**(2):156-168.
192. Borson ND, Salo WL, Drewes LR: **A lock-docking oligo(dT) primer for 5' and 3' RACE PCR.** *PCR Methods and Applications* 1992, **2**(2):144-148.
193. Robledo JA, Gauthier JD, Coss CA, Wright AC, Vasta GR: **Species-specificity and sensitivity of a PCR-based assay for *Perkinsus marinus* in the eastern oyster, *Crassostrea virginica*: a comparison with the fluid thioglycollate assay.** *J Parasitol* 1998, **84**(6):1237-1244.
194. Kumar S, Gadagkar SR: **Disparity index: a simple statistic to measure and test the homogeneity of substitution patterns between molecular sequences.** *Genetics* 2001, **158**(3):1321-1327.
195. Tamura K, Dudley J, Nei M, Kumar S: **MEGA4: Molecular Evolutionary Genetics Analysis (MEGA) software version 4.0.** *Mol Biol Evol* 2007, **24**(8):1596-1599.
196. Nicholas KB, Nicholas HB: **GeneDoc: a tool for editing and annotating multiple sequence alignments. Distributed by the authors.** 1997.
197. Mayer MG, Floeter-Winter LM: **Pre-mRNA trans-splicing: from kinetoplastids to mammals, an easy language for life diversity.** *Mem Inst Oswaldo Cruz* 2005, **100**(5):501-513.
198. Zhang H, Hou Y, Miranda L, Campbell DA, Sturm NR, Gaasterland T, Lin S: **Spliced leader RNA trans-splicing in dinoflagellates.** *Proc Natl Acad Sci U S A* 2007, **104**(11):4618-4623.
199. Tirard CT, Grossfeld RM, Volety AK, Chu F-LE: **Heat Shock Proteins of the Oyster Parasite *Perkinsus marinus*.** *Diseases of Aquatic Organisms* 1995, **22**:147-151.

200. Que Q, Helmann JD: **Manganese homeostasis in *Bacillus subtilis* is regulated by MntR, a bifunctional regulator related to the diphtheria toxin repressor family of proteins.** *Mol Microbiol* 2000, **35**(6):1454-1468.
201. Blumenthal T: **Trans-splicing and operons.** *WormBook* 2005:1-9.
202. Pouchkina-Stantcheva NN, Tunnaclyffe A: **Spliced leader RNA-mediated trans-splicing in phylum Rotifera.** *Mol Biol Evol* 2005, **22**(6):1482-1489.
203. Zhang H, Campbell DA, Sturm NR, Lin S: **Dinoflagellate spliced leader RNA genes display a variety of sequences and genomic arrangements.** *Mol Biol Evol* 2009, **26**(8):1757-1771.
204. Martinez-Calvillo S, Vizuet-de-Rueda JC, Florencio-Martinez LE, Manning-Cela RG, Figueroa-Angulo EE: **Gene expression in trypanosomatid parasites.** *J Biomed Biotechnol*, **2010**:525241.
205. Ivens AC, Peacock CS, Worthey EA, Murphy L, Aggarwal G, Berriman M, Sisk E, Rajandream MA, Adlem E, Aert R *et al*: **The genome of the kinetoplastid parasite, *Leishmania major*.** *Science* 2005, **309**(5733):436-442.
206. Berriman M, Ghedin E, Hertz-Fowler C, Blandin G, Renauld H, Bartholomeu DC, Lennard NJ, Caler E, Hamlin NE, Haas B *et al*: **The genome of the African trypanosome *Trypanosoma brucei*.** *Science* 2005, **309**(5733):416-422.
207. El-Sayed NM, Myler PJ, Bartholomeu DC, Nilsson D, Aggarwal G, Tran AN, Ghedin E, Worthey EA, Delcher AL, Blandin G *et al*: **The genome sequence of *Trypanosoma cruzi*, etiologic agent of Chagas disease.** *Science* 2005, **309**(5733):409-415.
208. El-Sayed NM, Myler PJ, Blandin G, Berriman M, Crabtree J, Aggarwal G, Caler E, Renauld H, Worthey EA, Hertz-Fowler C *et al*: **Comparative genomics of trypanosomatid parasitic protozoa.** *Science* 2005, **309**(5733):404-409.
209. Martinez-Calvillo S, Yan S, Nguyen D, Fox M, Stuart K, Myler PJ: **Transcription of *Leishmania major* Friedlin chromosome 1 initiates in both directions within a single region.** *Mol Cell* 2003, **11**(5):1291-1299.
210. LeBowitz JH, Smith HQ, Rusche L, Beverley SM: **Coupling of poly(A) site selection and trans-splicing in *Leishmania*.** *Genes Dev* 1993, **7**(6):996-1007.
211. Laird PW: **Trans splicing in trypanosomes--archaism or adaptation?** *Trends Genet* 1989, **5**(7):204-208.
212. Perry K, Agabian N: **mRNA processing in the Trypanosomatidae.** *Experientia* 1991, **47**(2):118-128.
213. Bastin P, Ellis K, Kohl L, Gull K: **Flagellum ontogeny in trypanosomes studied via an inherited and regulated RNA interference system.** *J Cell Sci* 2000, **113** (Pt 18):3321-3328.
214. LaCount DJ, Bruse S, Hill KL, Donelson JE: **Double-stranded RNA interference in *Trypanosoma brucei* using head-to-head promoters.** *Mol Biochem Parasitol* 2000, **111**(1):67-76.
215. Shi H, Djikeng A, Mark T, Wirtz E, Tschudi C, Ullu E: **Genetic interference in *Trypanosoma brucei* by heritable and inducible double-stranded RNA.** *RNA* 2000, **6**(7):1069-1076.
216. Wang Z, Morris JC, Drew ME, Englund PT: **Inhibition of *Trypanosoma brucei* gene expression by RNA interference using an integratable vector with opposing T7 promoters.** *J Biol Chem* 2000, **275**(51):40174-40179.

217. Joseph SJ, Fernandez-Robledo JA, Gardner MJ, El-Sayed NM, Kuo CH, Schott EJ, Wang H, Kissinger JC, Vasta GR: **The Alveolate *Perkinsus marinus*: Biological Insights from EST Gene Discovery.** *BMC Genomics* 2010, **11**(1):228-248.
218. Long JC, Sommer F, Allen MD, Lu SF, Merchant SS: **FER1 and FER2 encoding two ferritin complexes in *Chlamydomonas reinhardtii* chloroplasts are regulated by iron.** *Genetics* 2008, **179**(1):137-147.
219. Bengert P, Dandekar T: **A software tool-box for analysis of regulatory RNA elements.** *Nucleic Acids Res* 2003, **31**(13):3441-3445.
220. Piccinelli P, Samuelsson T: **Evolution of the iron-responsive element.** *RNA* 2007, **13**(7):952-966.
221. Loyevsky M, Mompoin F, Yikilmaz E, Altschul SF, Madden T, Wootton JC, Kurantsin-Mills J, Kassim OO, Gordeuk VR, Rouault TA: **Expression of a recombinant IRP-like *Plasmodium falciparum* protein that specifically binds putative plasmodial IREs.** *Mol Biochem Parasitol* 2003, **126**(2):231-238.
222. Hodges M, Yikilmaz E, Patterson G, Kasvosve I, Rouault TA, Gordeuk VR, Loyevsky M: **An iron regulatory-like protein expressed in *Plasmodium falciparum* displays aconitase activity.** *Mol Biochem Parasitol* 2005, **143**(1):29-38.
223. Loyevsky M, LaVaute T, Allerson CR, Stearman R, Kassim OO, Cooperman S, Gordeuk VR, Rouault TA: **An IRP-like protein from *Plasmodium falciparum* binds to a mammalian iron-responsive element.** *Blood* 2001, **98**(8):2555-2562.
224. Liu XF, Elashvili I, Gralla EB, Valentine JS, Lapinskas P, Culotta VC: **Yeast lacking superoxide dismutase. Isolation of genetic suppressors.** *J Biol Chem* 1992, **267**(26):18298-18302.
225. Evans CA, Harbuz MS, Ostefeld T, Norrish A, Blackwell JM: **Nramp1 is expressed in neurons and is associated with behavioural and immune responses to stress.** *Neurogenetics* 2001, **3**(2):69-78.
226. Richer E, Courville P, Bergevin I, Cellier MF: **Horizontal gene transfer of "prototype" Nramp in bacteria.** *J Mol Evol* 2003, **57**(4):363-376.
227. Richer E, Courville P, Cellier M: **Molecular Evolutionary Analysis of the Nramp Family.** New York, NY: Landes Bioscience/Kluwer Academic; 2004.
228. Robledo JA, Courville P, Cellier MF, Vasta GR: **Gene organization and expression of the divalent cation transporter Nramp in the protistan parasite *Perkinsus marinus*.** *J Parasitol* 2004, **90**(5):1004-1014.
229. Thomson JD, Gibson TJ, hIGGINS DG: **Curr Protoc Bioinformatics. Chapter 2; Unit 2.3;** 2002.
230. Edgar RC: **MUSCLE: a multiple sequence alignment method with reduced time and space complexity.** *BMC Bioinformatics* 2004, **5**:113.
231. Whelan S, Goldman N: **A general empirical model of protein evolution derived from multiple protein families using a maximum-likelihood approach.** *Mol Biol Evol* 2001, **18**(5):691-699.
232. Schmidt HA, von Haeseler A: **Maximum-likelihood analysis using TREE-PUZZLE,** vol. Chapter 6; Unit 6.6; 2007.
233. Rzhetsky A, Nei M: **A simple method for estimating and testing minimum evolution trees.** *Molecular Biology and Evolution* 1992, **9**:945-967.

234. Tamura K, Kumar S: **Evolutionary distance estimation under heterogeneous substitution pattern among lineages.** *Mol Biol Evol* 2002, **19**(10):1727-1736.
235. Eck RV, Dayhoff MO: **Atlas of Protein Sequence and Structure.** Silver Springs, MD: National Biomedical Research Foundation; 1966.
236. Felsenstein J: **limits on phylogenies: An approach using the bootstrap.** *Evolution* 1985, **39**:783-791.
237. Nei M, Kumar S: **Molecular Evolution and Phylogenetics.** New York: Oxford University Press; 2000.
238. Tajima F: **Simple methods for testing the molecular evolutionary clock hypothesis.** *Genetics* 1993, **135**(2):599-607.
239. Zhang Y: **I-TASSER server for protein 3D structure prediction.** *BMC Bioinformatics* 2008, **9**:40.
240. Courville P, Urbankova E, Rensing C, Chaloupka R, Quick M, Cellier MF: **Solute carrier 11 cation symport requires distinct residues in transmembrane helices 1 and 6.** *J Biol Chem* 2008, **283**(15):9651-9658.
241. Keeling PJ, Burger G, Durnford DG, Lang BF, Lee RW, Pearlman RE, Roger AJ, Gray MW: **The tree of eukaryotes.** *Trends Ecol Evol* 2005, **20**(12):670-676.
242. Rodriguez-Ezpeleta N, Brinkmann H, Burger G, Roger AJ, Gray MW, Philippe H, Lang BF: **Toward resolving the eukaryotic tree: the phylogenetic positions of jakobids and cercozoans.** *Curr Biol* 2007, **17**(16):1420-1425.
243. Sanchez-Puerta MV, Delwiche CF: **A hypothesis for plastid evolution in chromoalveolates.** *J Phycol* 2008, **44**:1097-1107.
244. O'Brien EA, Koski LB, Zhang Y, Yang L, Wang E, Gray MW, Burger G, Lang BF: **TBestDB: a taxonomically broad database of expressed sequence tags (ESTs).** *Nucleic Acids Res* 2007, **35**(Database issue):D445-451.
245. Takezaki N, Rzhetsky A, Nei M: **Phylogenetic test of the molecular clock and linearized trees.** *Molecular Biology and Evolution* 2004, **12**:823-833.
246. Tajima F, Nei M: **Estimation of evolutionary distance between nucleotide sequences.** *Mol Biol Evol* 1984, **1**(3):269-285.
247. Cohen A, Nelson H, Nelson N: **Metal-ion Transporters: from Yeast to Human Diseases.** New York, NY: Landes Bioscience/Kluwer Academic; 2004.
248. Kaiser BN, Moreau S, Castelli J, Thomson R, Lambert A, Bogliolo S, Puppo A, Day DA: **The soybean NRAMP homologue, GmDMT1, is a symbiotic divalent metal transporter capable of ferrous iron transport.** *Plant J* 2003, **35**(3):295-304.
249. Atkinson PG, Barton CH: **High level expression of Nramp1G169 in RAW264.7 cell transfectants: analysis of intracellular iron transport.** *Immunology* 1999, **96**(4):656-662.
250. Bandyopadhyay J, Song HO, Park BJ, Singaravelu G, Sun JL, Ahnn J, Cho JH: **Functional assessment of Nramp-like metal transporters and manganese in Caenorhabditis elegans.** *Biochem Biophys Res Commun* 2009, **390**(1):136-141.
251. Dix D, Bridgham J, Broderius M, Eide D: **Characterization of the FET4 protein of yeast. Evidence for a direct role in the transport of iron.** *J Biol Chem* 1997, **272**(18):11770-11777.

252. Eide D, Broderius M, Fett J, Guerinot ML: **A novel iron-regulated metal transporter from plants identified by functional expression in yeast.** *Proc Natl Acad Sci U S A* 1996, **93**(11):5624-5628.
253. West AH, Clark DJ, Martin J, Neupert W, Hartl FU, Horwich AL: **Two related genes encoding extremely hydrophobic proteins suppress a lethal mutation in the yeast mitochondrial processing enhancing protein.** *J Biol Chem* 1992, **267**(34):24625-24633.
254. Gietz RD, Schiestl RH: **Quick and easy yeast transformation using the LiAc/SS carrier DNA/PEG method.** *Nat Protoc* 2007, **2**(1):35-37.
255. Vert G, Grotz N, Dedaldechamp F, Gaymard F, Guerinot ML, Briat JF, Curie C: **IRT1, an Arabidopsis transporter essential for iron uptake from the soil and for plant growth.** *Plant Cell* 2002, **14**(6):1223-1233.
256. Cohen A, Nevo Y, Nelson N: **The first external loop of the metal ion transporter DCT1 is involved in metal ion binding and specificity.** *Proc Natl Acad Sci U S A* 2003, **100**(19):10694-10699.
257. Sacher A, Cohen A, Nelson N: **Properties of the mammalian and yeast metal-ion transporters DCT1 and Smf1p expressed in Xenopus laevis oocytes.** *J Exp Biol* 2001, **204**(Pt 6):1053-1061.
258. Luk E, Jensen LT, Culotta VC: **The many highways for intracellular trafficking of metals.** *J Biol Inorg Chem* 2003, **8**(8):803-809.
259. Montanini B, Blaudez D, Jeandroz S, Sanders D, Chalot M: **Phylogenetic and functional analysis of the Cation Diffusion Facilitator (CDF) family: improved signature and prediction of substrate specificity.** *BMC Genomics* 2007, **8**:107.
260. Lam-Yuk-Tseung S, Picard V, Gros P: **Identification of a tyrosine-based motif (YGSI) in the amino terminus of Nramp1 (Slc11a1) that is important for lysosomal targeting.** *J Biol Chem* 2006, **281**(42):31677-31688.
261. Courville P, Chaloupka R, Veyrier F, Cellier MF: **Determination of transmembrane topology of the Escherichia coli natural resistance-associated macrophage protein (Nramp) ortholog.** *J Biol Chem* 2004, **279**(5):3318-3326.
262. Forbes JR, Gros P: **Iron, manganese, and cobalt transport by Nramp1 (Slc11a1) and Nramp2 (Slc11a2) expressed at the plasma membrane.** *Blood* 2003, **102**(5):1884-1892.
263. Czachorowski M, Lam-Yuk-Tseung S, Cellier M, Gros P: **Transmembrane topology of the mammalian Slc11a2 iron transporter.** *Biochemistry* 2009, **48**(35):8422-8434.
264. Singh SK, Yamashita A, Gouaux E: **Antidepressant binding site in a bacterial homologue of neurotransmitter transporters.** *Nature* 2007, **448**(7156):952-956.
265. Faham S, Watanabe A, Besserer GM, Cascio D, Specht A, Hirayama BA, Wright EM, Abramson J: **The crystal structure of a sodium galactose transporter reveals mechanistic insights into Na⁺/sugar symport.** *Science* 2008, **321**(5890):810-814.
266. Weyand S, Shimamura T, Yajima S, Suzuki S, Mirza O, Krusong K, Carpenter EP, Rutherford NG, Hadden JM, O'Reilly J *et al*: **Structure and molecular mechanism of a nucleobase-cation-symport-1 family transporter.** *Science* 2008, **322**(5902):709-713.

267. Shaffer PL, Goehring A, Shankaranarayanan A, Gouaux E: **Structure and mechanism of a Na⁺-independent amino acid transporter.** *Science* 2009, **325**(5943):1010-1014.
268. Wu S, Zhang Y: **LOMETS: a local meta-threading-server for protein structure prediction.** *Nucleic Acids Res* 2007, **35**(10):3375-3382.
269. Wu S, Zhang Y: **MUSTER: Improving protein sequence profile-profile alignments by using multiple sources of structure information.** *Proteins* 2008, **72**(2):547-556.
270. Cellier M, Belouchi A, Gros P: **Resistance to intracellular infections: comparative genomic analysis of Nramp.** *Trends Genet* 1996, **12**(6):201-204.
271. Ben-Yona A, Kanner BI: **Transmembrane domain 8 of the α -aminobutyric acid transporter GAT-1 lines a cytoplasmic accessibility pathway into its binding pocket.** *J Biol Chem* 2009, **284**(15):9727-9732.
272. Kaufmann KW, Dawson ES, Henry LK, Field JR, Blakely RD, Meiler J: **Structural determinants of species-selective substrate recognition in human and Drosophila serotonin transporters revealed through computational docking studies.** *Proteins* 2009, **74**(3):630-642.
273. Lam-Yuk-Tseung S, Govoni G, Forbes J, Gros P: **Iron transport by Nramp2/DMT1: pH regulation of transport by 2 histidines in transmembrane domain 6.** *Blood* 2003, **101**(9):3699-3707.
274. Haemig HA, Moen PJ, Brooker R: **Evidence that Highly Conserved Residues of Transmembrane Segment 6 of Escherichia coli MntH Are Important for Transport Activity.** *Biochemistry*.
275. Chaloupka R, Courville P, Veyrier F, Knudsen B, Tompkins TA, Cellier MF: **Identification of functional amino acids in the Nramp family by a combination of evolutionary analysis and biophysical studies of metal and proton cotransport in vivo.** *Biochemistry* 2005, **44**(2):726-733.
276. Haemig HA, Brooker RJ: **Importance of conserved acidic residues in mntH, the Nramp homolog of Escherichia coli.** *J Membr Biol* 2004, **201**(2):97-107.
277. Nikko E, Sullivan JA, Pelham HR: **Arrestin-like proteins mediate ubiquitination and endocytosis of the yeast metal transporter Smf1.** *EMBO Rep* 2008, **9**(12):1216-1221.
278. Jensen LT, Carroll MC, Hall MD, Harvey CJ, Beese SE, Culotta VC: **Down-regulation of a manganese transporter in the face of metal toxicity.** *Mol Biol Cell* 2009, **20**(12):2810-2819.
279. Sunila I, Hamilton RM, Dungan CF: **Ultrastructural characteristics of the in vitro cell cycle of the protozoan pathogen of oysters, Perkinsus marinus.** *J Eukaryot Microbiol* 2001, **48**(3):348-361.
280. Matsuzaki M, Kuroiwa H, Kuroiwa T, Kita K, Nozaki H: **A cryptic algal group unveiled: a plastid biosynthesis pathway in the oyster parasite Perkinsus marinus.** *Mol Biol Evol* 2008, **25**(6):1167-1179.
281. Stelter K, El-Sayed NM, Seeber F: **The expression of a plant-type ferredoxin redox system provides molecular evidence for a plastid in the early dinoflagellate Perkinsus marinus.** *Protist* 2007, **158**(1):119-130.

282. Teles-Grilo ML, Tato-Costa J, Duarte SM, Maia A, Casal G, Azevedo C: **Is there a plastid in Perkinsus atlanticus (Phylum Perkinsozoa)?** *Eur J Protistol* 2007, **43**(2):163-167.
283. Bohnsack BL, Hirschi KK: **Nutrient regulation of cell cycle progression.** *Annu Rev Nutr* 2004, **24**:433-453.
284. Burhans WC, Heintz NH: **The cell cycle is a redox cycle: linking phase-specific targets to cell fate.** *Free Radic Biol Med* 2009, **47**(9):1282-1293.
285. Wright AC, Ahmed H, Gauthier JD, Silva AM, Vasta GR: **cDNA cloning and characterization of two iron superoxide dismutases from the oyster parasite Perkinsus marinus.** *Mol Biochem Parasitol* 2002, **123**(1):73-77.
286. Jabado N, Lam-Yuk-Tseung S, Forbes JR, Gros P: **The Nramp Family.** New York, NY: Kluwer Academic/ Landes; 2004.
287. Carpenter ML, Cande WZ: **Using morpholinos for gene knockdown in Giardia intestinalis.** *Eukaryot Cell* 2009, **8**(6):916-919.
288. Zhang H, Dungan CF, Lin S: **Introns, Alternative Splicing, Spliced Leader trans-Splicing and Differential Expression of pcna and cyclin in Perkinsus marinus.** *Protist* 2010.
289. Clayton C, Shapira M: **Post-transcriptional regulation of gene expression in trypanosomes and leishmanias.** *Mol Biochem Parasitol* 2007, **156**(2):93-101.